

KWAME NKRUMAH UNIVERSITY OF SCIENCE AND TECHNOLOGY, KUMASI
COLLEGE OF ENGINEERING
DEPARTMENT OF TELECOMMUNICATION ENGINEERING

FLEXIBLE AND WEARABLE PATTERN-RECONFIGURABLE PRINTED MONOPOLE
ANTENNA FOR ON-BODY COMMUNICATION.

By
ARTHUR PHILIP
(BSc TELECOMMUNICATION ENGINEERING)

A THESIS SUBMITTED TO THE DEPARTMENT OF
TELECOMMUNICATION ENGINEERING, KWAME NKRUMAH
UNIVERSITY OF SCIENCE AND TECHNOLOGY, IN PARTIAL
FULFILLMENT OF THE REQUIREMENT FOR THE DEGREE OF MPhil
TELECOMMUNICATION ENGINEERING

July, 2021

DECLARATION

I hereby declare that this submission is my own work towards the award of the MPhil degree and that, to the best of our knowledge, it contains no material previously published by another person or material which has been accepted for the award of any other degree of the university, except where due acknowledgment has been made in the thesis.

Arthur Philip (20692767) Signature Date
-----------------------------	--------------------	---------------

Certified by:

Dr. Mubarak Sani Ellis (Supervisor) Signature Date
--	--------------------	---------------

Certified by:

Dr. James Dzisi Gadze (Head of Department) Signature Date
---	--------------------	---------------

ABSTRACT

The fundamental feature of reconfigurable antenna (RA) systems is the ability to modify its functional operating characteristics compared to conventional antenna systems. As the size of electronic devices continues to shrink with stringent space constraints, reconfigurable antennas provide a low-cost approach for introducing adjustable properties on a single antenna element. This is to eliminate the need for multiple single-purpose antennas in diversity applications. Recently, reconfigurable antennas have gained popularity in wearable devices and finding applications in health care for the diagnosis and treatment of diseases such as stroke and cancer in tissues. Many applications of wearable antennas in personal communication devices, military gadgets and emergency apparatus are continuously growing. It is required that on-body antennas are unobtrusive and highly efficient with conformable features that can be easily suited to the configuration of the human body. However, due to the conductive nature of the human body, up to about 50% of the radiated energy from conventional printed monopole antennas can be absorbed. This effectively renders the omnidirectional antenna unidirectional when mounted on or close to the human body.

To this end, this current work proposes a simple technique to convert the conventional monopolar radiation pattern of a printed monopole antenna into a unidirectional radiation. This is shown among other advantages to significantly reduce specific absorption rate (SAR) and achieve circular polarization. The initial process begins with the design of a compact, low-profile, slotted-stepped planar monopole antenna (PMA) at the 2.45 GHz Industrial, Scientific and Medical (ISM) band. Further analysis presents an optimized reconfigurable extension of the antenna based on two switchable RF PIN diodes. This is incorporated in the antenna to asymmetrically steer the radiation pattern at different directions in specific operating modes. It is also shown that the frequency-radiation characteristics linkage that leads to shifts in the frequency while the radiation pattern is adjusted is fully decoupled in this design. Here, the switching effect of the radiation pattern does not cause any significant detuning in the operating frequency. This is further validated at varying antenna positions and excitation levels.

To present a conformable form of the reconfigurable antenna, a flexible substrate material is chosen for the design. Flexibility and wearability tests of the antenna are performed at various degrees of bending and subsequent placement on a human phantom model. The on-body effects on the antenna are characterized in simulation and measured on real human body. Simulated results show stable radiation patterns, reflection coefficient ($S_{11} < -20 \text{ dB}$) and a circular polarization at 2.45 GHz. Meanwhile, low simulated peak SAR of 0.46 W/kg and 0.39 W/kg averaged over $1g$ and $10g$ of tissue respectively are recorded when the antenna is mounted directly on the human body. This is achieved without the use of conventional large and bulky cavity-backed structures. Hence, the overall size of the antenna measures only a compact square size of 0.235λ , making it a very suitable candidate for on-body applications.

ACKNOWLEDGEMENTS

First and foremost thanks to God.

This research has been fully realized through the immense directions and insights of my supervisor, Dr. Mubarak Sani Ellis. His direct contributions, expertise, and dedication towards work have motivated the output of this thesis. I am highly indebted for his advice, financial support, great personality that created a thriving relationship for the success of this research.

I would also like to thank the management of the KNUST Engineering Education Project (KEEP) for the scholarship opportunity to pursue this two-year Master's Degree programme.

I also acknowledge the staff of my department and colleague research students for providing an enabling environment and support throughout this research.

TABLE OF CONTENTS

DECLARATION	ii
ABSTRACT	iii
ACKNOWLEDGEMENTS	iv
TABLE OF CONTENTS	v
LIST OF TABLES	viii
LIST OF FIGURES	ix
CHAPTER ONE	1
INTRODUCTION	1
1.1 Background and Significance of Study.....	1
1.2 Problem Statement	4
1.3 Research Objectives.....	5
1.3.1 General Objective	5
1.3.2 Specific Objectives	5
1.4 Motivation.....	6
1.5 Research Contributions.....	7
CHAPTER TWO	8
LITERATURE REVIEW	8
2.1 Introduction.....	8
2.2 Body-Centric Wireless Communication Networks	8
2.3 Characterization of Human Body Models for Body-centric Wireless Communication	9
2.4 Planar/Printed Monopole Antenna for On-body Communications	12
2.5 Reconfigurable Antenna Techniques.....	14
2.6 Reconfigurable Antenna Mechanisms	16
2.6.1 PIN Diodes.....	17
2.6.2 Basic Reconfigurable Antenna Topologies	21
2.6.3 Methods for Achieving Radiation Pattern Reconfigurability	21
2.7 Flexible, Wearable Reconfigurable Antennas and Applications.....	24
CHAPTER THREE	27
METHODOLOGY AND DESIGN	27
3.1 Introduction.....	27

3.2 A Compact Low Profile Unidirectional Antenna at 2.45 GHz for Body-Centric Communications	27
3.2.1 Introduction.....	27
3.2.2 Antenna Design.....	27
3.2.2.1 <i>Determination of the Resonant Frequency of the Antenna</i>	29
3.2.2.2 <i>Parametric Study</i>	31
3.2.3 Results and Discussions.....	32
3.2.4 Specific Absorption Rate (SAR) Simulation.....	34
3.2.5 Conclusion	35
3.3 A Compact Low-Profile Pattern-Reconfigurable Monopole Antenna for On-Body Communications	36
3.3.1 Introduction.....	36
3.3.2 Pattern-Reconfigurable Antenna Design	36
3.3.3 Antenna Reconfiguration and Principle of Operation	37
3.3.3.1 <i>DC Bias Circuit</i>	39
3.3.4 Results and Discussions.....	42
3.3.5 Radiation Patterns	42
3.3.6 Simulation of Specific Absorption Rate (SAR).....	42
3.3.7 Conclusion	44
3.4 A Flexible and Wearable Pattern-Reconfigurable Printed Monopole Antenna for On-Body Communications.....	44
3.4.1 Introduction.....	44
3.4.2 Flexible On-body Antenna Design	44
3.4.2.1 <i>Parametric Study</i>	46
3.4.3 Flexible Pattern-Reconfigurable Antenna Design and Operation	47
3.4.4 Radiation Patterns	49
3.4.5 Wearable Pattern-Reconfigurable Antenna Design and Operation	52
3.4.6 Radiation Patterns	54
3.4.7 Simulation of Specific Absorption Rate	55
CHAPTER FOUR.....	58
RESULTS AND DISCUSSIONS	58
4.1 Antenna Fabrication.....	58
4.2 Far Field Measurements.....	61

4.2.1 On-Body Measurements	61
4.2.2 Axial Ratio Bandwidth	62
CHAPTER FIVE	64
CONCLUSION AND FUTURE WORKS	64
5.1 Conclusion	64
5.2 Recommendation and Future Works	67
REFERENCES.....	68
APPENDIX A.....	73
APPENDIX B	75

LIST OF TABLES

Table 2.1 A summary of Available Technologies in Body-Centric Wireless Communications [10].....	10
Table 2. 2 Electromagnetic Properties of Human Body Tissue at 2.45 GHz [10].....	12
Table 2.3 Comparison of PIN diode, Transistor and MEMS Performance [52]	20
Table 3.1 Optimized Parameters of the Proposed Antenna	30
Table 3.2 Optimized Parameters of the Proposed Reconfigurable Antenna	37
Table 3.3 Operation Modes and Biasing Configuration of the Reconfigurable Antenna.....	38
Table 3.4 Optimized Parameters of the Proposed Flexible Reconfigurable Antenna	45
Table 3. 5 Simulated Maximum Spatial Average SAR Performance of the Proposed Flexible Reconfigurable Antenna	56
Table 5.1 Comparison of the Proposed Flexible Pattern-Reconfigurable Antenna with Previous Research Works	66
Table 5.2 Parameters Needed to Find Body Tissue Dielectric Constant and Conductivity at Any Frequency [10].	73

LIST OF FIGURES

Fig.1.1 Illustration of body-centric wireless communication [10].	2
Fig.1.2 Methods used in reconfigurable antennas [24].	3
Fig.2.1 Human body models (a) High resolution full biological voxel model (b) Three layer rectangular phantom (c) Three layer cylindrical phantom.	11
Fig.2.2 Monopole antenna on body phantom	13
Fig.2.3 Measured reflection coefficient of monopole antenna in proximity to human body phantom [10].	14
Fig.2.4 Reconfigurable antenna techniques (a) Electrical switching [43] (b) Mechanical tuning [43] (c) Optical switching [23] (d) Material change [44].	15
Fig.2.5 PIN Diode (a) Basic structure [50] (b) Equivalent forward bias circuit (c) Equivalent reverse bias circuit.	17
Fig.2.6 Single pole single throw switch (a) Series configuration (b) Shunt configuration	19
Fig.2.7 Beam-lead PIN diode (a) physical structure and dimension (b) typical isolation and insertion loss characteristics.	20
Fig.2.8 Basic planar reconfigurable antenna topologies [52] (a) component on main radiator element (b) component on stub (c) component on the feedline.	21
Fig.2.9 Methods of achieving unidirectional radiation pattern in printed microstrip antennas (a) Cavity-backed reflector (b) Full ground plane or Metallic reflector [67].	23
Fig.2.10 Application of wearable antennas.	25
Fig.3.1 Flow diagram of reconfigurable antenna design.	28
Fig.3.2 Topology and configuration of the proposed unidirectional antenna (a) Front view (b) Side view.	29
Fig.3.3 Combined simulated results of ANT_1 and ANT_2 (a) Radiation pattern. (b) Surface current distribution at 2.45 GHz (ANT_1—without side stub, ANT_2—with side stub).	30
Fig.3.4 Simulated S_{11} of the proposed antenna at different ground plane lengths.	31
Fig.3.5 Effects of stub position along y –axis on the reflection coefficient of the antenna.	32
Fig.3.6 Final simulated S_{11} of the proposed single side-stub planar monopole antenna.	33
Fig.3.7 Normalized radiation patterns of the proposed antenna in free space and on-body at 2.45 GHz (a) x - y plane (b) y - z plane.	33
Fig.3.8 Measured reflection coefficient in free space and at distance d from the body.	34
Fig.3.9 Simulated SAR performance of single side stub antenna (a) Antenna placed on head phantom (b) Antenna placed on hand phantom.	35

Fig.3.10 Design layout of low-profile, edge-stubbed pattern-reconfigurable antenna (a) Top view. (b) Side view.	36
Fig.3.11 (a) Design of the dual-stubbed pattern-reconfigurable monopole antenna (b) Equivalent PIN diode modelling of the side-stub as lumped <i>RLC</i> boundary.	37
Fig.3.12 Equivalent PIN diode circuit model simulation (a) Forward biased (b) Reverse biased.	38
Fig.3.13 Schematic diagram of DC bias circuit of the proposed pattern-reconfigurable antenna	40
Fig.3.14 Simulated <i>S</i> ₁₁ of the proposed antenna under varying operating conditions.	40
Fig.3.15 Normalized radiation patterns of the pattern-reconfigurable antenna at different frequencies (a) Mode-0 (b) Mode-1 (c) Mode-2.....	41
Fig.3.16 Simulated SAR performance of the proposed reconfigurable antenna at 2.45 GHz (a) Antenna placed on modeled head phantom (b) Antenna placed directly on a hand phantom.	43
Fig.3.17 Simulated radiation patterns of the reconfigurable antenna in free-space and on-body at 2.45 GHz (a) <i>x</i> – <i>y</i> plane (b) <i>y</i> – <i>z</i> plane.	43
Fig.3.18 Design configuration of the flexible pattern-reconfigurable antenna (a) Top layout (b) Side layout (c) Back view.	45
Fig.3.19 Effects of the width of the groundplane slot on the proposed flexible reconfigurable antenna.	46
Fig.3.20 Design of the flexible pattern-reconfigurable antenna; zoom in - Equivalent PIN diode modelling as a lumped <i>RLC</i> boundary.	47
Fig.3.21 Surface electric current distribution (a) Switch 1 (S1) ON (forward biased) (b) Switch 2 (S2) ON (forward biased) (c) Both Switch 1 (S1) and Switch 2 (S2) OFF (reverse biased).	47
Fig.3.22 Flexible antenna under various degrees of bending along <i>x</i> and <i>y</i> -axis (a) Outward bend at <i>R</i> = 45°, 90° (b) Inward bend at = 45°, 90°	48
Fig.3.23 Reflection coefficient (<i>S</i> ₁₁) of the flexible reconfigurable antenna in planar unbend (flat) and bend configurations.	49
Fig.3.24 Normalized radiation pattern modes of the of the proposed flexible reconfigurable antenna (a) S1 ON (b) S2 ON (c) S1 S2 OFF.....	50
Fig.3.25 Simulated radiation pattern of the flexible reconfigurable antenna in planar unbend (flat) and bend configurations.	51

Fig.3.26 Final reflection coefficient (S_{11}) of the flexible pattern-reconfigurable antenna.....	56
Fig.3.27 Rectangular and cylindrical three-layer phantom models.....	57
Fig.3.28 Antenna placement on body phantom.....	57
Fig.3.29 Simulated S_{11} of the flexible reconfigurable antenna in free space and on-body....	58
Fig.3.30 Normalized radiation pattern of the flexible reconfigurable antenna in free space and on-body at 2.45 GHz. (a) $x - y$ plane (b) $y - z$ plane.....	59
Fig.3.31 Specific absorption (SAR) rate performance of the flexible pattern-reconfigurable antenna at 2.45 GHz. (a) Directly on rectangular phantom (b) Directly on cylindrical phantom (c) Directly on hand phantom.....	60
Fig.3.32 Specific absorption (SAR) rate performance of the flexible pattern-reconfigurable antenna at 2.45 GHz on a Hugo voxel model (size = 2^3 mm^3).....	61
Fig.4.1 Fabricated prototype of the proposed pattern-reconfigurable antenna.....	62
Fig.4.2 Fabrication process of the flexible radiation pattern-reconfigurable antenna.....	63
Fig.4.3 Fujifilm Dimatix 3D materials printer (DMP-2850).....	63
Fig.4.4 Performance of the fabricated flexible pattern reconfigurable antenna on a stuffed animal body.....	64
Fig.4.5 Performance of the fabricated flexible pattern reconfigurable antenna on an adult human hand.....	65
Fig.4.6 3D gain plot of the proposed antenna on human voxel model (front and side view)..	66
Fig.4.7 Simulated axial ratio of the proposed flexible reconfigurable antenna.....	67
Fig.5.1 Electrical characteristics of tissues [8]: (a) relative permittivity; and (b) conductivity. Solid: muscle; dotted: fat.....	74
Fig.5.2 Design layout of the flexible reconfigurable antenna based on Rogers substrate (a) Flat (unbend, 0°) antenna (b) 45° and 90° bending.....	75
Fig.5.3 Simulated reflection coefficient (S_{11}) of the proposed flexible reconfigurable antenna without bending (flat, 0°).....	75
Fig.5.4 Simulated reflection coefficient (S_{11}) of the proposed flexible reconfigurable antenna at 90° based on Rogers substrate.....	76
Fig.5.5 Normalized radiation pattern of the proposed antenna without bending (flat, 0°).....	76
Fig.5.6 Normalized radiation pattern of the proposed antenna with bending at 45° (top) and 90° (down).....	77

CHAPTER ONE

INTRODUCTION

1.1 Background and Significance of Study

Antennas are well known to be indispensable components of every wireless communication system. The rapid advancement in modern wireless communication technology over the past decades has seen more functionality been integrated into even smaller electronic spaces. With the advent of 5G and the internet of things (IoT), small and electronically embedded wearable sensors for specialized applications are becoming increasingly popular. The wireless network of wearable computing devices placed around the body to provide communication is known as the wireless body area network (WBAN) [1]. In a WBAN, the antenna is a key component that establishes wireless communication in sensors, actuators, and IoT nodes on or off a human body. More specifically, on-body communication antennas are being used in telemedicine for patient vitals monitoring and diagnosis in the early detection and treatment of complicated diseases such as cancer and stroke. They are also widely used in military, emergency services, sports, and a plethora of personal communication gadgets including smartphones and watches. This presents unique requirements for such antennas to be unobtrusive while maintaining a low-profile and compact size with stable radiation patterns and impedance bandwidth. Additionally, these antennas must have flexible properties necessary for integration into conformal systems.

Furthermore, it is desired to dynamically adjust the antenna's radiation pattern [2]–[4], frequency of operation [5]–[7], and polarization [8], [9] in response to changing environmental conditions. To meet these requirements, multiple antennas are usually employed to achieve the design goal. However, this approach introduces undesirable features such as increased antenna size and cost, and possible electromagnetic interference. Thus, compact reconfigurable antennas have become a wide research area as a solution to introduce modifiable features in a conventional single antenna element or array that have fixed operational characteristics.

Body-centric wireless communication networks (BWCN) are essentially made up of three parts; on-body links describes the communication between devices that are mounted on the body while off-body networks represent links between on-body mounted devices and other terminals located in the surrounding environment of the body as shown in Fig.1.1 [10]. In-body links define the communication between implanted nodes and the on-body devices.

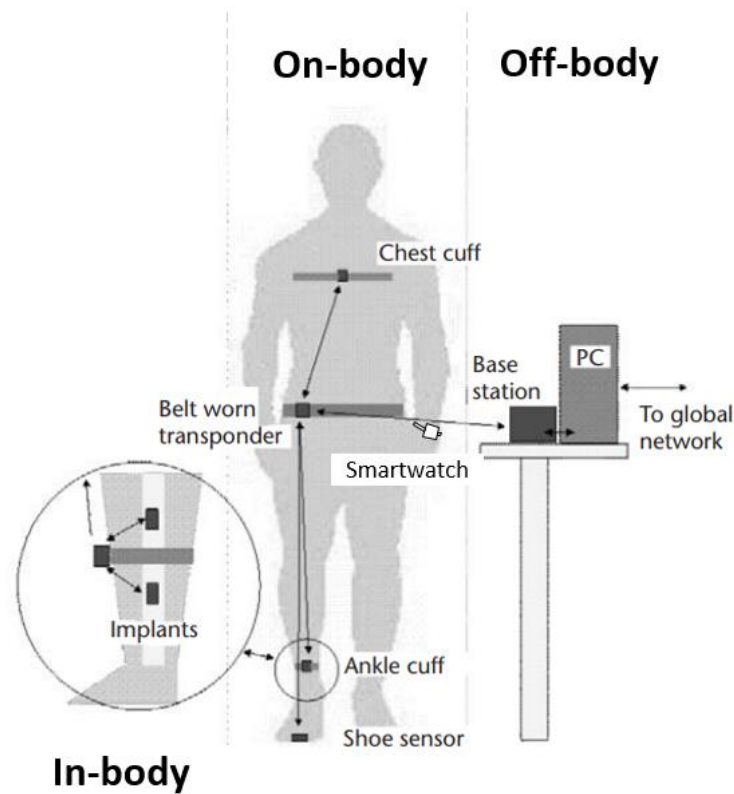


Fig.1.1 Illustration of body-centric wireless communication [10].

It is therefore highly desired for on-body antennas to be insensitive to detuning and impedance mismatch when mounted in close proximity to the body with a radiation pattern that minimizes the link loss [10], [11].

In many wireless applications, certain parameters of the radiating or receiving signal must be changed to meet specific outputs. Antenna reconfiguration has become an important feature in modern wireless communications such as MIMO systems, cognitive radio, 5G and satellite communication systems, IoT networks, and smartphones [12]. In its basic form, reconfigurability suggests the ability of a system to dynamically modify its performance characteristics [13]. The IEEE standards definitions of terms for antennas define reconfigurable antenna (RA) as an antenna capable of changing its performance characteristics (resonant frequency, radiation pattern, polarization, etc.) by mechanically or electrically changing its architecture [14]. In this way, a reconfigurable antenna can dynamically steer a far-field radiation pattern in a desirable fashion, shift the resonant frequency within a band, or switch between linear and circularly polarized modes. Hence, the basic goal of a reconfigurable antenna is to achieve more functionality with a single antenna element or array. It is noteworthy that single or array antenna elements fed by complex isolated programmable phase shift

systems to achieve beamforming are not classified as reconfigurable antennas since the fundamental functioning property of the antenna element is not altered, hence, out of the scope of this work.

Based on functionality, reconfigurable antennas can be classified into frequency reconfigurable, radiation pattern reconfigurable, and polarization reconfigurable antennas. A fourth category combines frequency, radiation pattern, and polarization mechanisms on a single antenna system known as compound reconfigurable antennas [13]. These antennas can radiate multiple patterns at different frequencies and polarizations. Generally, reconfigurable antennas can be realized by the use of multiple excitation points to generate differential operational modes or by incorporating active devices for structural changes in the antenna. The switching of the functional properties of a planar antenna can be mainly achieved via electrical or physical means. The electrical mechanism popularly involves the use of RF-MEMS, PIN diodes and, varactor diodes for switching [15]–[18]. Physical means of antenna reconfiguration introduces mechanical alterations in the radiating structures of some planar and non-planar antennas [19], [20]. Other forms of switching techniques involve the change in properties of materials such as ferrites, liquid crystals, and metasurfaces as depicted in Fig.1.2 [21]–[23]. Photoconductive devices have also been recently introduced for optical switching. This thesis will focus on the electronic reconfiguration method by using RF PIN diodes which possess advantages of low loss and reactive loading effect, high switching speed, compact size, good reliability, and automatic tuning over the mechanical and other switching techniques. The major goal in designing reconfigurable antennas is to ensure that the variation in one property of the antenna does not affect the others. To this end, a pattern-reconfigurable antenna must not cause a shift in frequency or polarization of the antenna. However, due to the linkage property of antennas as circuits and radiators, it has become a

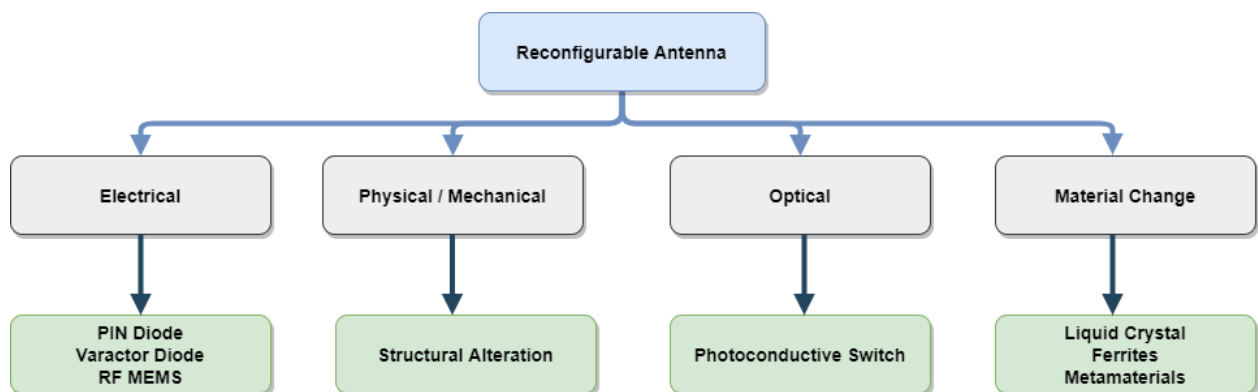


Fig.1.2 Methods used in reconfigurable antennas [24]

challenge in realizing a truly independent reconfigurable antenna whose characteristics are mutually exclusive of each other [13].

In this work, the printed monopole is selected as the antenna type based on microstrip technology due to its advantages of lightweight, broadband, low fabrication cost, and ease of integration in MMIC systems. Nonetheless, these antenna types are generally linearly polarized with an omnidirectional radiation pattern. When the antenna is operated close to or on the body with random deformation, it can result in severe polarization mismatch, unstable radiation pattern, varying impedance bandwidth, and high SAR levels primarily due to the lossy nature of the body. Several complex techniques have been introduced in literature to achieve pattern reconfiguration with low SAR levels in printed monopole antennas.

This thesis presents the design approach and analysis of a printed low-profile pattern-reconfigurable monopole antenna for on-body applications in five chapters. The introduction and literature review covers the first two chapters while chapter three explains the design procedure and development of the pattern reconfigurable antenna. In this chapter, circular polarization (CP) and conformable features are introduced in the antenna. A detailed summary of the final simulation and measurement results is presented in chapter four followed by the main conclusion, challenges, and future works in resolving them.

1.2 Problem Statement

Body-mounted (wearable) electronic devices have become increasingly popular in wireless sensor applications mainly for communication and medical purposes [25]. From smart watches and medical fit bits to industrial wearable gadgets, the antenna is a key component that establishes wireless communication in these devices. Some of the popular antennas used in these applications include the printed monopole antenna, planar inverted-F antennas (PIFA) and the printed loop antennas. Common among these antennas is their omnidirectional radiation pattern which is desired to provide all-round signal coverage for on-body communication. However, it is known that when the antenna is operated close to or directly on the body, about 40-50% of the radiated energy is absorbed. This is due to the conductive nature of the body which distorts the omnidirectional pattern and effectively makes the antenna unidirectional. This effect is also seen in the increased specific absorption rate (SAR) levels of the antenna beyond the acceptable limit. Popular techniques in the literature employ high impedance reflector surfaces, large or full ground planes, and other complex cavity-backed

structures to reduce SAR [26]–[28]. However, these approaches generally lead to large and bulky antenna size and increased fabrication cost.

Moreover, the increasing trend of miniaturization and computing power demands the RF front-end to be compact and adaptive. This means less space for hardware implementation in these wearable and IoT devices. Additionally, traditional antenna characteristics are fixed i.e. fixed radiation pattern, frequency and polarization. In this way, multiple antennas are required to serve different purposes in the system. This solution approach is employed in current smart mobile devices where separate antennas are used for GPS, near field communication (NFC), Bluetooth, WIFI/WLAN, and cellular 2G/3G/4G/5G communications. This is known as antenna diversity. As these devices become increasingly smaller, it has become more arduous to pack several antennas in space stringent applications without mutual coupling. Reconfigurable antenna provides a low cost solution approach compared to multi-antenna systems with the ability to switch radiation pattern, frequency and polarization. In particular, pattern-reconfigurable antennas are capable of transmitting or receiving signals from a desired point in space in order to increase signal coverage and avoid interference while reducing the amount of power required in transmission. However, these fundamental properties of the antenna are interlinked with each other in such a way that a change in one property causes a change in the others. This is known as antenna characteristic linkage [29]. Several techniques available in the literature involve complex reconfigurable designs with complicated biasing circuits that do not provide effective decoupling [30], [31]. Hence, compact reconfigurable antennas with isolated characteristic properties are highly desired.

1.3 Research Objectives

1.3.1 General Objective

The general aim of this research is to develop and analyze a compact, low-profile and low-cost reconfigurable printed monopole antenna for WLAN (2.45 GHz) body-centric wireless communication systems.

1.3.2 Specific Objectives

1. Design a simple antenna model in Ansys commercial full-wave electromagnetic solver; High Frequency Structure Simulator (HFSS) that converts the conventional omnidirectional radiation pattern of the basic antenna into a directional pattern by the use of a simple stub technique.

2. Introduce reconfigurable features into the designed antenna by incorporating a fewer number of PIN diodes.
3. Introduce flexible features in the reconfigured antenna.
4. Achieve low specific absorption rate (SAR) levels without the use of conventional complex and bulky cavity-backed structures.
5. Achieve stable radiation pattern and impedance bandwidth with decoupled antenna characteristic linkage property under various degrees of body deformations and bending.

1.4 Motivation

The advancement in miniaturization techniques and computation power has motivated the need for more compact and adaptive electronic components. Wearable devices have seen tremendous growth over the years with wide applications in remote health care, industrial apparatus, defense gear, personal communication and sports fit bits. The antenna plays a key role in establishing wireless communication in these devices. A common type of antenna used in these devices is the printed monopole antenna (PMA). It is known that the omnidirectional radiation from these antennas can be severely degraded when mounted close to or directly on the body. The absorption of the radiated energy by the body does not only increase specific absorption rate (SAR) levels but also effectively renders these antennas directional. Hence, this work proposes a simple technique to convert the omnidirectional pattern of a PMA into unidirectional radiation. Meanwhile, the achieved radiation pattern is reconfigured to switch between multiple directional patterns and an omnidirectional radiation in specific operating modes to increase capacity. This realizes functional agility in the antenna that would have otherwise been fixed and also eliminates the need for multiple antennas in these devices. However, the characteristic linkage of the antenna properties presents a unique challenge in achieving a truly reconfigurable antenna. Parts of this work seeks to address this problem. Moreover, the on-body implementation of the antenna requires it to be flexible and conformable to the human body. This work explores the human body loading effects on the antenna which are experimentally characterized to validate numerical results. Other key contributions of this work include the realization of a compact antenna size and circular polarization to maintain the communication link in multipath scenarios. Generally, a flexible and wearable pattern-reconfigurable printed monopole antenna with no cavity-backed structures for on-body applications is insufficiently reported in the literature.

1.5 Research Contributions

The outcome of this thesis provides the following contributions:

1. A simple yet compact printed pattern reconfigurable monopole antenna for 2.45 GHz WLAN and on-body applications. The proposed antenna employs a simple fork-shaped monopole printed on flexible substrates with a fewer number of PIN diodes for switching. The designed antenna is characterized in both flat and curved cylindrical orientations for conformability. It also seeks to serve as a model for designing low-profile functional reconfigurable antennas without the use of complex cavity structures and feeding methods.
2. Conversion of omnidirectional radiation into a directional pattern by the use of a simple stub and a defected ground plane structure (DGS). The same technique is also able to convert linear polarization into circular polarization in the singly fed monopole antenna.
3. Decoupling of frequency-radiation pattern characteristic linkage to present independent antenna property reconfiguration.
4. Realization of low SAR levels without the use of complex cavity-backed reflector structures that normally leads to bulky antenna size.

CHAPTER TWO

LITERATURE REVIEW

2.1 Introduction

The critical role of antennas in establishing wireless communication has made their design and characterization equally important for wireless systems. An antenna that can dynamically change its fundamental operating conditions based on demand has superior advantages over its fixed counterpart. In this chapter, the basic concept of antenna reconfigurability and the various techniques in its realization are discussed. An introduction of the printed planar monopole antenna and its parameters are presented. Since the electrical type is chosen as the reconfigurable method in this work, the switching technique using RF PIN diodes is explained together with the biasing circuit. Further details on conformable antennas based on flexible substrates and their fabrication processes are also provided. Meanwhile, some reviewed techniques in reducing SAR levels in on-body antennas are also reported.

2.2 Body-Centric Wireless Communication Networks

The continued miniaturization of electronic devices has seen a high proliferation of a wide range of portable devices that can be carried by the user or worn on the body. This has particularly found a growing interest in specialized areas such as defense, emergency services, and health care. To support a variety of real-time health monitoring and consumer electronics applications, the IEEE 802.15.6 international standard for wireless body area networks (WBANs) has been developed for low power, short-range and extremely reliable wireless communication within the surrounding area of the human body at high data rates [32]. In addition to the quality of services, the standard also provides strict compliance to the specific absorption rate of the antennas used. Wireless body area networks (WBANs), wireless sensor networks (WSNs), and wireless personal area networks together with their associated concepts can be essentially described in body-centric wireless communication networks (BWCNs) which is mainly divided into three parts based on the placement of the wireless sensor node as shown in Fig.1.1 under chapter 1.

- **On-body:** The communication between nodes located on the body surface is termed on-body. Most of the channel is on the surface of the body and both transceivers are on the body.
- **Off-body:** The communication between nodes on the body and a base station located in the surrounding environment of the body. Most of the channel is off the body and in the surrounding space with one antenna on the body.

- **In-body:** Describes the communication between implanted transceivers and the on-body units. Here, the majority of the channel is inside the body [10].

The existing industrial scientific and medical (ISM) band together with other approved bands has been allocated for BWC by the FCC (IEEE 802.15.6) and is detailed in Table 2.1. A plethora of applications in modern wireless communications has driven the need for wireless body area antennas in telemedicine for the remote monitoring and wellness management of patients, radiofrequency identification (RFID), military, emergency services, sports, and other personal communication gadgets such as smartwatches and handheld mobile devices. The focus of this work is in the on-body communication domain at the 2.45 GHz ISM band due to the numerous advantages it offers in data rate and coverage. Generally, one of the key requirements of on-body antennas is to maintain an omnidirectional radiation pattern to provide full-body coverage. However, about 40-50% of radiated energy is absorbed or attenuated by the human body which effectively renders it a directional antenna [33]–[35]. This is as a result of the highly conductive human body tissue that couples the antenna’s radiation. As a result, the antenna’s radiation efficiency is severely affected which ultimately increases the specific absorption rate (SAR) of the antenna. Other crucial factors demand the antenna to be mechanically robust, compact, flexible, and lightweight while maintaining a low profile with good impedance bandwidth and stable radiation patterns. Meanwhile, the human body is an uninviting environment for electromagnetic waves primarily due to the highly conductive nature of the individual tissues of the human body. Additionally, different forms of the positioning of the human body present a complex multipath scenario and highly complicated propagation channel for surface waves. These channel properties are not fully characterized by experimental means and therefore numerical modeling techniques are employed.

2.3 Characterization of Human Body Models for Body-centric Wireless Communication

In on-body communication, most of the propagation channel is known to exist on the surface of the body which creates an interaction between electromagnetic waves from the antenna and the human body. The channel performance is largely affected by the body tissue properties which depend on the type of tissue at the design frequency. At microwave frequencies, there is high variation in the individual tissue properties. This action of dielectric materials has been examined widely in literature using the head, hand, torso, and whole human body phantom models by authors in [36]–[39].

Table 2.1 A summary of Available Technologies in Body-Centric Wireless Communications

[10]

Standard	Frequencies (MHz)	Data Rate	Max. Power	Range (m)
UHF/VHF	~10	Very low	Very low	<=0.5
Medical Implant Communications Service (MICS)	402-405	Low	Low	<=2
Wireless Medical Telemetry Services (WMTS)	420-429 440-449 (Japan) 608-614 1395-1400 1427-1429.5 (USA)	Low	Low	~10
BodyLAN	900	32 kb/s	0 dBm	2-10
Bluetooth	2400-2480	1 Mb/s	0 dBm	0.1-10
Zigbee	2400 915 868	250 kb/s 40 kb/s 20 kb/s	Low	1-100
WLAN	2400, 5200	10-50 Mb/s	0 dBm	30-50
UWB	3100-10600	1 Gb/s	-41 dBm/MHz	10

One of the comprehensive studies carried out by authors in [39] to determine the relative permittivity (ϵ_r) of tissues over a range of frequencies from 10 MHz to 100 GHz as a function of angular frequency (ω) is based on the well-known Cole-Cole model. This generally describes the relaxation of dielectric materials [40], given by the expression:

$$\epsilon_r(\omega) = \epsilon_\infty + \frac{\Delta\epsilon}{1 + (j\omega\tau)^{(1-\alpha)}} \quad (1)$$

Where ϵ_∞ is the material's relative permittivity at terahertz frequency ($\omega\tau \gg 1$), τ and α are dispersion broadening parameters for each relaxation region. The magnitude of dispersion is given by $\Delta\epsilon = \epsilon_s - \epsilon_\infty$, where ϵ_s is the permittivity of the material at low frequency ($\omega\tau \ll 1$).

To appropriately describe the spectrum of a tissue, a conductivity term made up of the ionic conductivity (σ_i) and the free space permittivity (ϵ_o) is added to (1). Hence, the multiple Cole-Cole model is given as:

$$\epsilon_r(\omega) = \epsilon_\infty + \sum_n \left(\frac{\Delta\epsilon_n}{1 + (j\omega\tau_n)^{(1-\alpha_n)}} \right) + \frac{\sigma_i}{j\omega\epsilon_o} \quad (2)$$

The properties of selected tissues at 2.45 GHz as shown in Table 2.2 are therefore predicted using the 4- Cole-Cole model whose input parameters can be found in appendix A.

To achieve an efficient on-body antenna design in terms of its lightweight, minimum power consumption, stable radiation, and impedance bandwidth, it is important to understand the properties of different human body models and their operating frequencies. By this, simple numerical models to simulate tissues like the skin, muscle, and bone are designed while a realistic full human body voxel model that simulates complex organs and tissues are also considered as shown in Fig.2.1. The simple layered shapes i.e. rectangular and cylindrical (Fig.2.1 b and c) are homogenous phantoms that are used to evaluate the characteristics of radiated energy from EM sources. However, to fully characterize the on-body antenna, it is necessary to use high-resolution phantoms that simulate realistic human body conditions. Although the voxel models present a greater degree of tissues, they demand very high computer resources as compared to the simple phantoms that are practical but require less computer resource in simulation. Hence, the simple layered phantom model together with the human voxel model is adopted in this work.

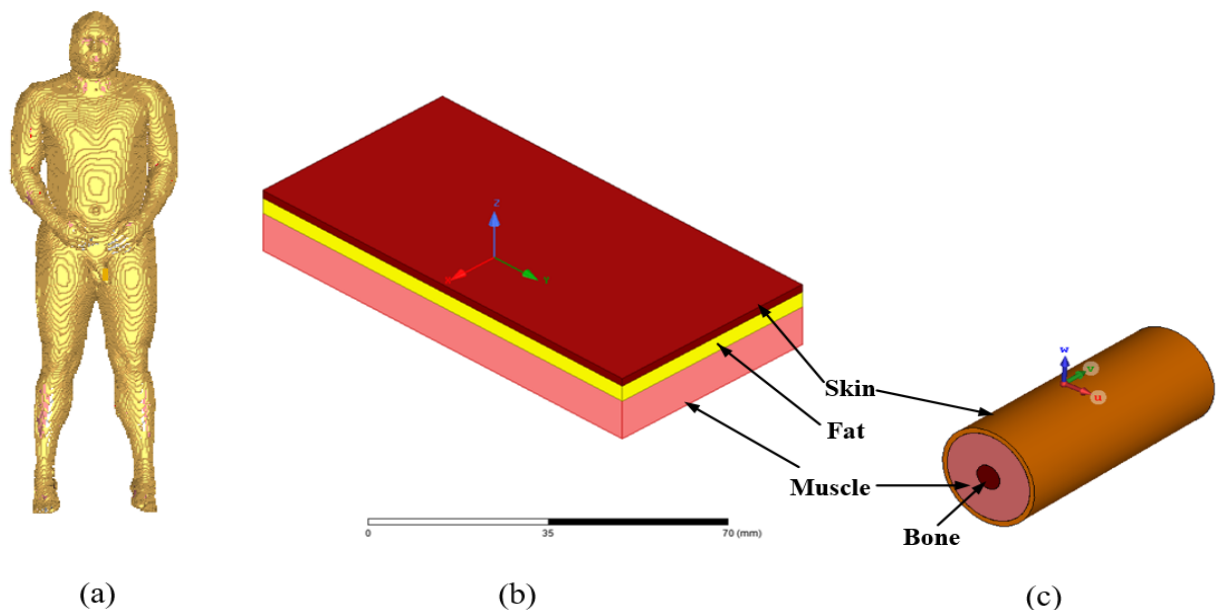


Fig.2.1 Human body models (a) High resolution full biological voxel model (b) Three layer rectangular phantom (c) Three layer cylindrical phantom.

Table 2. 2 Electromagnetic Properties of Human Body Tissue at 2.45 GHz [10]

<i>Tissue Name</i>	<i>Conductivity [S/m]</i>	<i>Relative Permittivity</i>	<i>Loss Tangent</i>	<i>Penetration Depth [m]</i>
Aorta	1.467	42.47	0.24837	0.023761
Bladder	0.69816	17.975	0.27927	0.032545
Blood	2.5878	58.181	0.31981	0.015842
Bone (Cancellous)	0.82286	18.491	0.31996	0.028087
Bone (Cortical)	0.40411	11.352	0.25597	0.044616
Brain (Gray Matter)	1.843	48.83	0.27137	0.02031
Breast Fat	0.14067	5.137	0.1969	0.085942
Cartilage	1.7949	38.663	0.3338	0.018638
Cerebro Spinal Fluid	3.5041	66.168	0.38078	0.012537
Cornea	2.3325	51.533	0.32544	0.016548
Eye Sclera	2.0702	52.558	0.28321	0.018773
Fat	0.10672	5.2749	0.14547	0.11455
Gall Bladder Bile	2.8447	68.305	0.29945	0.015592
Heart	2.2968	54.711	0.30185	0.017286
Kidney	2.4694	52.63	0.33736	0.015811
Liver	1.7198	42.952	0.2879	0.020434
Lung (Inflated)	0.81828	20.444	0.28779	0.02963
Muscle	1.773	52.668	0.24205	0.021886
Skin (Dry)	1.4876	37.952	0.28184	0.022198
Skin (Wet)	23.984	20.369	0.84665	0.0010736
Small Intestine	3.2132	54.324	0.42529	0.012438
Stomach	2.2546	62.078	0.26114	0.018707
Testis	2.2084	57.472	0.27628	0.018394
Tongue	1.8396	52.558	0.25167	0.021083

2.4 Planar/Printed Monopole Antenna for On-body Communications

The choice of antenna type for on-body wireless communication is strongly influenced by several factors due to the unique propagation characteristics presented by the human body that

is different from the conventional free space channel. Generally, BWC propagation modes can be categorized into three main domains based on the nature of the radiated energy;

- i. Surface or creeping wave: propagates along the surface of the body i.e. on-body communication.
- ii. Space wave: propagates away from the body, i.e. off-body communication.
- iii. Penetrating wave: propagates into the body, i.e. in-body communication.

To demonstrate the excitation of creeping waves, a conventional non-planar monopole antenna of height $h = \lambda/4$ on an infinite ground plane and located at a distance, d from the body is depicted in Fig.2.2. The near field radiations from the antenna when it is vertically oriented are shown to propagate well along the surface of the body while the horizontal orientation does not. Although the omnidirectional patterns of the monopole and loop antennas are generally desired, it is important to screen the antenna from the body to prevent the losses in the tissue from degrading the efficiency of the antenna. This can be achieved by using larger ground planes than are possible in miniaturized equipment [10]. The proximity of the body strongly affects the antenna which can cause frequency detuning and impedance mismatch leading to poor efficiency. Fig.2.3 depicts the shift in frequency with a deteriorating return loss as the distance between the phantom and antenna decreases to $d = 0$ mm. In free space, the efficiency of the antenna is around 90%. When the antenna is directly mounted on the phantom model, the measured efficiency is about 40-50%. Moreover, the on-body antenna must have a compact size with desired radiation characteristics while maintaining a low profile and altogether being lightweight. Furthermore, to analyze the antenna's conformability to the body, different random body postures must be accounted for. These highly random body postures can significantly prevent communication.

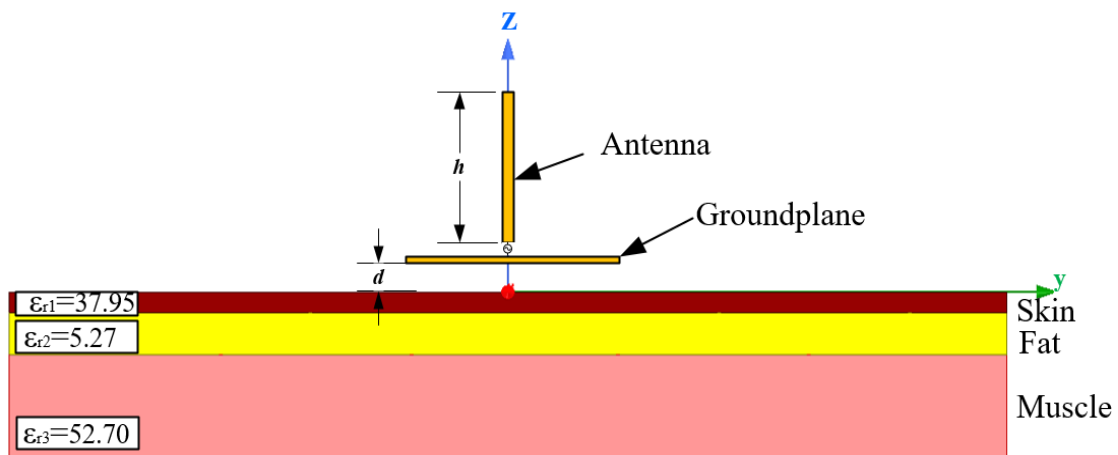


Fig.2.2 Monopole antenna on body phantom

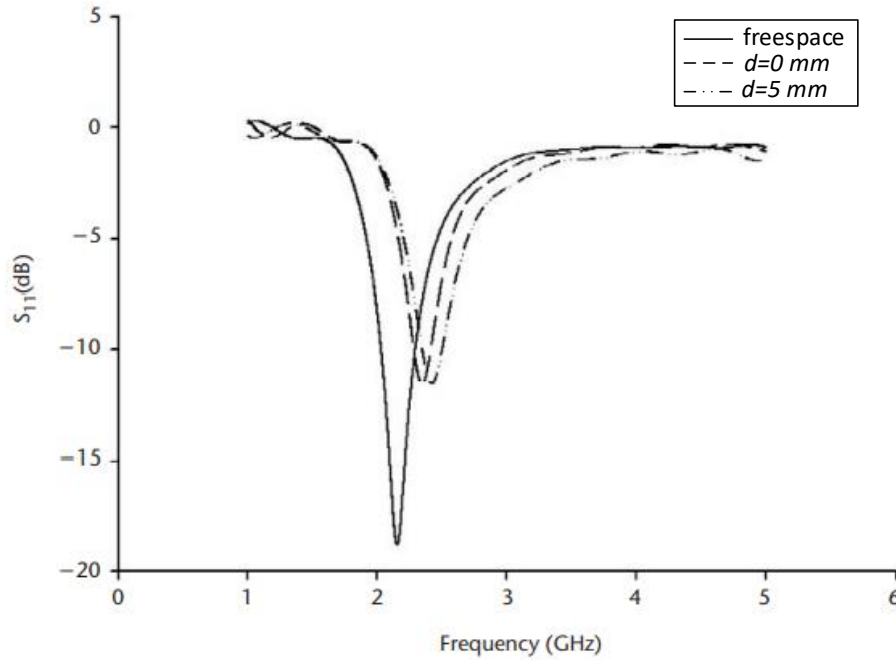


Fig.2.3 Measured reflection coefficient of monopole antenna in proximity to human body phantom [10].

2.5 Reconfigurable Antenna Techniques

Since the introduction of the reconfigurable antenna concept in the early 1930s with its practical demonstration almost seven decades later [29], major developments of the concept have been witnessed in both industry and academia primarily for military and space applications [24]. Over the last decades, reconfigurable antennas have gained wide traction in health, emergency services, and emerging fields such as cognitive radio [41]. The primary goal of reconfigurable antennas is to control the distribution of electric and magnetic currents on the antenna via structural adjustments of the radiating elements [13]. This dynamically enables the modification of the fundamental properties of the antenna. It is worthy of note that the reconfiguration technique is implemented directly on the antenna and does not suggest that the antenna is ‘smart’ which is a case of an isolated programmable feature outside the antenna. The main antenna reconfigurable types are functionally based on the frequency, radiation pattern, and polarization. In other cases, a combination of either or all the reconfigurable types is termed as a compound reconfigurable antenna [42]. The following sections describe the various topologies and techniques used in achieving reconfigurable features in planar antennas. Generally, four main techniques are employed in switching the base properties of the antenna as represented in Fig.2.4.

- i. **Electrical mechanism:** This involves the use of popular RF switches such as PIN diodes, field-effect transistors (FETs), varactor diodes, and RF MEMS in tuning the parameter of interest.
- ii. **Physical/mechanical mechanism:** Tuning of antenna parameter is done by manually altering the structure of the antenna to vary the equivalent inductance and capacitance of the antenna.
- iii. **Optical mechanism:** The use of photoconductive (silicon) switches that are activated or deactivated by illumination to cause parameter switching effect.
- iv. **Material change mechanism:** The molecular structure of materials like liquid crystals, ferrites and metamaterials can be changed by electric or magnetic field excitation which causes it to act as a switch.

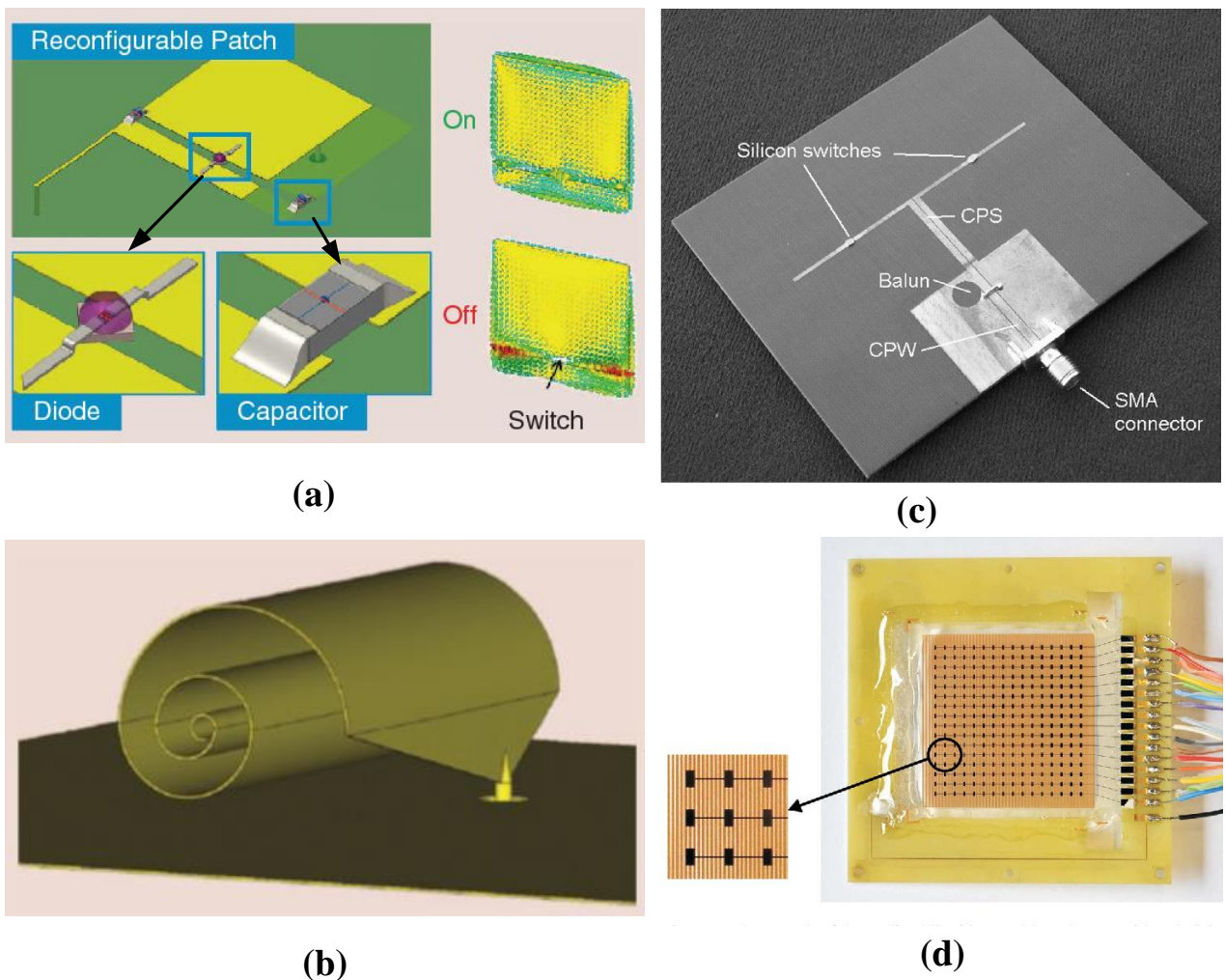


Fig.2.4 Reconfigurable antenna techniques (a) Electrical switching [43] (b) Mechanical tuning [43] (c) Optical switching [23] (d) Material change [44].

2.6 Reconfigurable Antenna Mechanisms

Antenna reconfiguration mechanisms can generally be summarized into four main groups based on functionality;

1. Frequency response reconfigurability
2. Radiation pattern reconfigurability
3. Polarization reconfigurability
4. Combination of frequency, radiation pattern, and polarization.

Various methods discussed in chapter 1 (Fig.1.2) can be used in achieving the different types of reconfigurable features in antennas. This work focuses on the radiation pattern reconfiguration method on a printed monopole antenna for on-body applications. As part of efforts, many pattern-reconfigurable planar monopole antennas have been recently developed for both narrowband and wideband applications. Switchable loaded-parasitic elements based on RF PIN diodes are proposed in [3], [45], [46]. In these works, broadband radiation was achieved over a wideband by switching passive antenna elements at different angles to serve as reflectors in directing the main beam. In [3], the arc-shaped reflectors and the circular patch were open-circuited which required more PIN diodes in performing the switching together with multiple bias points. The reconfigured patterns in [55] were realized on separate antennas which resulted in three different antennas for each pattern reconfigured. Eight radially symmetrically distributed microstrip monopoles were employed in [56] to achieve pattern reconfiguration in a wide band. The design equally employs up to eight diodes in switching each monopole element at a time while the others are turned off and act as reflectors to direct the beam. Generally, it is observed in these antennas that, varying resonant frequencies occur as the radiation pattern is being tuned. This is primarily due to the concept of coupled frequency-radiation characteristic linkage that causes frequency shifts at varying radiation patterns and vice versa. This shift in frequency leads to antenna detuning that can cause it not to radiate at the design frequency together with other detuning effects studied in [47], [48]. Meanwhile, the electronic switching technique involving PIN diodes is used in this work to realize a pattern reconfigurable feature on a flexible printed monopole antenna. This section introduces the basic concept in the operation of PIN diodes and explores previous works in the design of reconfigurable antennas using PIN diodes.

2.6.1 PIN Diodes

A switch is governed by ON and OFF states with an infinite impedance in the OFF state and a null impedance when ON [49]. When operated at high frequencies, additional parameters in the form of inductance, capacitance, and resistance begins to appear and the equivalent circuit model of the switch becomes complicated. These must be taken into account to ensure optimum performance. The integrable switches considered for RA design mainly include the PIN diode, field-effect transistor (FET), and microelectromechanical switches (MEMS).

A PIN diode is a current-controlled device that can operate as a variable resistor at RF and microwave frequencies. It is formed from semiconductors made up of a highly positively doped (P) layer, an undoped intrinsic (I) layer and a highly negatively doped (N) layer as shown in Fig.2.5 (a) [50].

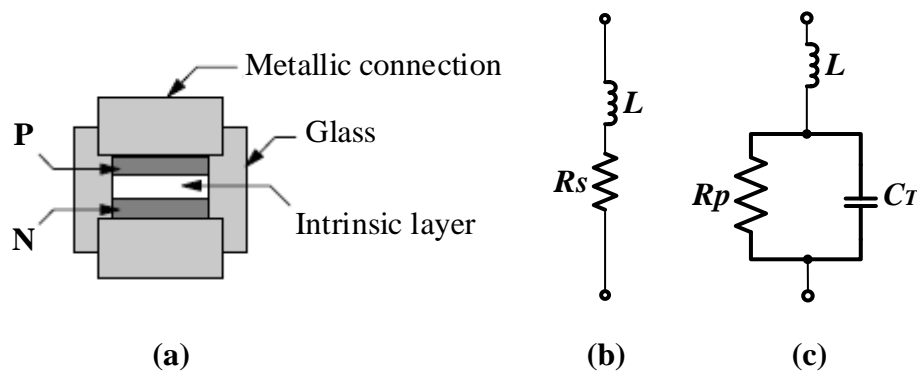


Fig.2.5 PIN Diode (a) Basic structure [50] (b) Equivalent forward bias circuit (c) Equivalent reverse bias circuit.

The PIN diode is a semiconductor device widely used in microwave circuits to produce variable attenuators, modulators, and commutators. This is mainly due to their low series resistance (R_s) and total capacitance (C_T). The PIN diode also has high switching speeds in nano-seconds with high voltage and power handling capabilities. The PIN diode conducts current in one direction only and therefore determines the ON and OFF states respectively. When the diode is forward biased (ON state) the equivalent circuit is a combination of parasitic inductance L and a series resistance R_s as shown in Fig.2.5 (b). When a reverse-biased voltage is applied, there is no stored charge in the I-region, and the diode is known to operate in the OFF state with the equivalent circuit model containing a very large parallel resistance (R_p) in the order of $k\Omega$ in shunt with a capacitor as shown in Fig.2.5 (c). Other semiconductor switching devices like the metal-semiconductor-field effect transistor (MESFET) and MEMS are also widely used in embedded applications [51]. Several of key parameters affect the performance of PIN diodes.

The insertion loss represents the transmission loss through the PIN diode when it is forward-biased. In the ON state, microwave and bias currents flow through the switch causing Ohmic losses. This is critical in reducing the system's noise figure, hence, a relatively low insertion loss value ($I_L < 0.25 \text{ dB}$) is mostly desired. However, when the switch is turned off, the isolation measures the leakage of current through the switch due to inherent transmission losses. This is determined by calculating the difference between the power measured at the switch output port in the ON state and the power measured at the switch output port in the OFF state.

$$I_{so}(\text{dB}) = (P_{out})_{ON} - (P_{out})_{OFF} \quad (3)$$

$$FOM = \frac{1}{(2\pi \times C_{OFF} R_{ON})} \quad (4)$$

Among other performance parameters of diodes, the figure of merit (FOM) is denoted as in (4) and is used to rate the achievable bandwidth of the diode. Due to a lower OFF state capacitance (C_{OFF}) for a given ON resistance (R_{ON}), PIN diodes generally have a high operating frequency advantage with the maximum operating frequency component reaching up to 180 GHz, while it is about 26 GHz for a MESFET. The switch is normally operated in a configuration based on the switching need and condition of the circuit. The typical series and shunt single pole single throw (SPST) switch configurations are shown in Fig.2.6 with the biasing network to provide the appropriate current and voltage conditions for the ON and OFF states of the diode. The anode of the diode is connected in a configuration for positive biasing with blocking capacitors C1 and C2 to prevent the leakage of high RF current into the diode as shown in Fig.2.6 (a, b). In the same manner, the RF choke (L) is used to direct any RF signal to the ground through the capacitor C3 and in the end, allow only the DC current in biasing the diode. In the series SPST configuration, the maximum obtainable isolation (I_{so}) and insertion loss (I_L) depends on the capacitance (C_T) and series resistance (R_s) of the diode in the reverse and forward conditions respectively. This can be describe by the following equations:

$$I_{so} = 10 \log \left[1 + \frac{1}{(4\pi f C_T Z_o)^2} \right] \text{ dB} \quad (5)$$

$$I_L = 20 \log \left(1 + \frac{R_s}{2Z_o} \right) \text{ dB} \quad (6)$$

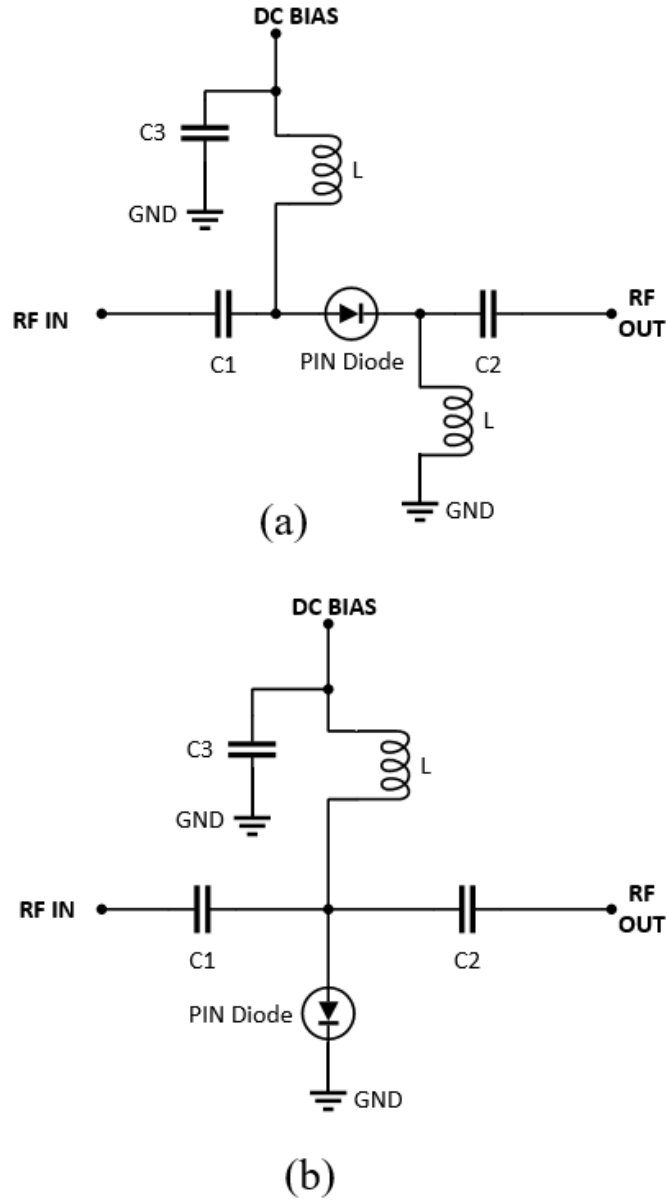


Fig 2.6 Single pole single throw switch (a) Series configuration (b) Shunt configuration

Where f is the operating frequency of the diode at a matched characteristic impedance $Z_o = 50 \Omega$. In the shunt SPST switch, high isolation over a broadband frequency range with a low insertion loss is achieved due to no switching element connected in series with the transmission element. In contrast to the series SPST, the I_{so} is a function of R_s and the I_L depends on the C_T in the design equations below:

$$I_L = 10 \log[1 + (\pi f C_T Z_o)^2] \text{ dB} \quad (7)$$

$$I_{so} = 20 \log\left(1 + \frac{Z_o}{2R_s}\right) \text{ dB} \quad (8)$$

Table 2.3 Comparison of PIN diode, Transistor and MEMS Performance [52]

	PIN diode (silicon)	MESFET	PHEMT	MEMS
Typical R_{ON} (Ω)	1.7	1.5	1.2	0.5
Typical C_{OFF}	0.05pF	0.4pF/mm	0.32pF/mm	
Insertion loss (dB)	0.5	0.5	1	0.25
Isolation (dB min)	30	30	40	40
Figure of Merit (GHz)	1872	265	414	208
Breakdown Voltage	50	15	8	$\sim 44/\mu V$
Low limit frequency	10MHz	DC	DC	12 KHz
Biassing constraints	5-10mA ON 0-30 V OFF	0 V ON -5 V OFF	+0.5 V ON -5 V OFF	20-200 V (Actuation voltage)

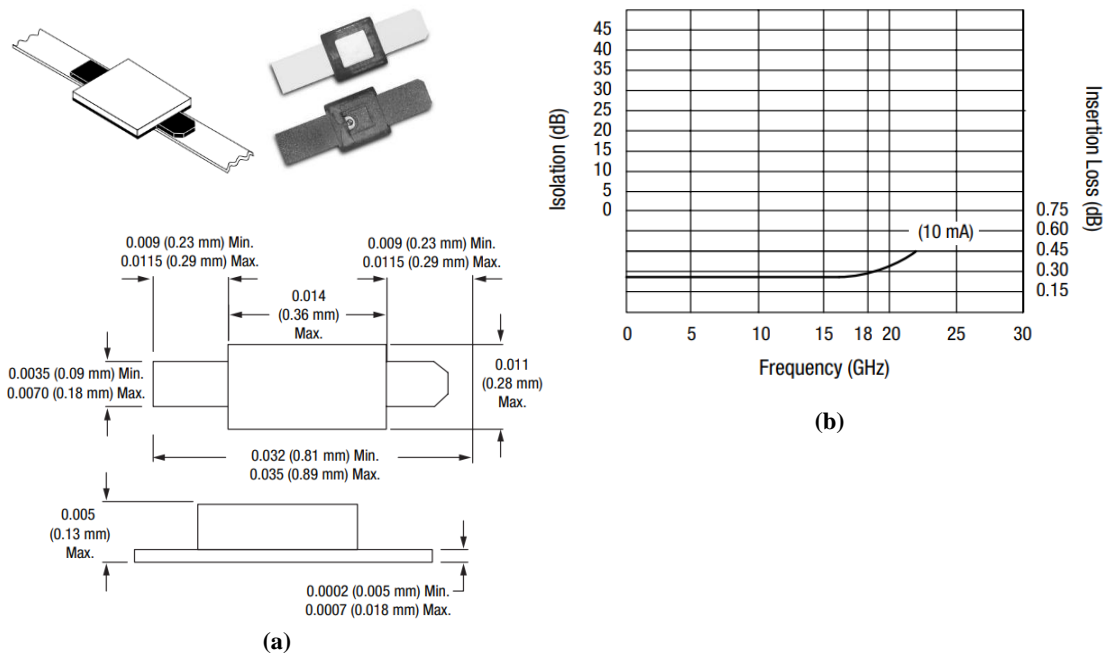


Fig.2.7 Beam-lead PIN diode (a) physical structure and dimension (b) typical isolation and insertion loss characteristics.

A summary of the performance characteristics of PIN diodes compared with other switching devices is shown in Table 2.3 [52]. Commercial RF switches are generally packaged in bulky cases but the beam-lead technology is commonly used to realize smaller diodes that are easily integrated into antennas. The typical performance of the DSM8100-000 PIN diode is shown in Fig.2.7.

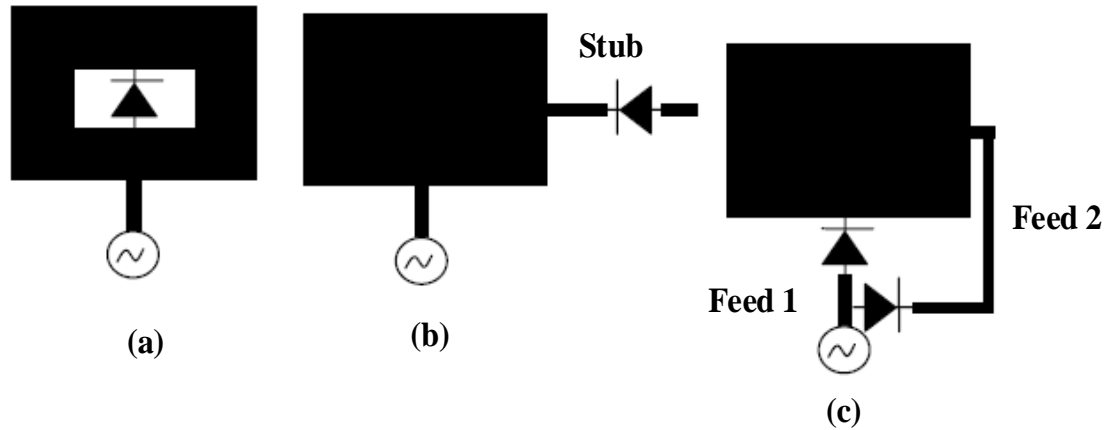


Fig.2.8 Basic planar reconfigurable antenna topologies [52] (a) component on main radiator element (b) component on stub (c) component on the feedline.

2.6.2 Basic Reconfigurable Antenna Topologies

The method of incorporating active components on planar antennas can generally be classified into three main categories;

- The first method involves the integration of the active device into the main surface area of the radiator element.
- Embedding the active device into the connected stub of the antenna.
- Incorporating the component into the feedline of the antenna.

Figs.2.8 (a) - (c) depicts the basic RA topologies where more compact structures are achieved with the first topology type but coupling effects from the non-ideal behavior of the active device when switched on or off may significantly reduce the efficiency and cause an undesirable shift in the resonant frequency of the antenna. The second topology type presents good isolation between the component and the near field of the antenna which significantly reduces the coupling effects. Integration of the active components in the feedline is mainly employed in antenna diversity to switch either of the two orthogonal linear polarizations modes. However, this technique may require complex feeding networks and corresponding biasing [52].

2.6.3 Methods for Achieving Radiation Pattern Reconfigurability

An antenna that can switch its radiation between omnidirectional and unidirectional patterns is greatly desired not only to improve coverage but also to reduce the power required in transmission in multipath applications like MIMO. On-body antennas are desired to be insensitive to detuning and impedance mismatch while maintaining a stable radiation pattern

near the human body [10], [53], [54]. As part of efforts, some planar antennas with unidirectional properties have been studied over the years for their suitability as on-body antennas. Many design considerations involving printed monopoles and dipoles [35], [55]–[58], microstrip patch [34], [59], [60], yagi-uda [61][62], slot [63], [64] and planar inverted-F antennas (PIFA) [65], [66] have been reported in literature. Generally, conventional methods of realizing a unidirectional radiation pattern in printed monopole antennas involve the use of large full ground planes, metamaterials, and cavity-backed structures acting as reflectors and also to improve performance in microstrip patch antennas.

In its basic form, increasing the spacing between the antenna and the human body about a quarter-wavelength ($\lambda/4$) and placing the cavity-backed structure at a distance greater than $\lambda/10$ proves to reduce the SAR by 50% with unidirectional radiation as shown in Fig.2.9 [67]. The coplanar waveguide dipole antenna presented in [68] is designed with a slot on the radiator together with a full ground plane to achieve one-sided radiation. Although a higher gain is realized at 5 GHz, the backward propagation of the ground plane does not achieve a high front-to-back (F/B) ratio and also produces an unstable and nearly omnidirectional radiation pattern. (EBG) structures have been investigated as high impedance periodic dielectric materials that can be used to suppress surface waves as shown in Fig.2.9 (a). This reduces backward radiation and enhances radiation in the forward direction; hence, it is popularly used as a reflector. A large pyramidal-shaped cavity with a height of 15 mm is introduced in [7] to cause the directional radiation pattern of the planar monopole antenna in the ultra-wideband. Similar EBG-backed materials have been used by authors in [33], [34], [69] not only in the realization of unidirectional patterns but also to significantly reduce SAR levels. Although these cavity-backed reflectors can achieve an average of 60-70% reduction in SAR levels, it leads to a generally bulky and complex antenna size that is obtrusive and not compact enough for on-body applications.

Recently, some techniques [35] [70] have been studied to realize directional radiation patterns without the use of large ground planes and cavity-backed structures. The quasi-self-complementary antenna presented in [35] exploits the defected ground plane structure (DGS) coupling effect on the semi-circular printed monopole antenna for the ultra-wideband. However, the radiation patterns obtained when the antenna is operated close to the body demonstrate high rates of absorption to cause the unidirectional effect.

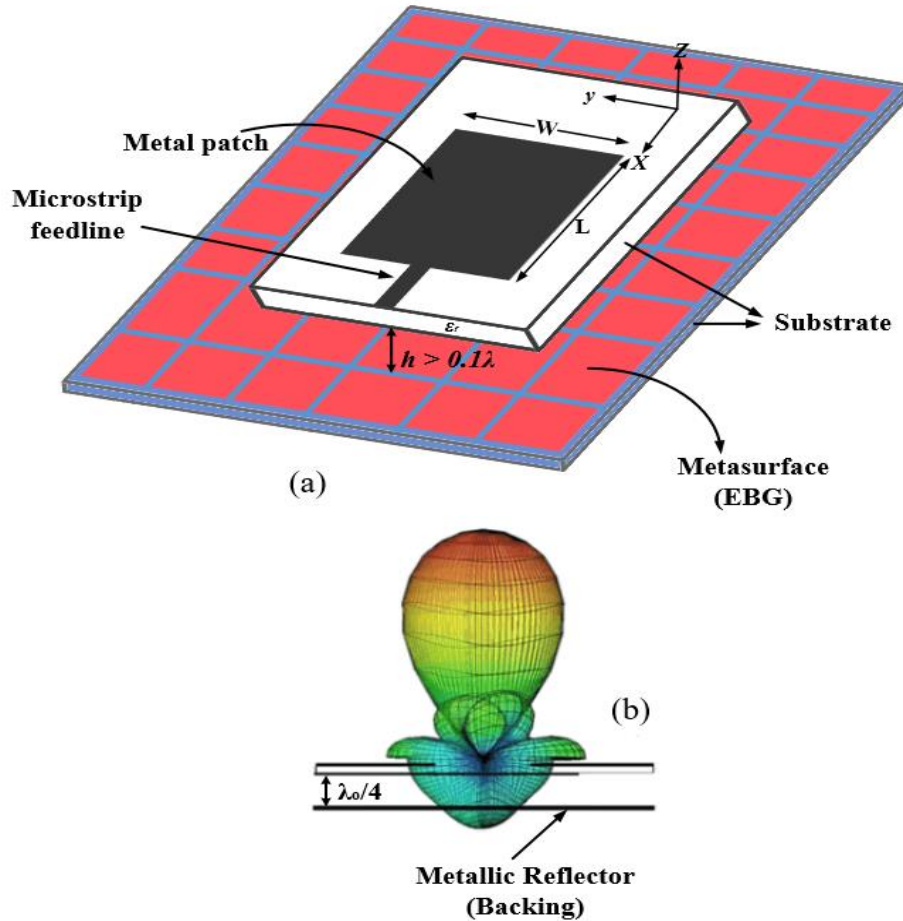


Fig.2.9 Methods of achieving unidirectional radiation pattern in printed microstrip antennas (a) Cavity-backed reflector (b) Full ground plane or Metallic reflector [67].

Moreover, the radiation patterns observed are unstable with great offsets and high impedance detuning under body loading which suggests the antenna does not possess unique unidirectional characteristics. Meanwhile, the dual-band printed monopole antenna in [70] is comprised of top and bottom microstrip patches separated by a 1.6mm FR4 substrate for the medical implantable communication service (MICS) and the industrial, scientific, and medical (ISM) bands respectively. The zeroth-order resonance (ZOR) which exploits the infinite wavelength ($\lambda_g = \infty$) property to present uniform surface currents on the resonator is employed to make the antenna insensitive to the human body coupling effects that lead to frequency shifting. By this, compact size is achieved through the shunt capacitive and inductive loading of the antenna. More recently, a simple approach to achieving unidirectional radiation pattern in wideband printed monopoles have been demonstrated in [71], [72]. By introducing a shorting stub, one edge of the radiator acts as a reflector causing the monopole to radiate strongly in one direction. This technique eliminates the need for conventional large and complex reflector surfaces.

However, the complex body loading effects and its characterization on the antenna in terms of SAR, impedance bandwidth, and radiation pattern stability based on these techniques are not reported in literature to date.

2.7 Flexible, Wearable Reconfigurable Antennas and Applications

The demand for body-worn computer systems to establish wireless body area communication has been growing rapidly. Classic applications in defense (police, military) for instance, have employed “bodycams” and wearable radios for soldiers’ live-location tracking and the real-time transmission of audio, image, and video to enable instant decentralized communications as shown in Fig.2.23. In healthcare, the noninvasive medical imaging of tumors and cancer cells in tissues, as well as stroke diagnosis, have led to the early detection and treatment of complicated illnesses that otherwise may be limited via traditional methods [73] (see Fig.2.10). Many other applications exist in smart personal communication and monitoring devices like cellular phones, smartwatches, and smart clothing have essentially driven the need to integrate antennas into WBANs. The key design requirements of wearable antennas are lightweight, compact size, low profile, low cost of fabrication, and conformity to the stochastic human body movements and positions. Functionally, the compact antenna size must not degrade its performance in terms of stable radiation pattern and impedance bandwidth, minimize radiation towards the body, and low transmission power to prolong battery life according to IEEE 802.15.6 international standard. Besides, the highly random human body postures and movements can significantly prevent communication. This must be accurately characterized by taking into account different degrees of bending on the antenna by the human body. Critical in the development of on-body flexible antennas is the choice of conductive and substrate materials that ultimately determines the type of fabrication process. Mainly, flexible antennas are realized using polymer-based materials that have resistant properties to moisture content and possess stretchable characteristics. Popular printed circuit board (PCB) substrates such as FR4, Rogers, and Teflon have been used in developing conformal antennas whereas some flexible substrates such as flexible FR4, flexible Rogers, textile, Polyethylene terephthalate (PET), Kapton polyimide, paper, etc., have also been widely used [74], [75].

In [76], Saeed et al proposed a wearable flexible reconfigurable antenna integrated with artificial magnetic conductor. The proposed design consists of three layers of flexible material which results in an overall large and bulky antenna size. Although no significant detuning was observed in the S_{11} and radiation pattern, higher degrees of curvature in different orientations

of the antenna were not considered. A more compact flexible L-shaped stub monopole antenna was presented in [77] by Ghaffar et al. In the conformability test, the antenna was bent in the x and y –axis which revealed shifts in the reflection coefficient and radiation patterns respectively. Similarly, the composite right/left handed (CRLH) technique was also employed in [78] to realize a very compact antenna size. However, the artificial magnetic conductor backing for reduced SAR altogether increases the antenna size. Additionally, the reconfigurable radiation pattern antenna reported in [79] switches from broadside to conical radiation using switched feed network. Meanwhile, highly efficient nano silver composite materials have been used in the fabrication of flexible printed monopole antennas in [80] and [81] respectively. However, these works are non-reconfigurable. Some of the highly advanced fabrication processes of these antennas include screen printing, chemical etching, inkjet printing.

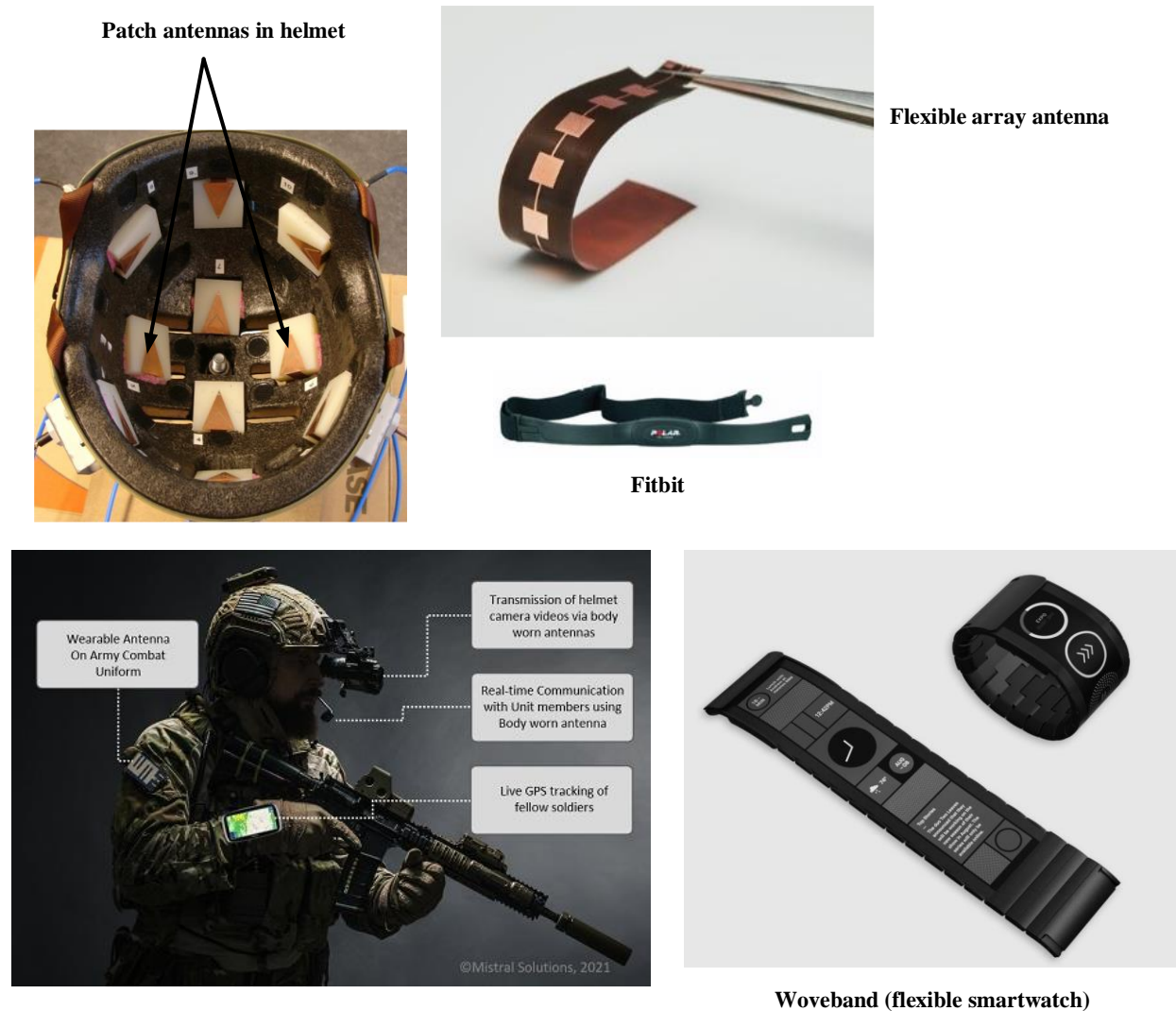


Fig.2.10 Application of wearable antennas

There have been a number of other flexible PMAs reported in the recent literature. However, there has been a paucity of flexible radiation pattern reconfigurable printed monopole antennas in the literature. In this work, the flexible FR4 and Rogers RO4003 substrates are chosen for the design while the inkjet printing process is recommended in the fabrication of the wearable antenna.

In subsequent sections of the next chapter, the design of a compact, low-profile slotted-stepped monopole antenna is presented based on a rectangular shorting side stub to achieve a unidirectional radiation pattern at the 2.45 GHz ISM band. To verify the antenna's on-body performance, it is characterized on phantom models to simulate the SAR, impedance bandwidth, and radiation patterns. It is known that under various complicated body posture and orientations, slight radiation pattern, impedance bandwidth, and polarization detuning is expected. A radiation pattern-agile antenna that is insensitive to body loading effects is greatly desired in on-body scenarios. A reliable solution is the design of a radiation pattern reconfigurable antenna. It is also noteworthy that previous works reported are mostly linearly polarized which severely suffers from polarization mismatch under such complex body constraints. Further sections of the chapter are dedicated to the design and operation of a radiation pattern reconfigurable printed monopole antenna with circular polarization using two RF PIN diodes. Later, flexibility and conformable features are incorporated into the reconfigurable antenna based on extremely low-loss flexible substrates.

CHAPTER THREE

METHODOLOGY AND DESIGN

3.1 Introduction

The method adopted for this research primarily involves the development of a reconfigurable antenna from an initial simple planar monopole design based on a comprehensive literature review as shown in Fig.3.1. The initial design is validated from the theory introduced in chapter 2 with specific parameters to be optimized for the desired output. The Ansys High-frequency Structure Simulator (HFSS) and computer simulation technology (CST) are used in the development and simulation modeling of the antenna. The simulation model is further enhanced through optimization and parametric study of various characteristics of the antenna. The optimal parameters are used to finalize the design to produce optimum results in simulation. Analysis of results is extensively performed using HFSS, CST, and Matlab software. A prototype of the antenna is then fabricated with appropriate far-field and return loss measurements carried out to ensure desired results agree with the simulation.

3.2 A Compact Low Profile Unidirectional Antenna at 2.45 GHz for Body-Centric Communications

3.2.1 Introduction

This work proposes a compact, low-profile slotted-stepped monopole antenna with a simple technique for achieving a unidirectional radiation pattern on a planar monopole antenna designed for the 2.45 GHz ISM band. By employing a shorting side stub, out-of-phase electric currents in one end of the radiator are shorted to the ground making that edge non-radiative resulting in a unidirectional radiation pattern. This technique is shown to significantly reduce SAR without the use of complex cavity-backed materials in simulation on a modeled phantom and on a real human body which shall be shown in later sections. The antenna also maintains a stable radiation pattern and reduced frequency shifting across the bandwidth.

3.2.2 Antenna Design

Fig.3.2 illustrates the layout of the proposed planar monopole antenna and its dimensions. The basic structure of the antenna consists of a slotted-stepped rectangular patch fed by a 3 mm 50Ω microstrip feedline. Printed at the back of the antenna is a rectangular ground plane fabricated on a 1.6 mm thick FR-4 substrate with a dielectric constant $\epsilon_r = 4.4$. The overall topology of the antenna measures a square compact size of $0.235\lambda_0$ (λ_0 = free space wavelength at 2.45 GHz) with the optimized parameters listed in Table 3.1.

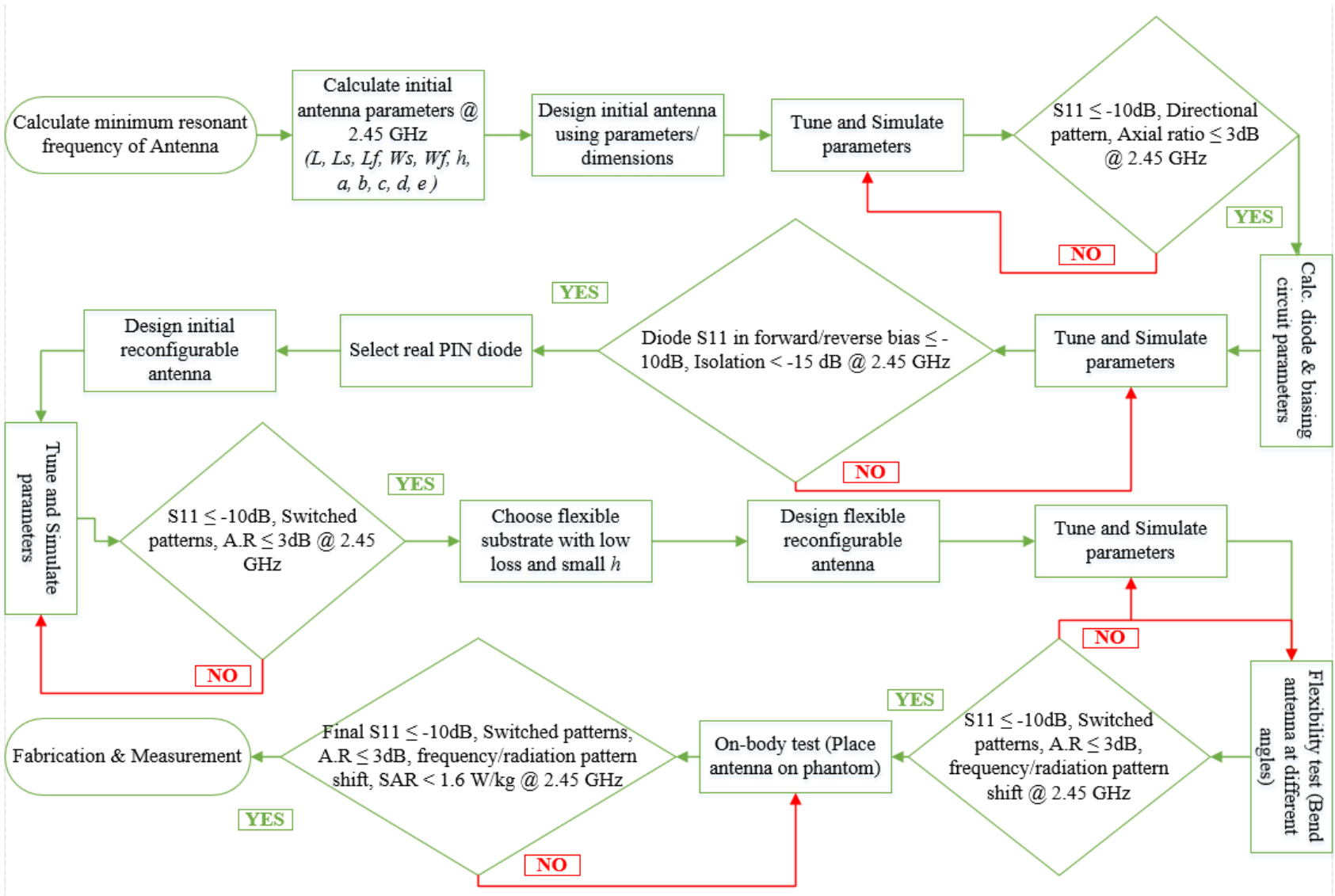


Fig.3.1 Flow diagram of reconfigurable antenna design.

3.2.2.1 Determination of the Resonant Frequency of the Antenna

The estimation of the lower resonant frequency of a regular-shaped planar monopole antenna is calculated from its physical dimensions corresponding to the equivalent area of a cylindrical monopole of the same length L and radius r , given by the relation in [82]:

$$2\pi rL = LW \quad (9)$$

For printed square monopole antennas (PSMA) of width = L , then

$$r = \frac{L}{2\pi} \quad (10)$$

Hence, the lower resonant frequency f_L of the square monopole is determined by:

$$f_L = \frac{7.2}{(L + p + r)} \text{ GHz} \quad (11)$$

Where the probe length p , L and r are in centimeters. From (10) and (11), the PSMA with dimensions $L = 2.88$ cm, and $p = 0.01$ cm yields $f_L = 2.15$ GHz for $|S_{11}| \approx -10$ dB. These initial parameters demonstrate the resonance of the antenna which is further optimized as listed in Table 3.1 and validated by the final S_{11} result in Fig.3.16. It is worthy of note that the optimized parameters are achieved through the optimetrics tool in HFSS based on predefined algorithms.

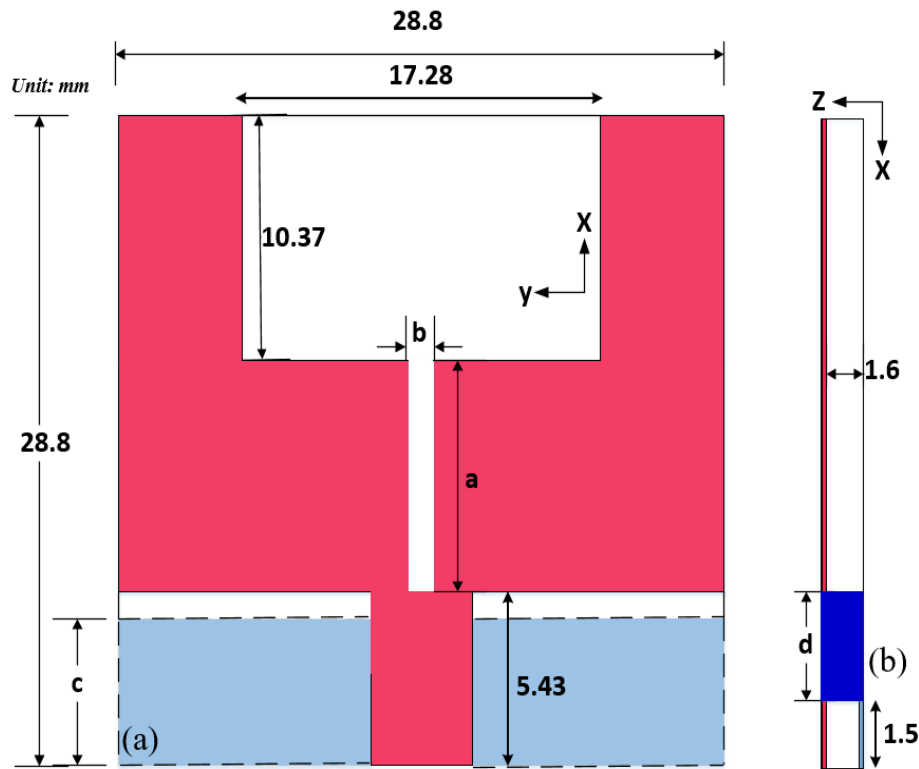


Fig.3.2 Topology and configuration of the proposed unidirectional antenna (a) Front view (b) Side view.

Table 3.1 Optimized Parameters of the Proposed Antenna

Dimension	Value (mm)	Dimension	Value (mm)
a	13.34	d	4.5
b	1.28	e	1.5
c	5.04	—	—

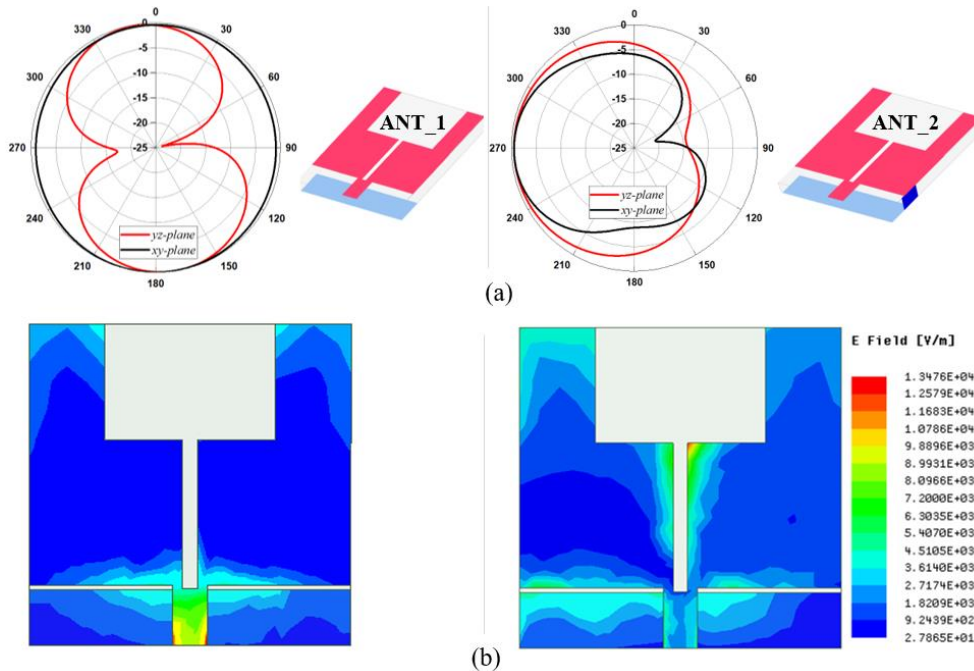


Fig.3.3 Combined simulated results of ANT_1 and ANT_2 (a) Radiation pattern. (b) Surface current distribution at 2.45 GHz (ANT_1—without side stub, ANT_2—with side stub).

In this proposed design, the monopole is formed into a fork-shaped radiator similar to that in [71] and [72]. To achieve unidirectional radiation, a rectangular stub is inserted at the edge of the substrate to connect the right arm of the monopole and the ground plane as shown in Fig.3.2 (b). The radiation mechanism can further be understood from Fig.3.13 (a) by comparing the simulated antenna without a side stub and the same antenna with an optimized side stub. It is observed that ANT_1 without a side stub exhibits a regular omnidirectional radiation pattern. However, introducing the side stub causes ANT_2 to produce a unidirectional pattern concentrated in the $-y$ direction in both the azimuth and elevation planes. This is basically due to the conduction of opposite surface currents by the stub that is out-of-phase with the adjacent radiator arm and the ground plane. In this way, the nearby radiator arm becomes non-radiative

and acts as a reflector which aids in steering the broadside radiation towards the opposite azimuth plane similar to the principle of operation proposed in [72]. This is further verified by the dominance of distributed surface currents on the left monopole shown in the fields plot in Fig.3.3 (b) as compared to ANT_1.

3.2.2.2 Parametric Study

The effect of the design parameters a, b, c, d have been observed in simulation and subsequently optimized for optimum performance of the antenna. It is expedient to note that for conciseness, the effects of the length a and width b of the vertical slot are not presented in this work as their variations do not greatly affect the performance of the S_{11} and radiation pattern. However, the slots contribute to increasing miniaturization and slightly to improving the impedance matching of the antenna. It is shown that an improved S_{11} is realized when the length of the ground plane, c is chosen from optimization as $c = 5.04$ mm as depicted in Fig.3.4. By connecting right arm of the radiator with the metallic side stub to the ground plane, existing symmetric currents on the radiator are observed to be out of phase. These out-of-phase currents are then shorted to the ground causing the right arm of the monopole to be non-radiative leading to unidirectional radiation along the $-y$ direction. The optimal placement of the rectangular side stub of length $d = 4.5$ mm to connect the ground plane and the monopole also achieves an improved $S_{11} < -10$ dB at 2.45 GHz.

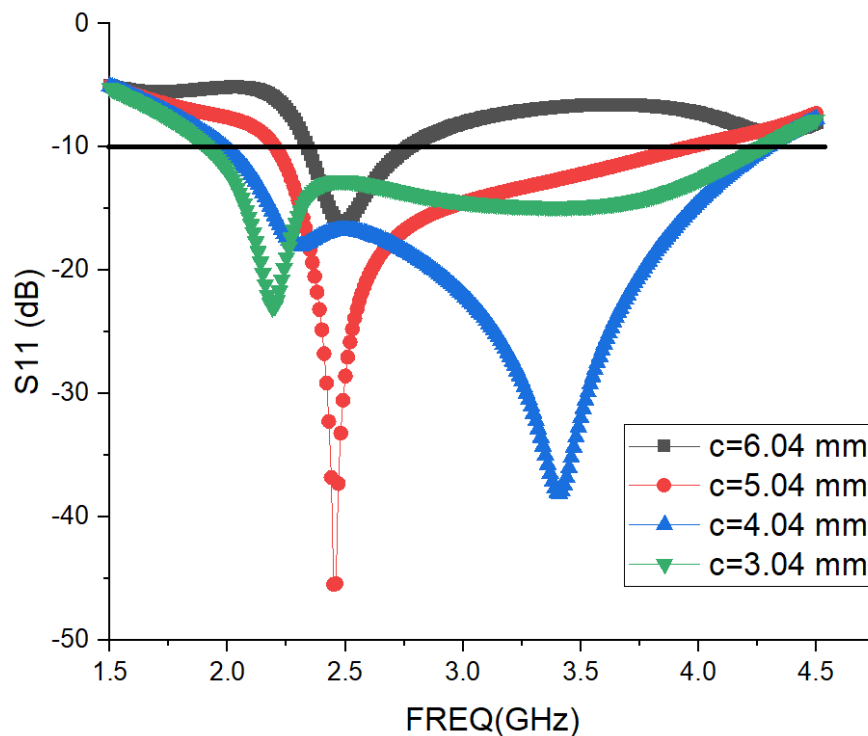


Fig.3.4 Simulated S_{11} of the proposed antenna at different ground plane lengths.

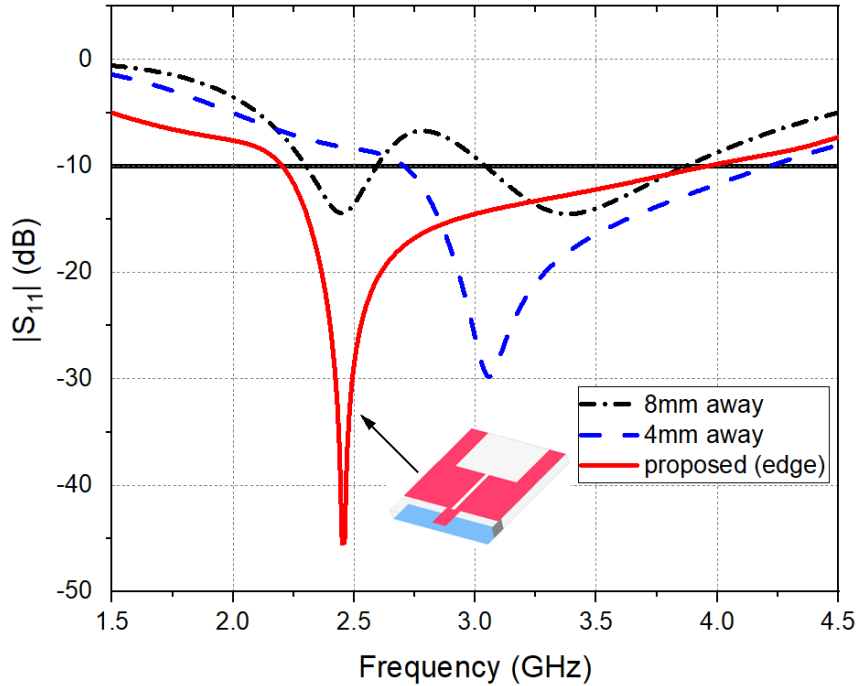


Fig.3.5 Effects of stub position along y –axis on the reflection coefficient of the antenna.

It is observed that moving the stub 4 mm away from the edge in the $-y$ direction, the resonant frequency is shifted to about 3.05 GHz while the antenna’s return loss deteriorates when the stub is further moved 8 mm away from the edge and closer to the feedline as shown in Fig.3.5. At this point, the unidirectional radiation pattern of the antenna is lost which demonstrates the critical role of the shorting side stub in achieving a directional pattern. This feature will further be exploited in section 3.3 to achieve a pattern-reconfigurable design with the help of RF switches. The length of the stub and its movement along the y -axis were observed in simulation to have little impact on the antenna’s performance characteristics and hence have not been shown for brevity.

3.2.3 Results and Discussions

Fig.3.6 represents the final simulated return loss of the single side-stub planar monopole antenna. The resonant frequency is observed at 2.45 GHz with $S_{11} < -20$ dB indicating a good antenna matching. In the fabricated antenna, similar measurements are performed to validate the simulation results by attaching a sub-miniature version A (SMA) connector and a coaxial cable with the help of a vector network analyzer (VNA). Far-field radiation pattern simulations were carried out in free space and on-body. The radiation patterns were measured in the xy (E –plane) and yz (H –plane) planes showing unidirectional radiation in the principal plane-cuts in both free space and on-body at the design frequency as illustrated in Fig.3.7.

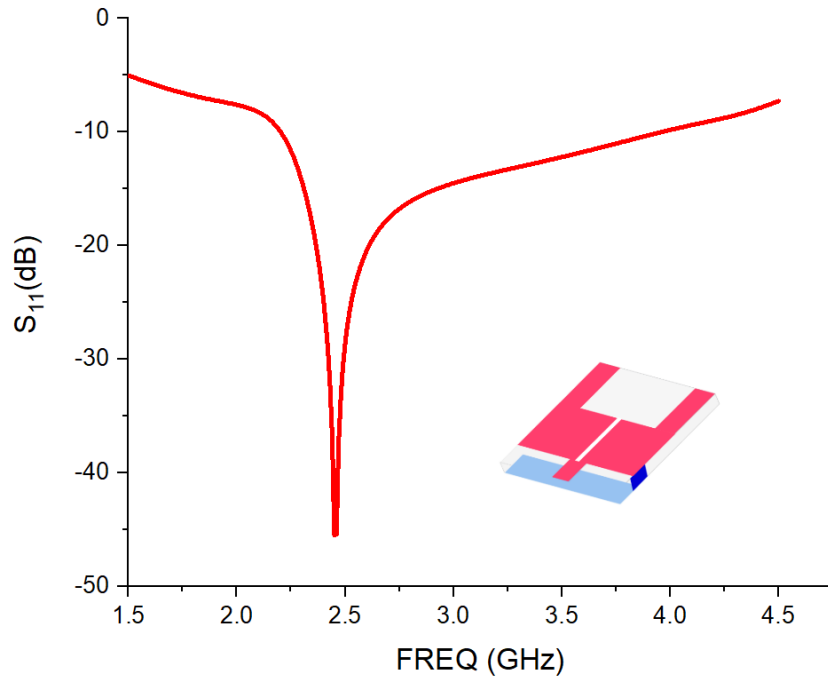


Fig.3.6 Final simulated S_{11} of the proposed single side-stub planar monopole antenna.

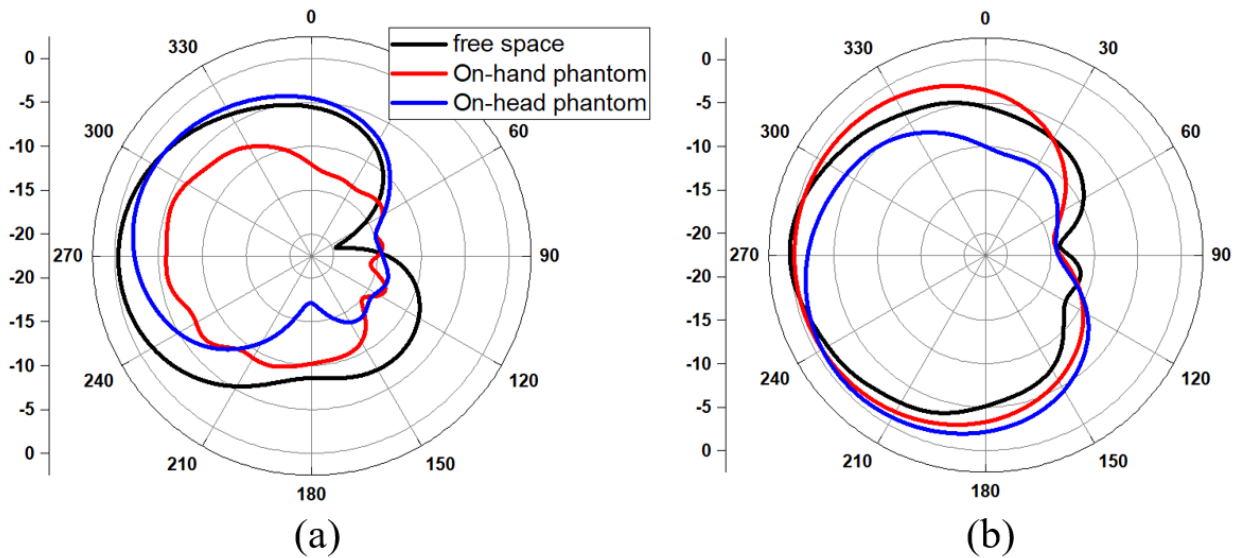


Fig.3.7 Normalized radiation patterns of the proposed antenna in free space and on-body at 2.45 GHz (a) x - y plane (b) y - z plane.

A semi-circular bowl phantom to simulate the human head with relative permittivity and conductivity of skin ($\epsilon_r = 37.952$ $\sigma = 1.4876$ s/m), bone ($\epsilon_r = 11.352$ $\sigma = 0.40411$ s/m) and brain ($\epsilon_r = 48.83$ $\sigma = 1.843$ s/m) was modeled for the on-body far-field simulations with dimensions as provided in [10]. This is an IEEE standardized measurement procedure for the characterization of random on-body effects on an antenna. A similar experiment was conducted

on a real body (i.e. average age man) and the measured radiation patterns were observed to be in agreement. The effect of the antenna position with respect to its proximity on the body has been studied at various separation distances, d up to 10 mm away from the body. The Simulated S_{11} results in Fig.3.8 show reduced detuning in the antenna's impedance bandwidth while also maintaining a stable radiation pattern without offsets even when the antenna is placed directly on the body is depicted by the normalized radiation pattern in Fig.3.7.

3.2.4 Specific Absorption Rate (SAR) Simulation

The specific absorption rate which is defined as the amount of electromagnetic energy absorbed per-unit mass by the human body when using a wireless communication device can be represented mathematically as:

$$SAR = \frac{\sigma \times E^2}{\rho} \quad (12)$$

Where σ is the conductivity of the body tissue (S/m), E expresses the root mean square (RMS) electric field intensity (V/m) and ρ denotes the mass density of the body tissue in kg/m^3 . The IEEE C95.1-2005 standard for safety levels with respect to human exposure to RF energy and the International Commission on Non-Ionizing Radiation Protection (ICNIRP), the SAR limit is set to 2 W/kg over 10 g of tissue. Similarly, the Federal Communications Commission (FCC) specifies a peak power of 1.6 W/kg over 1 g of contiguous tissue that must be strictly complied with by all on-body wireless communication devices before it can be marketed.

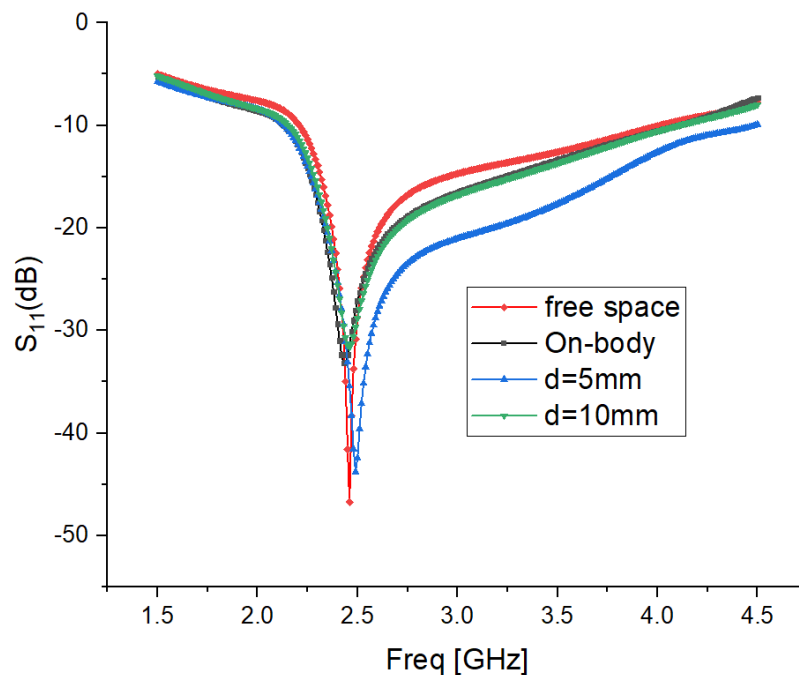


Fig.3.8 Measured reflection coefficient in free space and at distance d from the body.

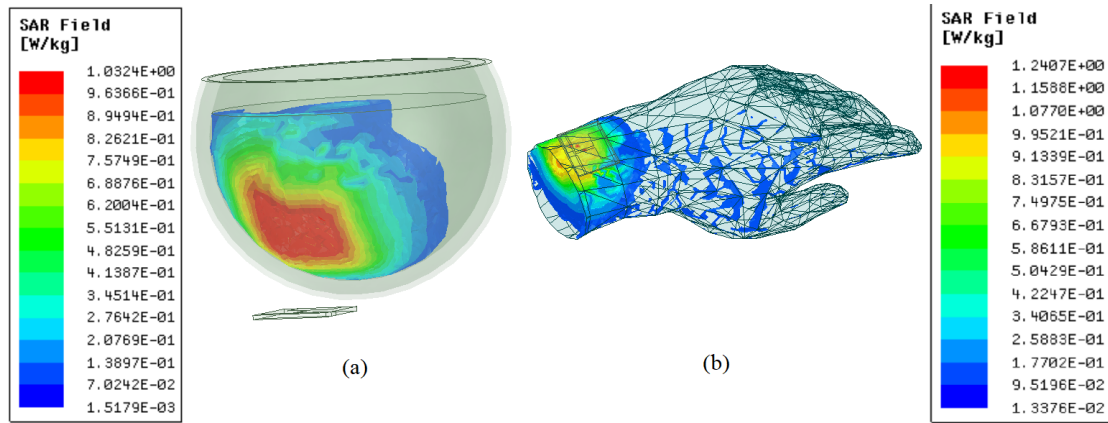


Fig.3.9 Simulated SAR performance of single side stub antenna (a) Antenna placed on head phantom (b) Antenna placed on hand phantom.

As a result, the spatial peak SAR performance of the proposed antenna was evaluated over 10 g spherical and hand phantom with standard body tissue properties commonly used to simulate the human head and hand as outlined in the IEEE P1528-2002 standard. The maximum average SAR recorded for the simulated head and hand phantoms of the antenna were 1.03 W/kg and 1.24 W/kg respectively for an input power of 1 W at the resonant frequency of 2.45 GHz as illustrated in Fig.3.9. Similar measurements carried out on real tissue also recorded low SAR values which are all below the safety limits.

3.2.5 Conclusion

In this section, a compact size, slotted-stepped planar monopole antenna with a low-profile design has been proposed for on-body applications in the 2.45 GHz ISM band. The conventional omnidirectional radiation pattern of the antenna is converted to unidirectional radiation in the $-y$ direction to reduce the on-body coupling effects on the antenna. Unidirectionality is achieved by employing a rectangular shorting side stub to reduce the absorption of electromagnetic radiation by the body. The technique also showed the SAR of the proposed antenna to be within acceptable limits without the use of complex cavity-backed structures and large reflector elements commonly used in on-body antennas. Simulation and measurement results have demonstrated that the antenna provides reduced frequency detuning and stable radiation pattern characteristics at the resonant frequency in free space and on-body.

3.3 A Compact Low-Profile Pattern-Reconfigurable Monopole Antenna for On-Body Communications

3.3.1 Introduction

In this work, by incorporating PIN diodes as RF switches, the unidirectional radiation of the single-stubbed monopole antenna presented in the previous section can be reconfigured to tune the realized symmetric radiation pattern in both $-y$ and $+y$ directions together with the monopole-like radiation at different operating modes in the same frequency. In this way, the radiation pattern can be dynamically adjusted to provide communication in the random positioning of the human body that creates a typical multipath situation.

3.3.2 Pattern-Reconfigurable Antenna Design

In the previous section, the design of a low-profile single side-stub planar monopole antenna that converts an omnidirectional pattern to unidirectional radiation has been presented. Based on this design concept, an improved reconfigurable extension of the antenna is developed by choosing a suitable voltage-controlled RF switching device to independently vary between two rectangular side-stubs. The design layout of the edge-stubbed pattern-reconfigurable antenna is presented in Fig.3.10 with the optimized parameters summarized in Table 3.2. This section demonstrates the concept and realization of the switching technique via RF PIN diodes incorporated in the antenna to obtain tunable radiation patterns.

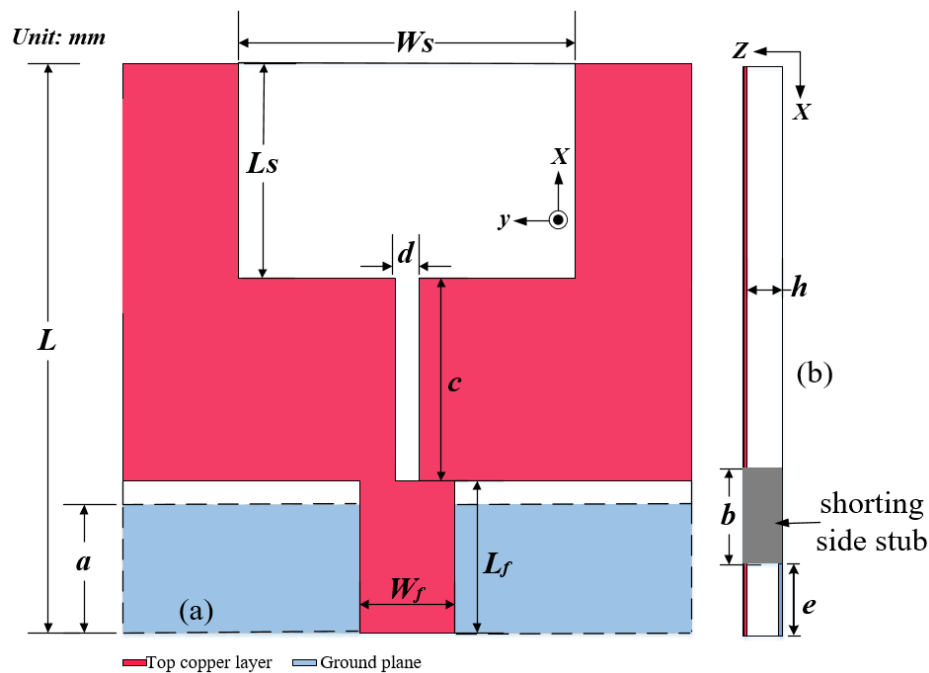


Fig.3.10 Design layout of low-profile, edge-stubbed pattern-reconfigurable antenna (a) Top view. (b) Side view.

Table 3.2 Optimized Parameters of the Proposed Reconfigurable Antenna

Dimension	Value (mm)	Dimension	Value (mm)
L	28.8	a	5.04
L_s	10.37	b	4.5
L_f	5.43	c	13.34
W_s	17.28	d	1.28
W_f	3.06	e	1.5
h	1.6	—	—

3.3.3 Antenna Reconfiguration and Principle of Operation

The principle of obtaining unidirectional radiation has been discussed in section 3.2. Here in this section, the radiation pattern of the antenna is reconfigured by the independent switching of PIN diodes connecting the patch and the ground plane. In [3], arc-shaped stubs were connected to the ground plane extension via PIN diodes which were left open-circuited with the circular patch to effectively realize a reflector element.

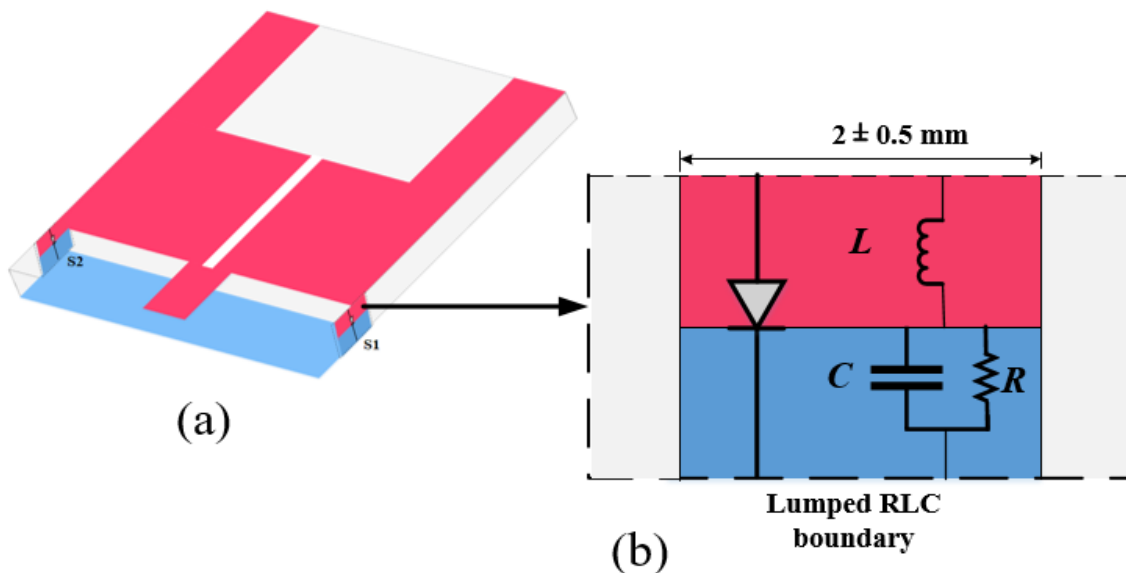


Fig.3.11 (a) Design of the dual-stubbed pattern-reconfigurable monopole antenna (b) Equivalent PIN diode modelling of the side-stub as lumped RLC boundary.

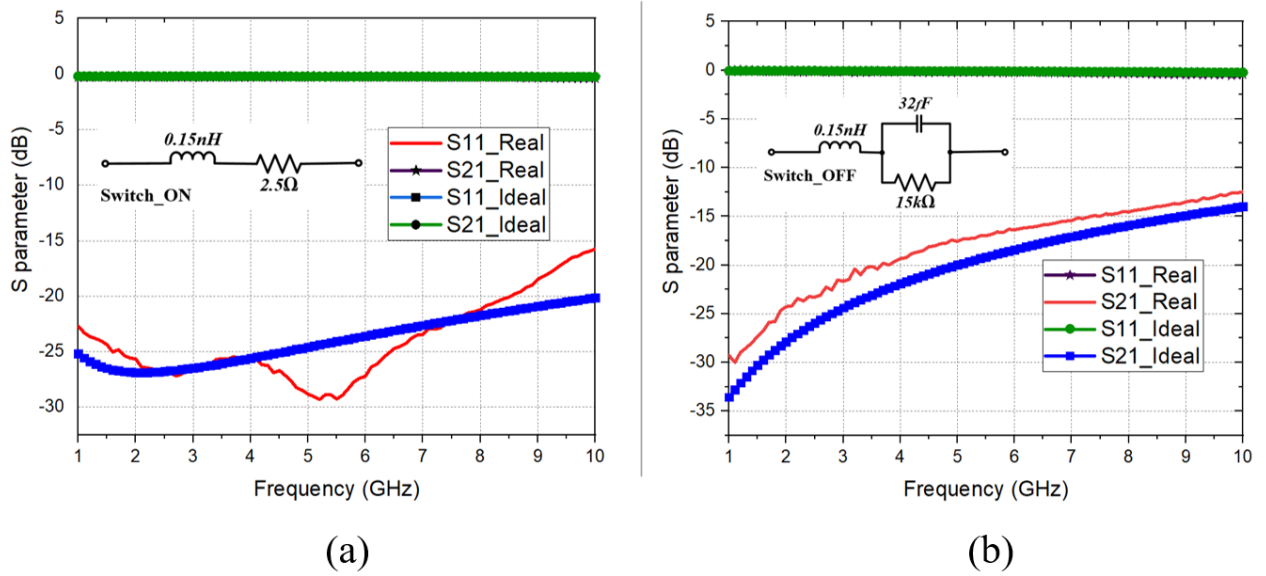


Fig.3.12 Equivalent PIN diode circuit model simulation (a) Forward biased (b) Reverse biased.

Table 3.3 Operation Modes and Biasing Configuration of the Reconfigurable Antenna

Operation Mode	S1	S2	V1	V2
Mode-0	OFF	OFF	0 V	0 V
Mode-1	ON	OFF	+5 V	0 V
Mode-2	OFF	ON	0 V	+5 V

This work achieves pattern diversity by connecting the patch and the ground plane using PIN diodes. As a proof of concept, the two metallic side stubs S1, S2 are modeled as an equivalent 2 mm lumped resistor, inductor and capacitor (RLC) perfect electric conductor boundary in HFSS at a height of the substrate to depict the PIN diodes as shown Fig.3.11. Thus, when the switch is in the ON state (forward-biased) the equivalent circuit of the RF PIN diode is ideally represented as a series 2.5 Ω resistor and 0.15 nH inductor while the OFF state (reverse biased) is modeled as a shunt combination of a 15 k Ω resistor and a 32 fF capacitor in series with the inductor [7] (zoom-in—Fig.3.11). Hence, the RLC boundary can be considered as the equivalent RF switch and their ON or OFF states represent the short or open circuit conditions of the side stubs respectively. The ideal characteristics of the modeled PIN diodes exhibit a low reflection coefficient less than -20 dB in the ON condition with high isolation in the OFF state better than -15 dB for frequencies up to 10 GHz. However, implementation of the actual RF

PIN diode presents real characteristics that are influenced by several factors including ohmic contact losses, power dissipation, substrate losses, and other manufacturing tolerances. To verify the operation of a real PIN diode, the DSM8100-000 beam-lead PIN diode with a very low total capacitance from Skyworks Inc. is chosen after rigorous investigation and simulations to meet the design goal [83]. The return loss and isolation of the actual PIN diode are found to agree well with the ideal simulated values as shown in Fig.3.12. By employing the PIN diodes, the maximum directive radiation pattern can be symmetrically steered between -90° and $+90^\circ$ along the y –axis with a high front-to-back ratio. Altogether, the antenna can switch between three modes, namely the omnidirectional mode (Mode-0) and the two symmetric modes of -90° (Mode-1) and $+90^\circ$ (Mode-2). The switch modes of S1 and S2 together with the respective voltage configurations are presented in Table 3.3. As a side attraction, the antenna achieves a miniaturized structure without the use of multiple switched radiator elements to realize reconfigured patterns compared to [84].

A similar reconfigurable concept presented in [45] demonstrates the switching of the radiator elements at different angles to create three different versions of the same antenna. However, in this approach, the three different states of the antenna cannot be simultaneously tuned on a single fabricated prototype. In addition, the tuned angles (i.e., $= 90^\circ, 30^\circ$ and 150°) of the loaded radiators suffer significant frequency detuning due to uncontrolled shifts in length of the monopole. This present design simultaneously tunes the antenna’s radiation pattern by the independent switching of the PIN diodes on the same fabricated prototype without any variations in the operating frequency. The design also implements a smaller number of RF switches (2) and no excess vias are needed to connect the patch and the ground plane therefore significantly reducing fabrication complexity.

3.3.3.1 DC Bias Circuit

The DC biasing network required to switch the two PIN diodes S1, S2 is designed to primarily isolate the RF and DC signal paths as shown in Fig.3.13. The two PIN diodes are controlled by a simple shunt single pole double throw (SPDT) switch configuration which offers high isolation with extremely low insertion loss over a broad frequency range. The isolation (I_{so}) is found to be approximately 21 dB in the OFF state of the RF PIN diode from the given equation below [49],

$$I_{so} = 20\log\left(1 + \frac{Z_0}{2R_s}\right) \quad (13)$$

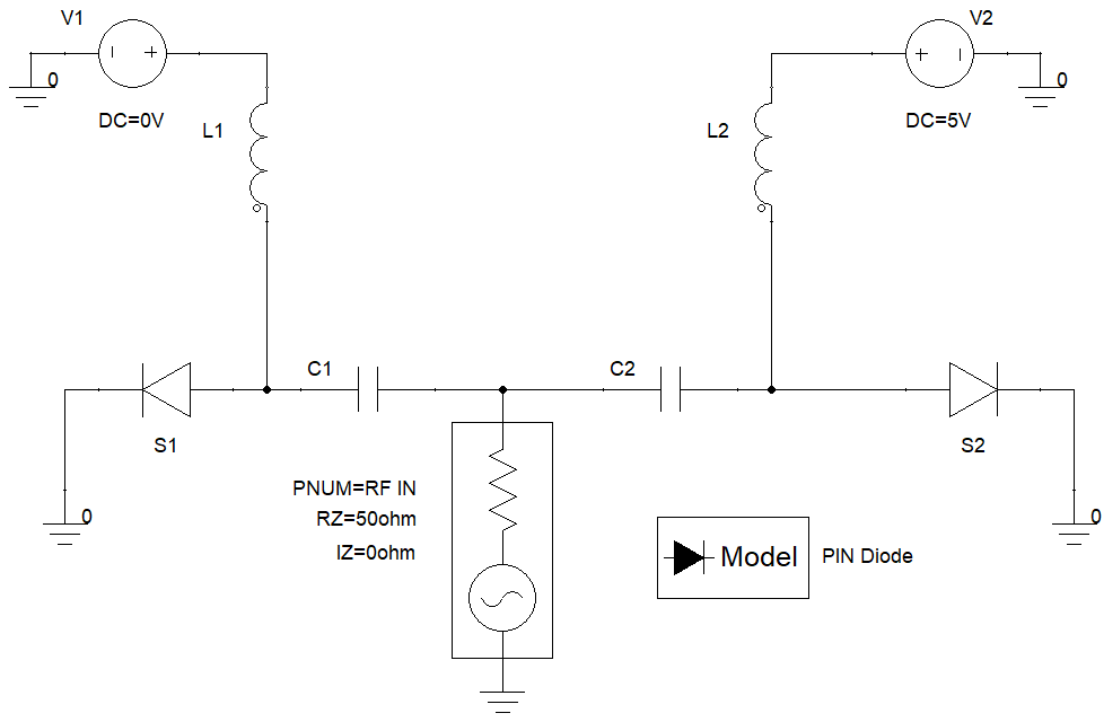


Fig.3.13 Schematic diagram of DC bias circuit of the proposed pattern-reconfigurable antenna

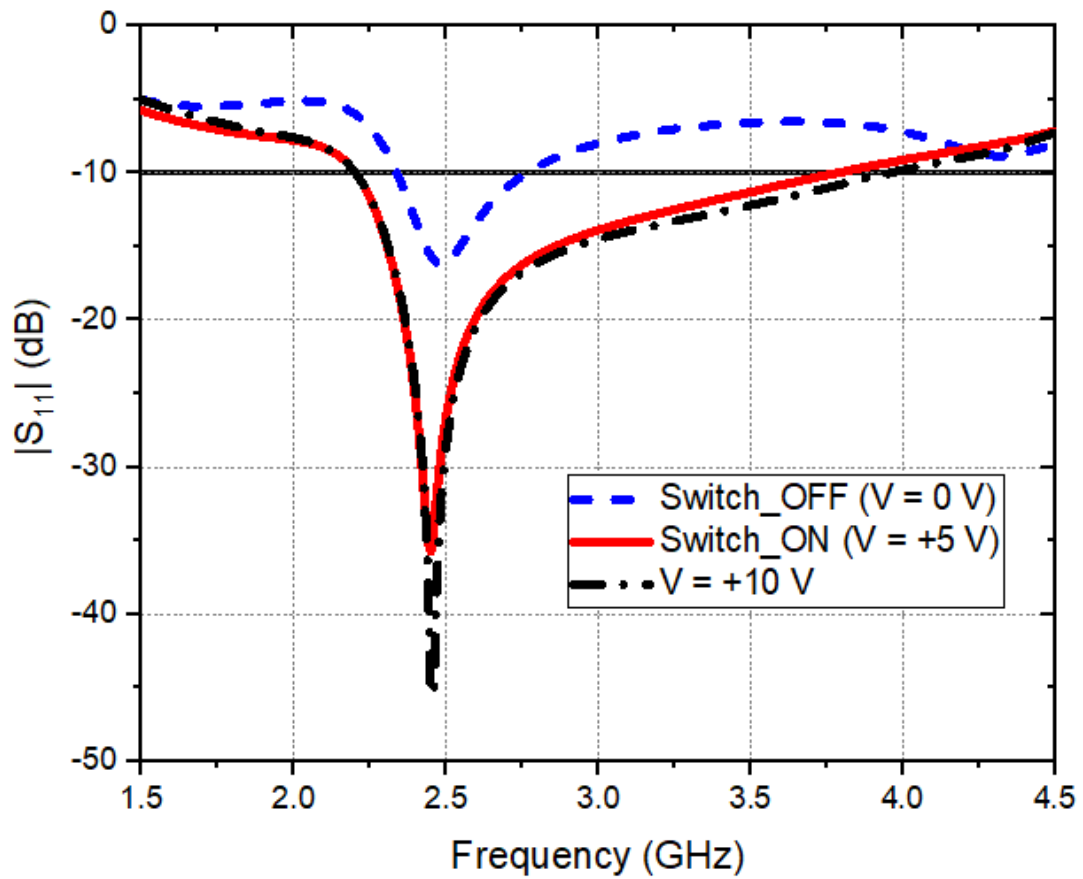


Fig.3.14 Simulated S_{11} of the proposed antenna under varying operating conditions.

Where R_s is the diode's series resistance at an input impedance characteristic of $Z_0 = 50 \Omega$. From the design structure of the antenna, the left and right edges of the patch are directly connected to the ground plane by the PIN diodes and therefore do not require additional capacitors to separate the DC and RF signals. Thus, only two blocking capacitors $C_1, C_2 = 1 \mu\text{F}$ and two RF choke inductors $L_1, L_2 = 0.1 \mu\text{H}$ are needed to prevent the RF currents from flowing back into the bias circuit before connecting them to the external DC bias voltages V_1 and V_2 respectively. Voltages V_1 and V_2 alternately biases the PIN diodes and are supplied at 0 V and 5 V respectively to either turn S1 ON/OFF and vice versa for S2.

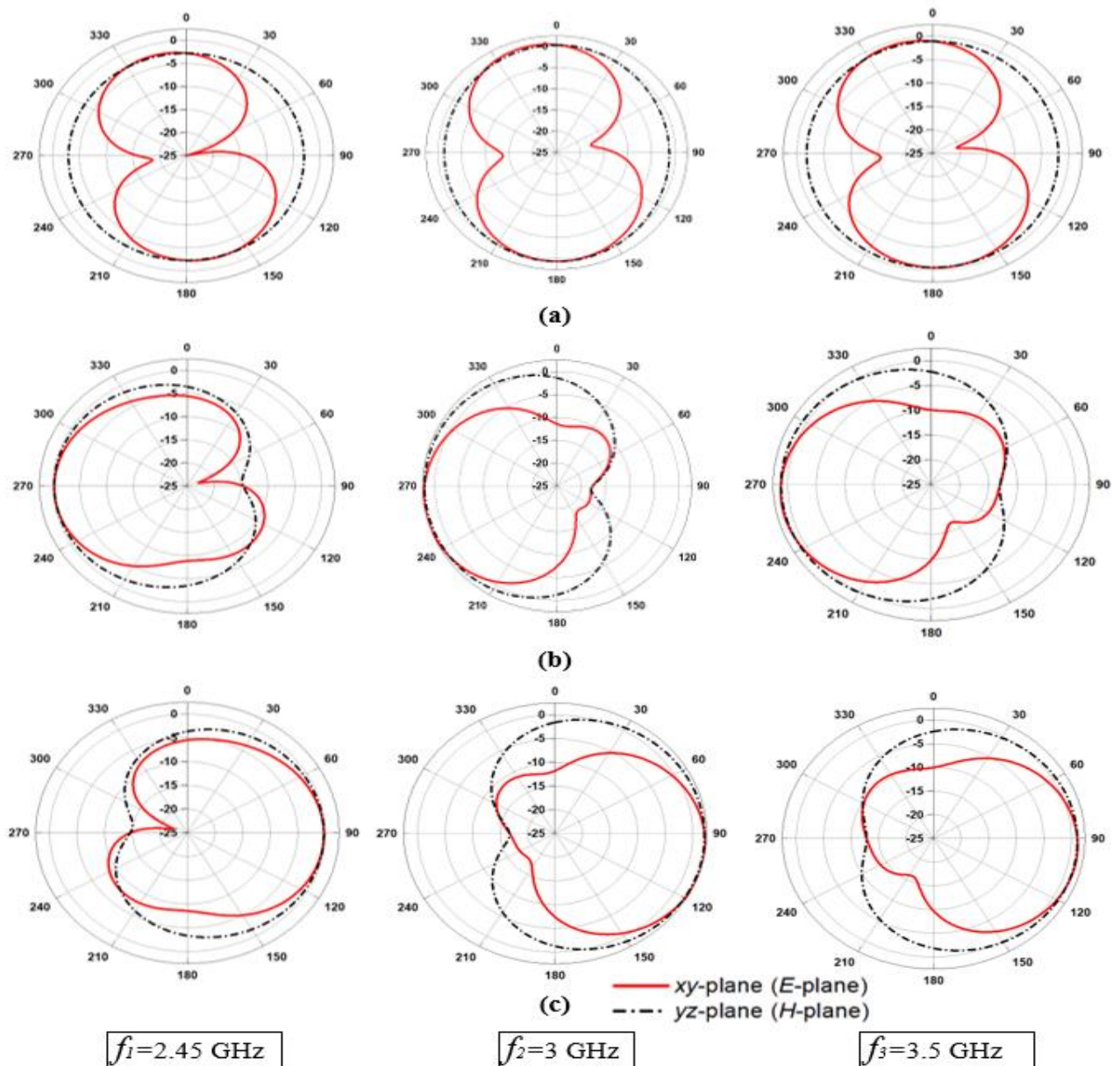


Fig.3.15 Normalized radiation patterns of the pattern-reconfigurable antenna at different frequencies (a) Mode-0 (b) Mode-1 (c) Mode-2.

3.3.4 Results and Discussions

The printed pattern-reconfigurable monopole antenna based on switched dual side-stubs using RF PIN diodes has been designed to discretely switch between omnidirectional and unidirectional radiations in both azimuth and elevation planes. The optimized antenna employs two sets of DSM8100-000 RF PIN diodes with a total capacitance of $C_T = 0.025$ pF and a small internal resistance in the range of $R_S = 2.5\text{--}3.5$ Ω . The reflection coefficient (S_{11}) of the proposed antenna operating in different modes of supplied voltages is presented in Fig.3.14. The bias voltages for Mode-1 and Mode-2 are varied between V_1 and V_2 . V_1 is fixed at 0 V while V_2 is varied and vice versa. It can be observed that a further increase in the voltage supply above +5 V only improves the reflection coefficient of the antenna while the operating frequency remains unaffected even when the diode is reverse-biased at 0 V. This effect explains the complete decoupling of the frequency-radiation pattern characteristic linkage that most reconfigurable antennas suffer from. This is also an ideal feature that is specifically desired in on-body communications where complex antenna propagation patterns exist due to highly random body deformations. In such cases, the proposed antenna dynamically switches the radiation pattern without any effect on the operating frequency. Moreover, the input impedance of the antenna is properly matched at the resonance with $S_{11} \leq -10$ dB and a realized VSWR of less than 2:1.

3.3.5 Radiation Patterns

The normalized far-field radiation patterns of the proposed reconfigurable antenna are characterized in HFSS as shown in Fig.3.15 for different frequencies and operating modes. The simulated results in the E –plane and H –plane reveal typical omnidirectional radiation for Mode-0 similar to that in [3], [6] while Mode-1 and mode-2 exhibit unidirectional radiation concentrated in the $-y$ and $+y$ directions respectively. Stable radiation patterns with no significant offsets are observed across the entire bandwidth.

3.3.6 Simulation of Specific Absorption Rate (SAR)

The specific absorption rate (SAR) which expresses the amount of electromagnetic energy absorbed per unit mass by the human body when using a wireless electronic device is evaluated for compliance. The peak SAR performance of the proposed antenna was simulated on a human hand phantom and semi-circular bowl phantom models designed to simulate the human hand and head respectively as shown in Fig.3.16. The tissue properties in terms of the permittivity, permeability, conductance, and loss tangent are as provided in [10]. The peak average SAR at

the resonant frequency of 2.45 GHz for a 1W input power of the proposed pattern-reconfigurable antenna was found to be between 0.56 W/kg and 0.76 W/kg over a10 g tissue mass for the head and hand phantoms respectively. The SAR values recorded are all below the safety limits which make the antenna a suitable candidate for body-centric wireless applications. The antenna also exhibits no significant detuning in the impedance bandwidth when placed directly on the body and at a distance $d = 5$ mm, 10 mm away respectively. This result did not show any significant variation from the one presented in Fig.3.8 in section 3.2, hence, has not been shown for conciseness. Similarly, stable radiation patterns simulated in free space and on-body are shown in Fig.3.17.

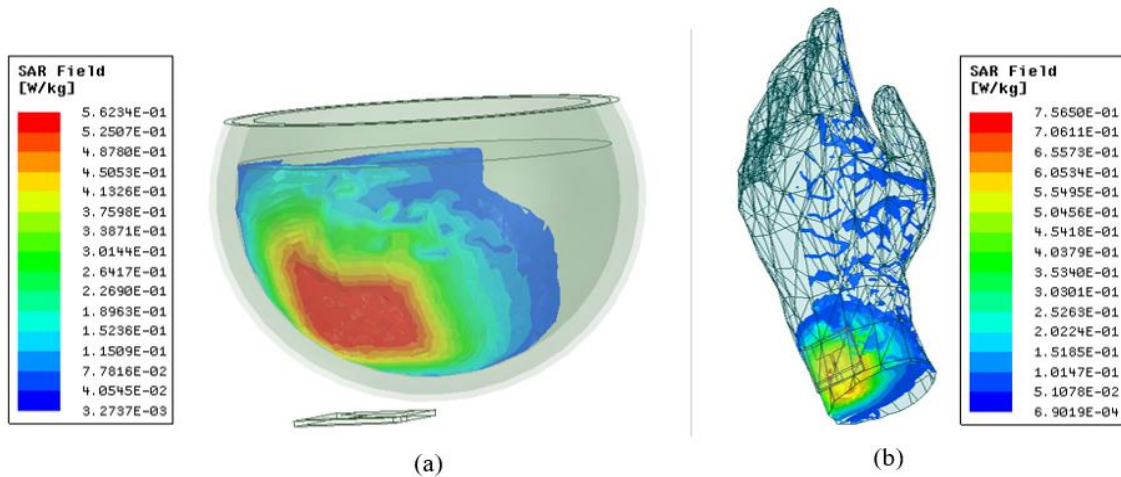


Fig.3.16 Simulated SAR performance of the proposed reconfigurable antenna at 2.45 GHz (a) Antenna placed on modeled head phantom (b) Antenna placed directly on a hand phantom.

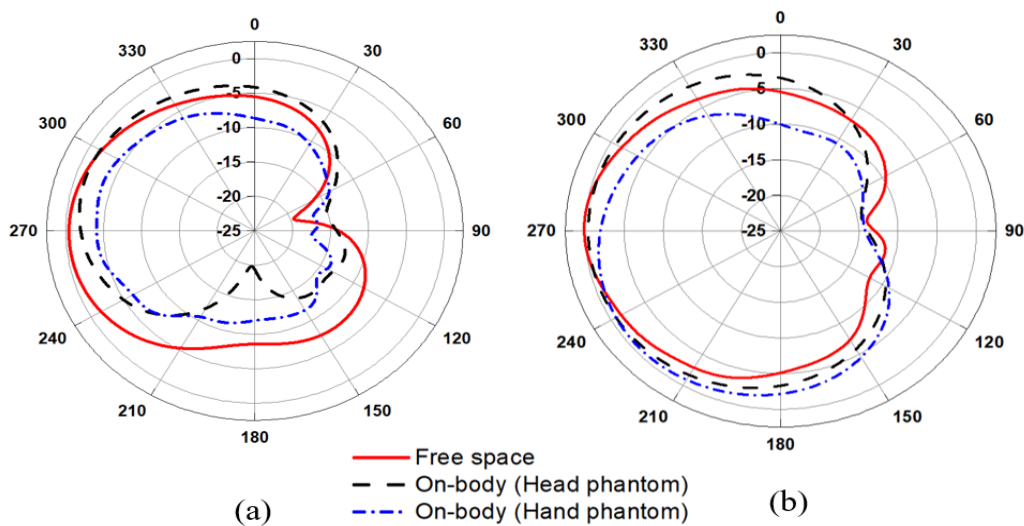


Fig.3.17 Simulated radiation patterns of the reconfigurable antenna in free-space and on-body at 2.45 GHz (a) $x - y$ plane (b) $y - z$ plane.

3.3.7 Conclusion

In this section, a pattern-reconfigurable mode of the antenna has been demonstrated based on the independent switching of the dual side-stubs by incorporating two RF PIN diodes. This technique ultimately converts the omnidirectional radiation of the monopole antenna into unidirectional patterns with a bidirectional degree of freedom in the maximum radiation angles from -90° to $+90^\circ$ along the y – axis to extend the diversity and radiation coverage of the antenna. Results from simulation and measurement confirm the successful decoupling of the frequency-radiation pattern characteristic linkage with stable reconfigured patterns across a wideband. The proposed design also exhibits a good SAR performance with no significant frequency detuning when the antenna is operated on or close to the body. This is achieved without the use of cavity-backed structures and large reflector elements that are common with most body-centric antennas. Thus, the antenna maintains a simple and compact structure that is desirable in space stringent applications such as in wearable technology.

3.4 A Flexible and Wearable Pattern-Reconfigurable Printed Monopole Antenna for On-Body Communications.

3.4.1 Introduction

This section presents the design and analysis of a flexible pattern-reconfigurable printed monopole antenna for BWC applications. The wearable feature is a key requirement of flexible antennas to present a conformal nature to the configuration of the human body. Based on previous designs, the printed monopole antenna is optimally modified in terms of geometry and the selection of appropriate flexible substrates (flexible FR4 and Rogers) with low loss tangent (δ) and thickness. It has been established that random body postures can cause severe attenuation in communication. Hence, the need to obtain circular polarization and also switch the radiation pattern of the antenna in different modes to maintain the communication link. In this section, the flexible reconfigurable antenna is demonstrated under different bending conditions and the results in terms of frequency and radiation pattern stability are analyzed. To demonstrate the conformability of the antenna, it is mounted directly on phantom models and the body coupling effects are subsequently investigated in terms of the radiation pattern and frequency characteristic linkage together with the specific absorption rate performance.

3.4.2 Flexible On-body Antenna Design

The design and configuration of the flexible radiation pattern reconfigurable antenna is presented in Fig.3.18. Optimized parameters of the designed antenna are listed in Table 3.4.

By the concept of design, the slotted monopole is printed on a flexible FR4 substrate with a dielectric constant of 4.4, the thickness of 0.25 mm, and a loss tangent of 0.025. The antenna is fed by a thin 50Ω microstrip feedline. Already discussed in previous works, two switchable rectangular side stubs are used to connect the edge of the radiator to the defected ground plane structure (DGS) with an embedded slot. The slot in the ground plane is necessary to achieve the desired matching and impedance bandwidth at the resonant frequency. The overall size of the antenna is only $0.235\lambda_0 \times 0.235\lambda_0 \times 0.002\lambda_0$. It is emphasized that the operating principle behind the radiation pattern reconfiguration of the antenna based on RF PIN diodes together with the bias circuitry has also been discussed in detail in the previous section. Thus, the operating modes and biasing conditions of the reconfigurable antenna are the same as those presented in Table 3.3.

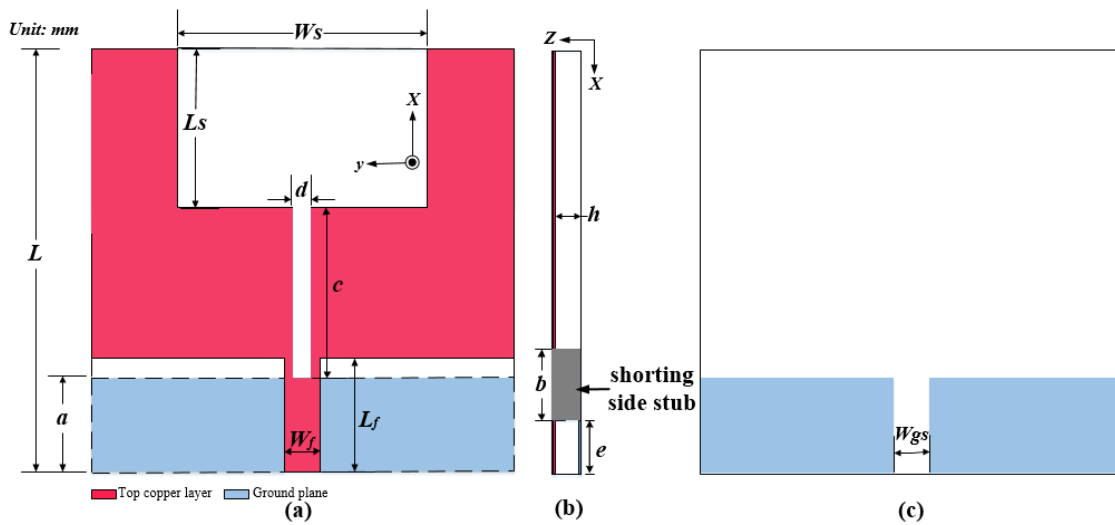


Fig.3.18 Design configuration of the flexible pattern-reconfigurable antenna (a) Top layout (b) Side layout (c) Back view.

Table 3.4 Optimized Parameters of the Proposed Flexible Reconfigurable Antenna

Dimension	Value (mm)	Dimension	Value (mm)
L	28.8	a	4.44
L_s	10.37	b	1.51
L_f	5.43	c	13.99
W_s	15.28	d	0.62
W_f	1.26	e	4.05
h	0.25	W_{gs}	0.93

3.4.2.1 Parametric Study

It is well known that the thickness of the substrate considerably affects the radiation of a microstrip antenna. Hence, thicker substrates with low permittivity are usually employed for efficient radiation characteristics of the antenna [85]. In this current design, the thickness of the substrate represents about an 84% reduction in size from the 1.6 mm FR-4 substrate used in the previous antennas. A simple technique, without overly modifying the antenna structure is therefore required to achieve a good impedance matching that leads to efficient radiation of the antenna. A vertical slot is created in the truncated horizontal ground plane to achieve the best impedance matching at 2.45 GHz. The width (W_{gs}) of the vertical slot in the ground plane is varied from 0.53 mm to 1.23 mm and its effect on the simulated reflection coefficient is shown in Fig.3.19. It is observed that the impedance is significantly improved at the resonant frequency when the width of the vertical slot is 0.93 mm. Moreover, the fork-shaped slot helps to improve the impedance matching and achieve a good radiation efficiency in terms of the F/B of the antenna. However, this does not cause any change in the S_{11} and radiation pattern, hence its effect has not been shown.

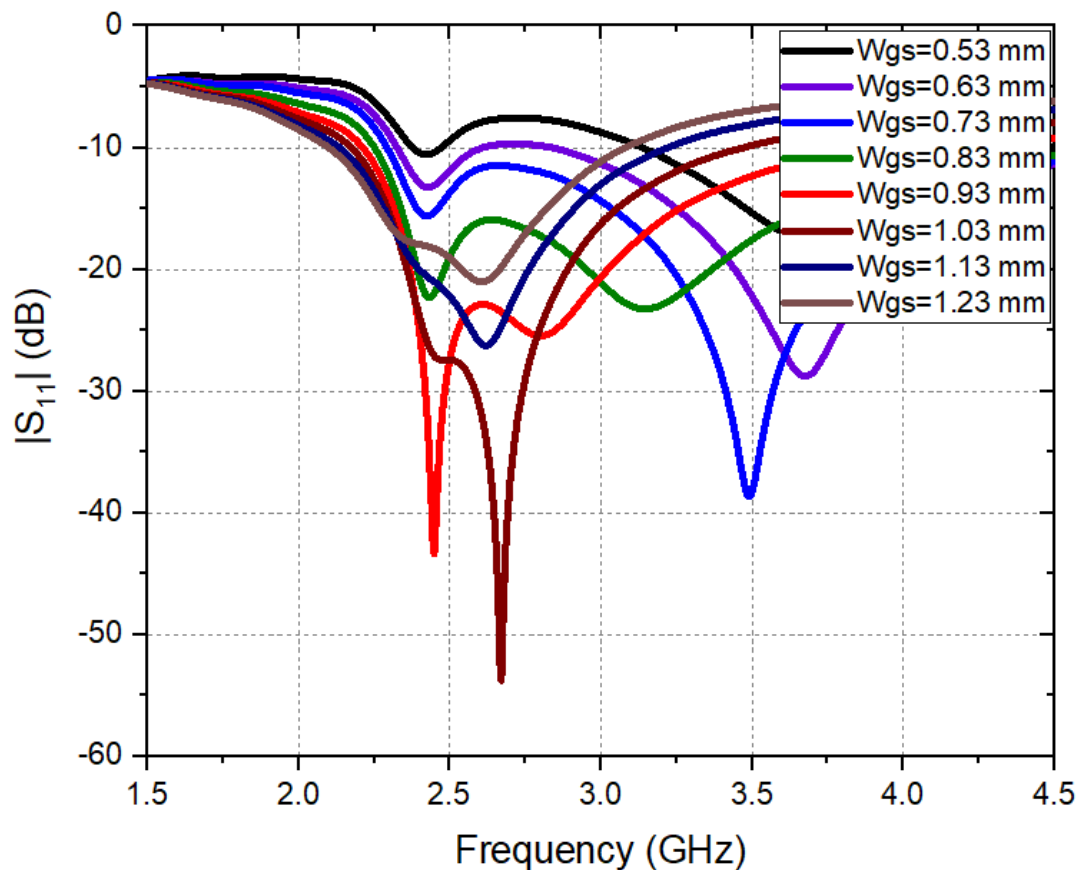


Fig.3.19 Effects of the width of the groundplane slot on the proposed flexible reconfigurable antenna.

3.4.3 Flexible Pattern-Reconfigurable Antenna Design and Operation

Based on the design concept introduced, the radiation pattern of the flexible antenna is reconfigured by the use of RF PIN diodes to alternately switch the side stubs to obtain three independent modes of radiation. The approach for obtaining pattern diversity by incorporating two PIN switches as shown in Fig.3.20 has been discussed in section 3.3.

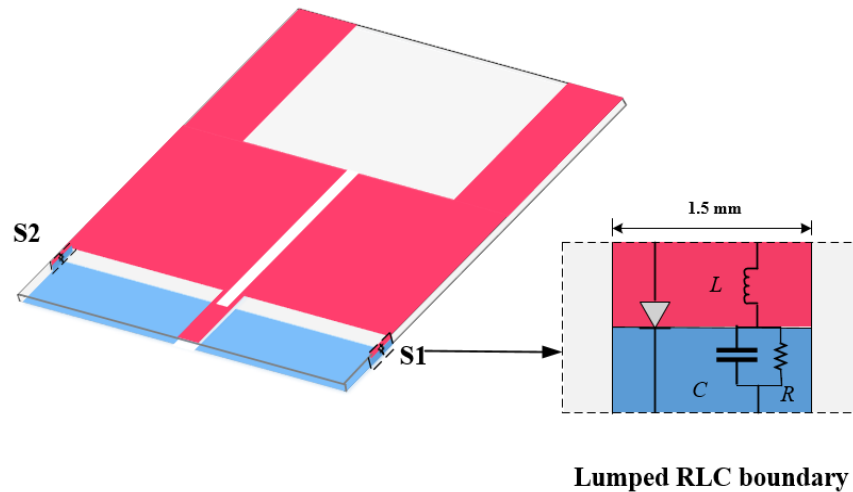


Fig.3.20 Design of the flexible pattern-reconfigurable antenna; zoom in - Equivalent PIN diode modelling as a lumped RLC boundary.

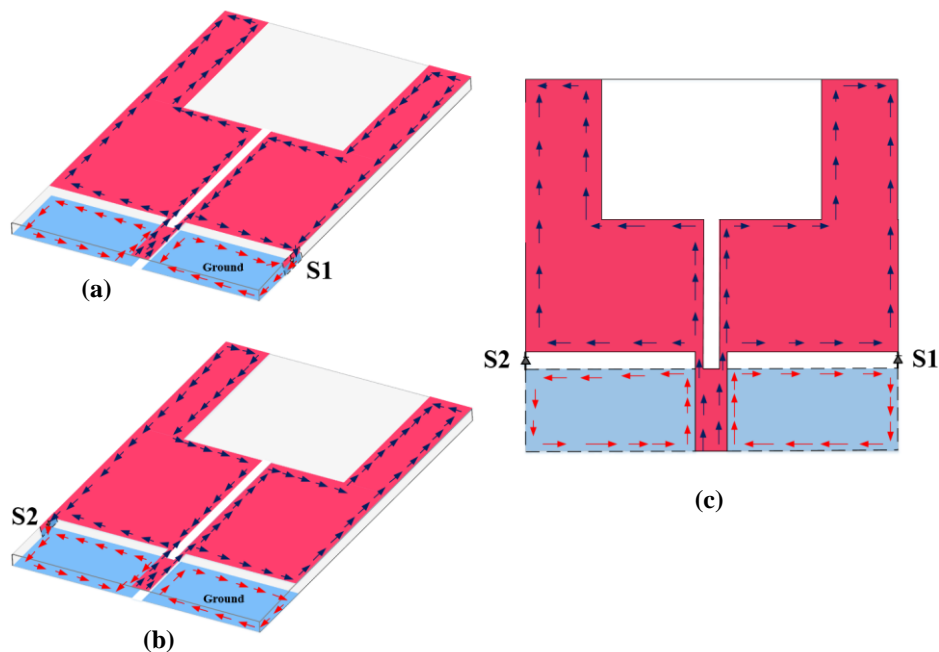


Fig.3.21 Surface electric current distribution (a) Switch 1 (S1) ON (forward biased) (b) Switch 2 (S2) ON (forward biased) (c) Both Switch 1 (S1) and Switch 2 (S2) OFF (reverse biased).

In this design, the two switches S1 and S2 can be conveniently modeled as a 1.5 mm perfect electric conductor boundary (zoom-in) in HFSS with the same lumped RLC component values as in the previous section. The DSM8100-000 beam-lead PIN diode with a very low total capacitance from Skyworks Inc. is chosen together with a simple biasing network also provided in the same section. Thus, when switch 1 (S1) is in the ON state or forward biased with an appropriate DC source, the right edge of the monopole is shorted to ground and becomes non-radiative. This is evident in the asymmetric surface current distribution on the monopole as illustrated in Fig.3.21 (a). Similarly, when S2 is activated, the left arm of the monopole is shorted to ground and the surface electric current distribution is observed to be out-of-phase with the right arm of the monopole as shown in Fig.3.21 (b). As a result, only the right arm of the monopole radiates leading to unidirectional radiation along the +y axis. However, when both S1 and S2 are reversed biased, the ground plane and the radiator are open-circuited and symmetric current is observed to be distributed on the monopole as depicted in Fig.3.21 (c). To demonstrate the flexibility of the reconfigurable antenna, various simplified bending characteristics are explored and its effect on the return loss and radiation pattern is subsequently studied. Various degrees of bending in the range of radius $R = 0^\circ - 180^\circ$ at 45° interval is performed on the antenna along the x and y-axis as shown in Fig.3.22. The inward and outward bending conditions are also taken into consideration.

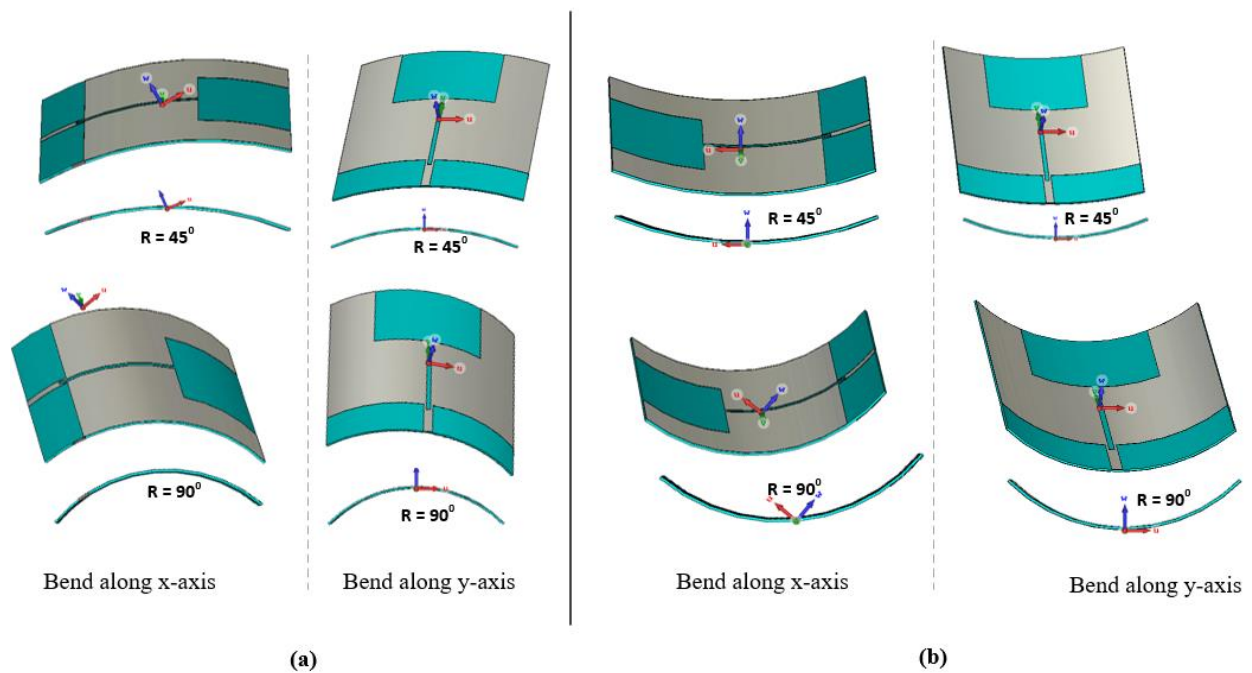


Fig.3.22 Flexible antenna under various degrees of bending along x and y-axis (a) Outward bend at $R = 45^\circ, 90^\circ$ (b) Inward bend at $R = 45^\circ, 90^\circ$.

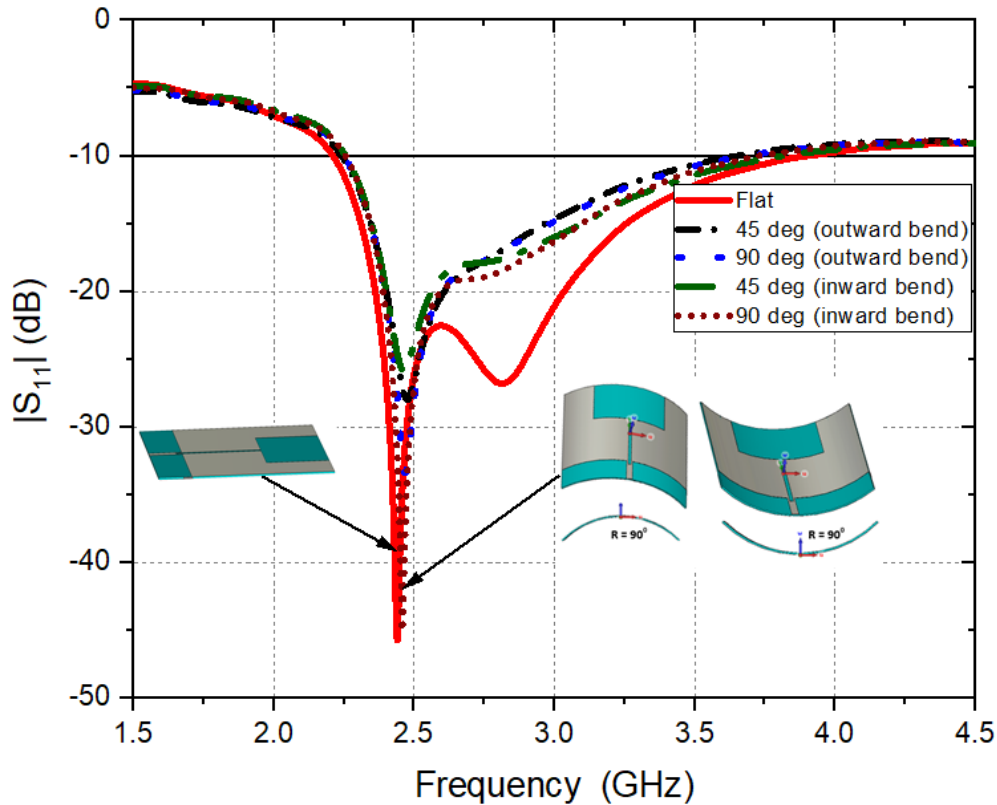


Fig.3.23 Reflection coefficient (S_{11}) of the flexible reconfigurable antenna in planar unbend (flat) and bend configurations.

The effect of these bending scenarios on the reflection coefficient is plotted in Fig.3.23. The simulated S_{11} result shows no variation in the reflection coefficient for the various bending configurations as against the planar unbend antenna (flat). It is noteworthy, that similar bending scenarios were performed for other angles 135° , 180° and there was no noticeable difference hence these have not been shown for brevity.

3.4.4 Radiation Patterns

The three dominant radiation modes of the antenna based on the state of the PIN diode is evident in the normalized radiation pattern plot in Fig.3.24. The normalized radiation pattern plots in the $x - y$ and $y - z$ planes for the flat (unbend) antenna and the average bending characteristics of the antenna at 90° is shown in Fig.3.25. The plot reveals no offsets in the main lobe radiation in the elevation $E -$ plane and horizontal $H -$ planes. The stable patterns maintain the unidirectional state of the flexible antenna. It can therefore be deduced that the bending effects present no significant detuning on the antenna's impedance bandwidth and radiation pattern which is critical to explaining the decoupling of the frequency-radiation pattern characteristic linkage property. In this way, both properties of the antenna i.e. reflection

coefficient and radiation pattern can be individually tuned without any significant effect on the other properties as have been shown in the simulation. It is emphasized that the decoupling of individual properties in reconfigurable antennas without the use of complex techniques has seldom appeared in the literature. Previous works that attempt this feature of the reconfigurable on-body antenna usually end up with wide impedance detuning and unstable radiation patterns due to inefficient decoupling strategies and other RF switch effects as a result of complicated biasing networks [47], [48]. The final simulated reflection coefficient of the flexible radiation pattern reconfigurable antenna is shown in Fig.3.26 with high resonance occurring at the design frequency of 2.45 GHz and a magnitude of $S_{11} < -40$ dB. The antenna also achieves a wideband impedance from 2.2 GHz to 4 GHz which is an inherent characteristic of printed monopoles that is desirable for applications in the higher ISM and WLAN bands. It is noteworthy that the pattern-reconfigurable antenna was also designed using the flexible Rogers RO4003 substrate with a thickness of 0.2 mm, $\epsilon_r = 3.55$, and $\delta = 0.0027$ and the S_{11} and far field results are provided in appendix B.

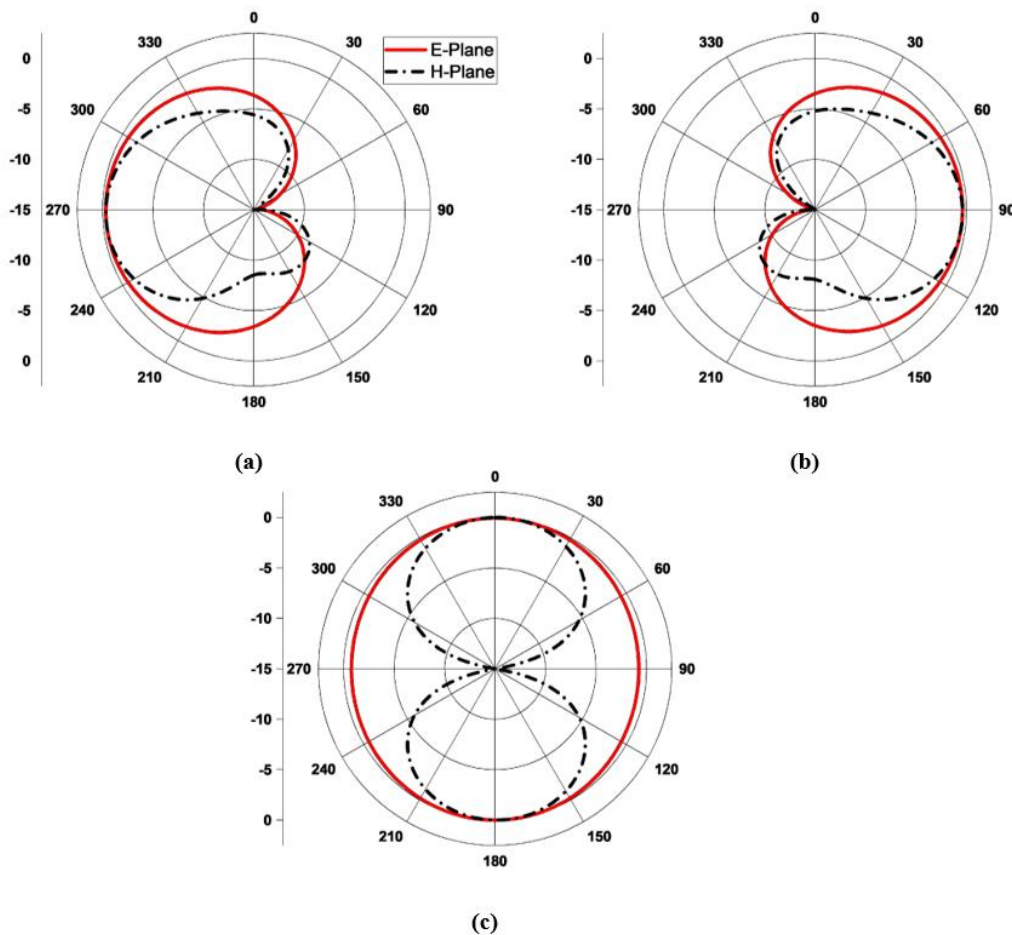
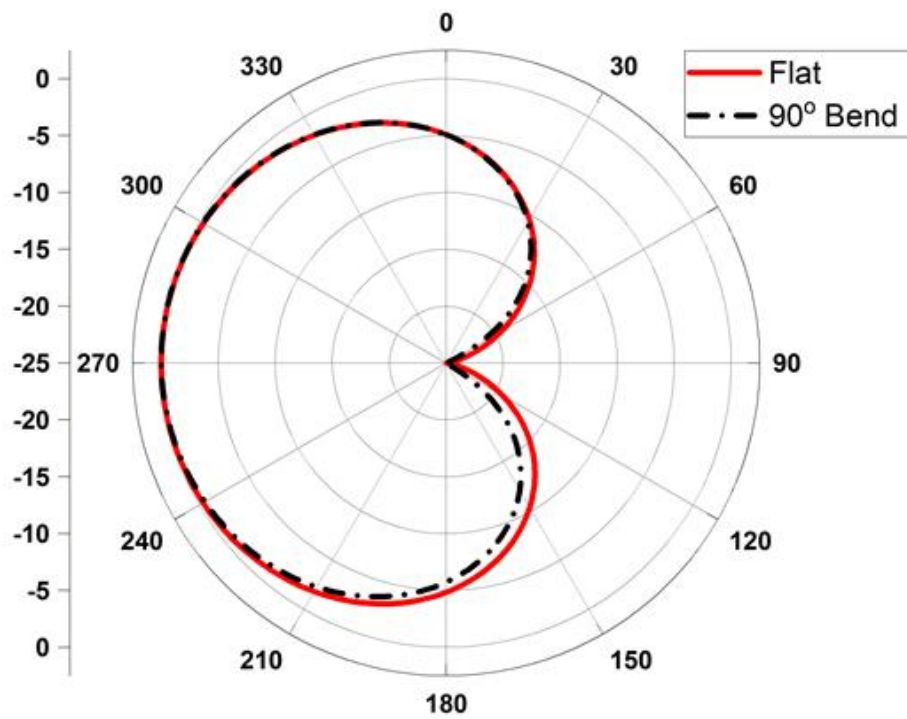
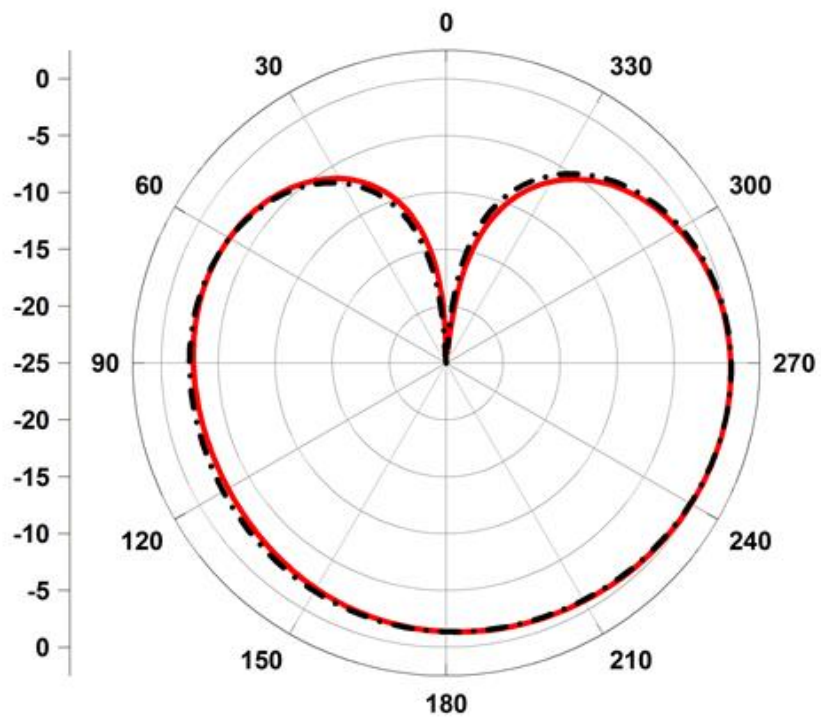


Fig.3.24 Normalized radiation pattern modes of the of the proposed flexible reconfigurable antenna (a) S1 ON (b) S2 ON (c) S1 S2 OFF.



(a)



(b)

Fig.3.25 Simulated radiation pattern of the flexible reconfigurable antenna in planar unbend (flat) and bend configurations.

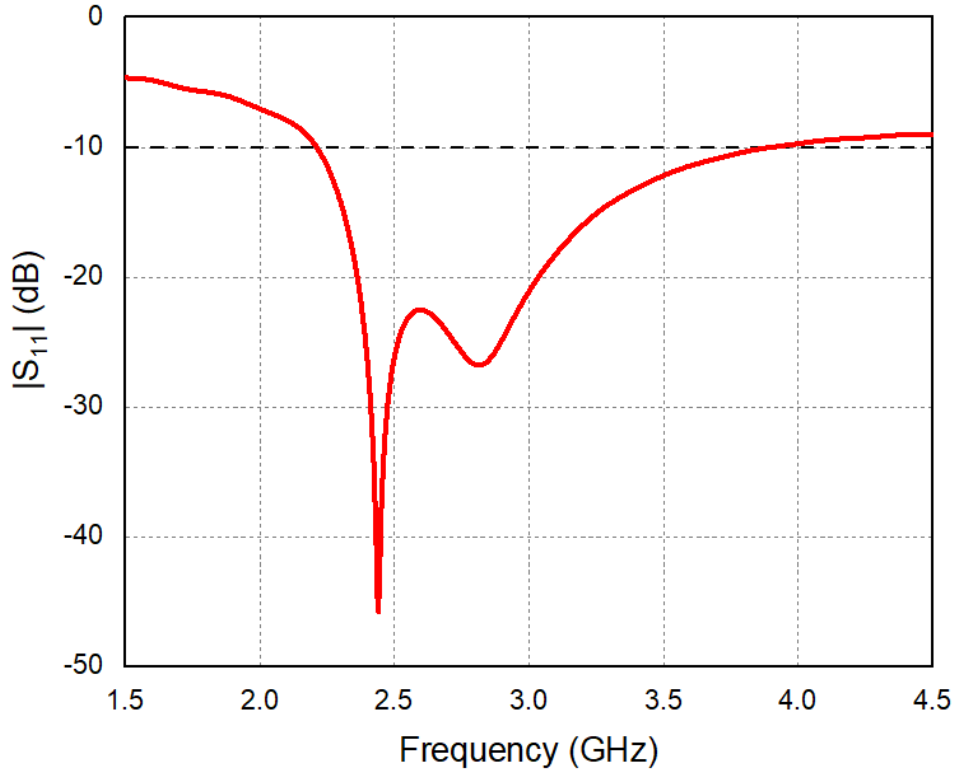


Fig.3.26 Final reflection coefficient (S_{11}) of the flexible pattern-reconfigurable antenna.

3.4.5 Wearable Pattern-Reconfigurable Antenna Design and Operation

In the previous section, the pattern-reconfigurable antenna was designed with flexible features that showed enhanced performance characteristics under various degrees of deformations and curvature. However, these bending tests were performed in free space. Since body-worn devices are operated on real body surfaces, the effects of the body on the antenna performance must be properly analyzed in simulation to effectively characterize the antenna. In this way, the result largely reflects the real human body effects with very minor discrepancies. To calculate the on-body effects of the antenna, appropriate phantom models that simulate the real human body are used. There are many types of biological phantom models that are widely used in the on-body simulation of electromagnetic (EM) structures. In this work, the simple rectangular and cylindrical phantom models are employed in the on-body performance of the flexible reconfigurable antenna. Additionally, the male right-hand model provided in HFSS together with the complete human voxel model in CST is also used in the simulation. The three-layer phantom model consists of 2 mm skin ($\epsilon_r = 38, \sigma = 1.5 \text{ s/m}$), 4 mm fat ($\epsilon_r = 5.3, \sigma = 0.1 \text{ s/m}$), and a 10 mm muscle ($\epsilon_r = 52.1, \sigma = 1.7 \text{ s/m}$) with a full length of 100 mm \times 100 mm. Its equivalent cylindrical model with a bone structure ($\epsilon_r = 18.5, \sigma = 0.8 \text{ s/m}$) are both illustrated in Fig.3.27, where ϵ_r and σ are the material's permittivity and conductivity

properties respectively. To observe the body effects on the antenna, it is initially placed directly on the body without any separation distance between the antenna and the skin layer as depicted in Fig.3.28.

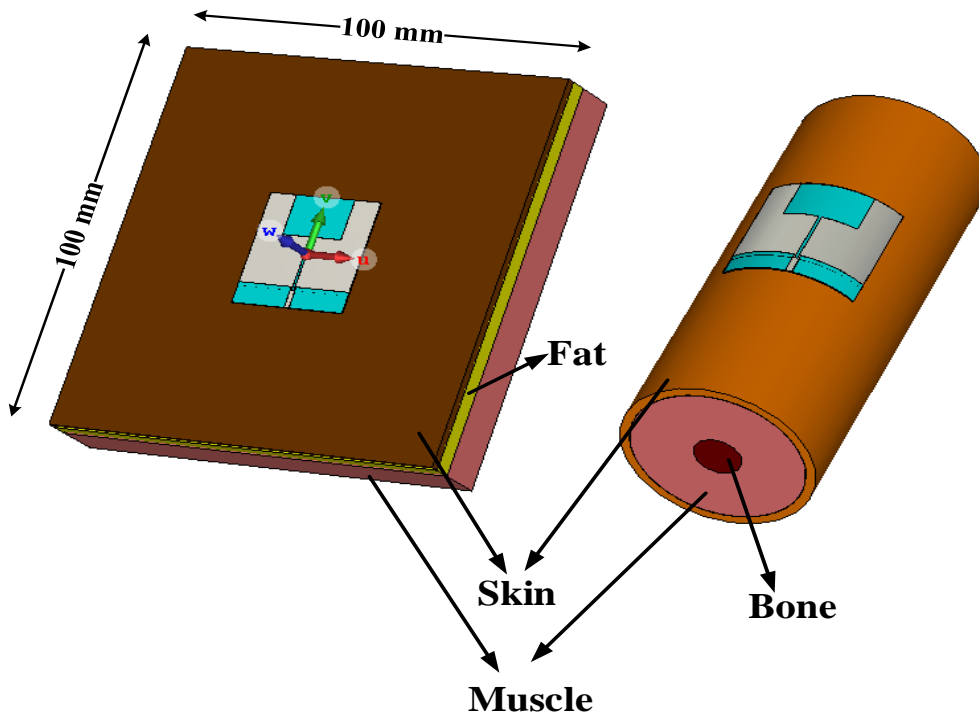


Fig.3.27 Rectangular and cylindrical three-layer phantom models.

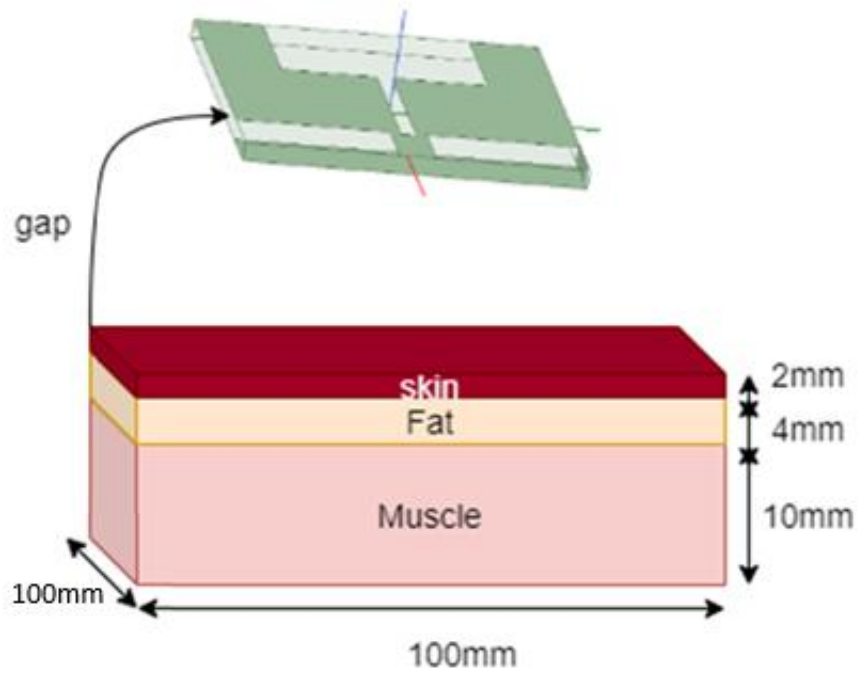


Fig.3.28 Antenna placement on body phantom

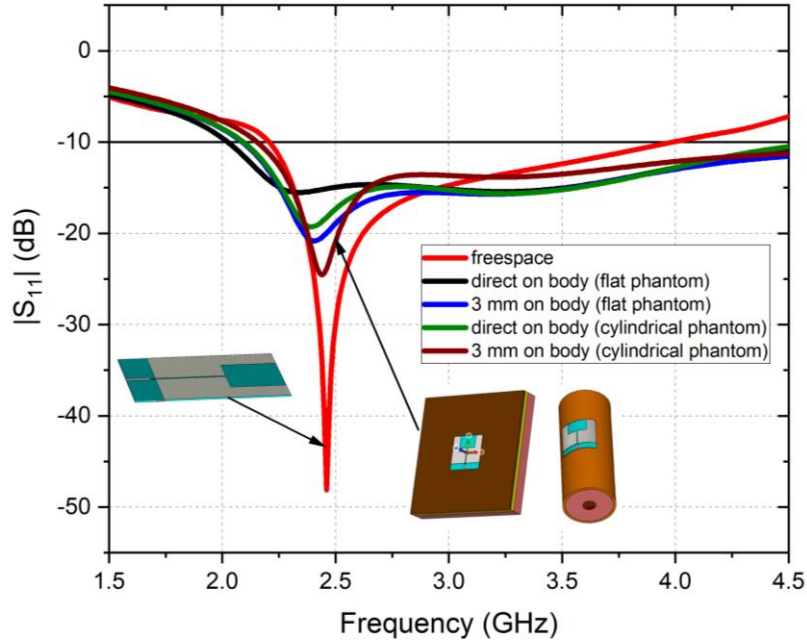


Fig.3.29 Simulated S_{11} of the flexible reconfigurable antenna in free space and on-body.

However, a gap between the antenna and the body layer is increased to up to 3 mm to account for clothing and other conditions when the antenna is operated at a distance away from the body. The simulated S_{11} of the flexible reconfigurable antenna is analyzed for the rectangular and cylindrical phantoms as presented in Fig.3.29. It can be observed, that there is no detuning in the resonant frequency at 2.45 GHz when the antenna is directly placed on the body and operated at a 3 mm distance from the body. Although the magnitude of the S_{11} is noticed to be high when the antenna is directly placed on the body, this is expected due to the conductive nature of the tissues involved. However, their magnitudes are still well under -10 dB. This ensures that the impedance of the antenna is not mismatched at the resonant frequency as compared to [86], [87].

3.4.6 Radiation Patterns

The radiation pattern obtained in free space is compared with the on-body performance of the antennas. It is evident in Fig.3.30 that the directionality of the antenna is well preserved in both E-plane and H-plane when the antenna is operated directly on or close to the body at a distance of 3 mm. It is also shown that fairly stable radiation patterns without any significant offsets in the main lobe radiation patterns are achieved. As expected, the directivity of the antenna is slightly reduced at the minimum input power of 0 dBm of the radiated energy as the unidirectional radiation attained in free space is not distorted in the body environment.

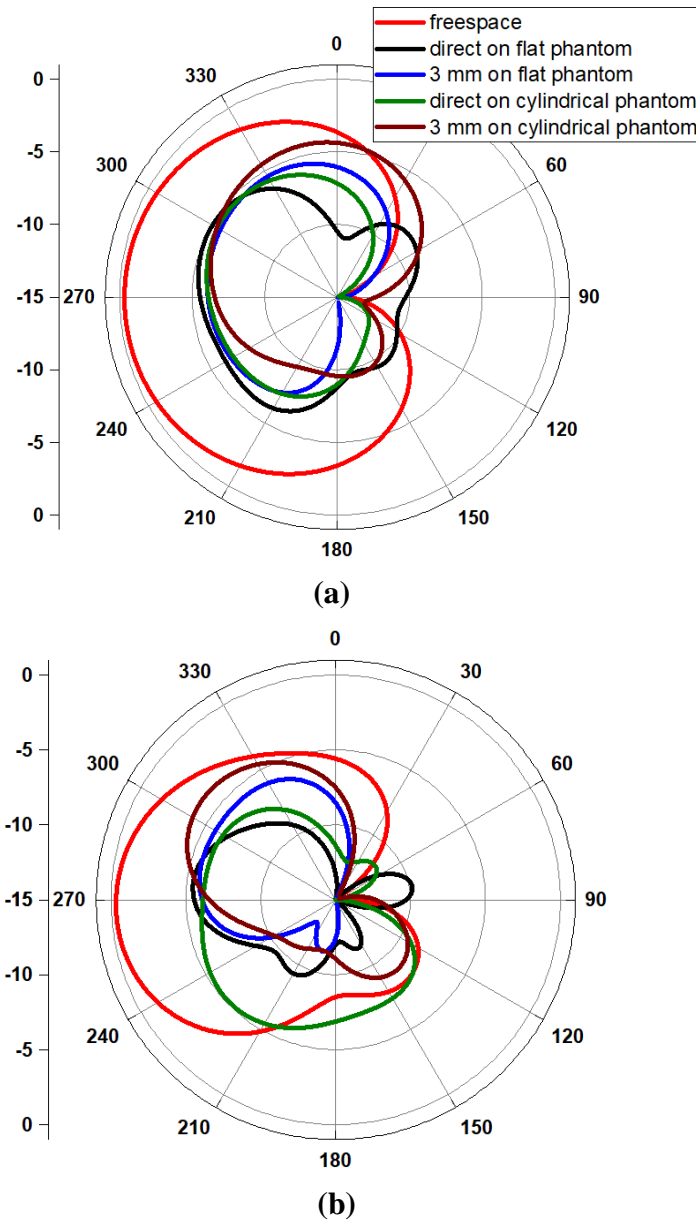


Fig.3.30 Normalized radiation pattern of the flexible reconfigurable antenna in free space and on-body at 2.45 GHz. (a) $x - y$ plane (b) $y - z$ plane.

This is validated by the 1 g peak spatial average specific absorption rate (SAR) performance of the flexible reconfigurable antenna as shown in Fig.3.31.

3.4.7 Simulation of Specific Absorption Rate

It is shown that extremely low SAR levels of approximately 0.39 W/kg, 0.23 W/kg and 0.15 W/kg are recorded even when the antenna is mounted directly on the 1000 kg/m^3 rectangular, cylindrical, hand and high resolution Hugo voxel phantoms respectively in Fig.3.31 and Fig.3.32. The simulated SAR is well below the standard safety limit of 1.6 W/kg

set by the FCC. Additionally, the 1 *g* and 10 *g* averaging SAR is also conducted on the antenna directly placed on-body and 3 mm away from the body and the results are summarized in Table 3.5. All simulations were carried out in the commercial high-frequency structure simulator (HFSS) and the computer simulation technology (CST) software. It is important to state that the low-level SARs was achieved without the use of additional large reflector surfaces that generally leads to bulky and large antenna sizes which are not compact enough for on-body implementation.

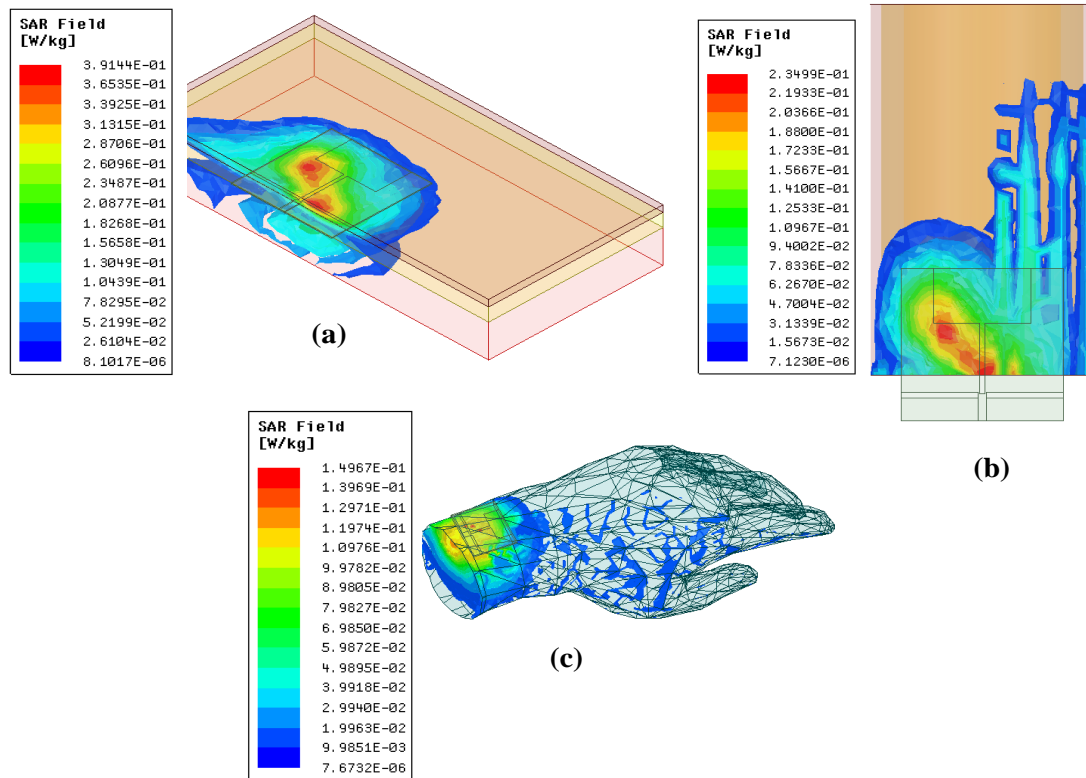


Fig.3.31 Specific absorption (SAR) rate performance of the flexible pattern-reconfigurable antenna at 2.45 GHz. (a) Directly on rectangular phantom (b) Directly on cylindrical phantom (c) Directly on hand phantom.

Table 3. 5 Simulated Maximum Spatial Average SAR Performance of the Proposed Flexible Reconfigurable Antenna

SAR Averaging	Direct on body (Rectangular phantom) [W/kg]	3 mm away from body (Rectangular phantom) [W/kg]	Direct on body (Cylindrical phantom) [W/kg]	3 mm away from body (Cylindrical phantom) [W/kg]	On Hugo voxel model
1 <i>g</i>	0.39	0.1	0.23	0.16	0.46
10 <i>g</i>	0.28	0.08	0.15	0.14	0.28

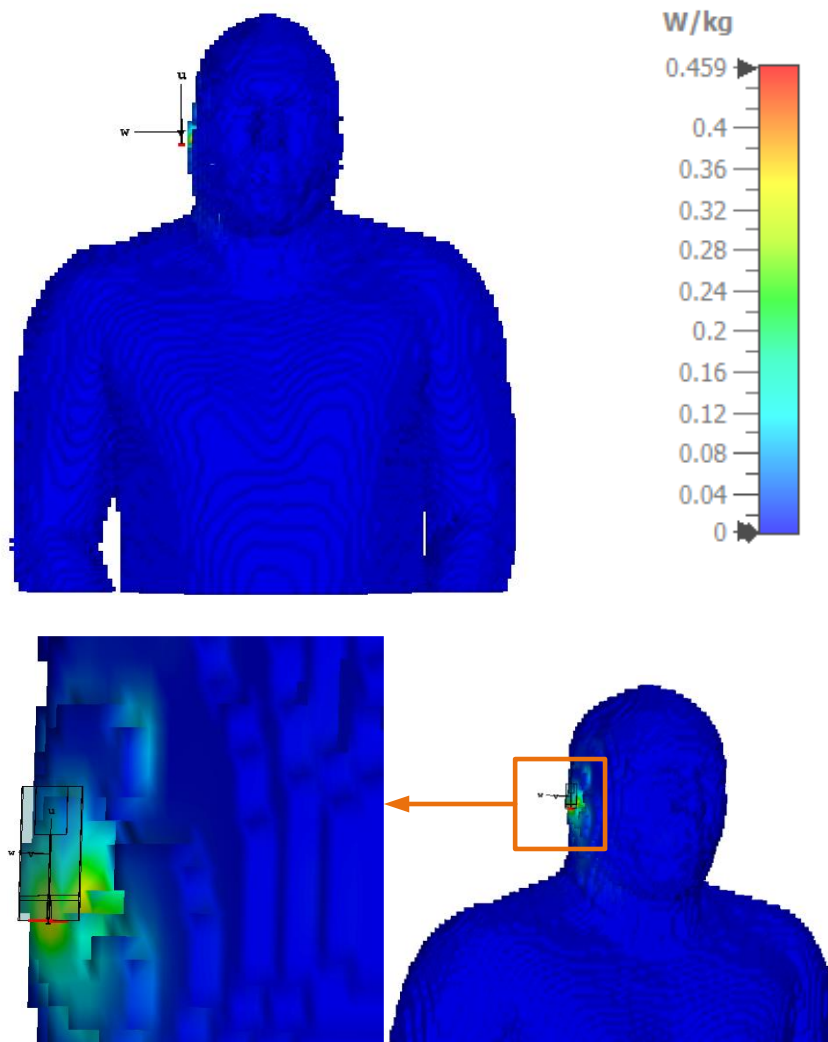


Fig.3.32 Specific absorption (SAR) rate performance of the flexible pattern-reconfigurable antenna at 2.45 GHz on a Hugo voxel model (size = 2^3 mm^3).

CHAPTER FOUR

RESULTS AND DISCUSSIONS

4.1 Antenna Fabrication

The design and operation of a single side stubbed unidirectional monopole antenna printed on a rigid FR-4 substrate have been introduced in the previous chapter and the simulation results equally presented. The reconfigurable extension of the antenna has also been demonstrated using two RF PIN diodes incorporated as the metallic side stubs to generate switched radiation patterns based on the defined switching modes. Meanwhile, the flexible pattern-reconfigurable antenna based on flexible FR-4 and flexible Rogers RO4003 substrates has also been designed. The single side-stub antenna is fabricated on a rigid FR-4 substrate and typically connected to an SMA connector for measurement. Similarly, the reconfigurable version is also fabricated on the same substrate as shown in Fig.4.1. Meanwhile, the RF PIN diodes are incorporated by creating a via to connect the monopole and the ground plane. Another way of realizing the DSM8100-000 PIN diode is by simple soldering. This approach is known to introduce some degree of parasitics. However, for best results, the thermocompression bonding technique which involves the pressing of the beam leads against the metalized antenna substrate under proper conditions of heat and pressure is recommended [83]. The fabrication process of the ultra-thin flexible reconfigurable antenna is different from the technique used in realizing the rigid substrate antenna.

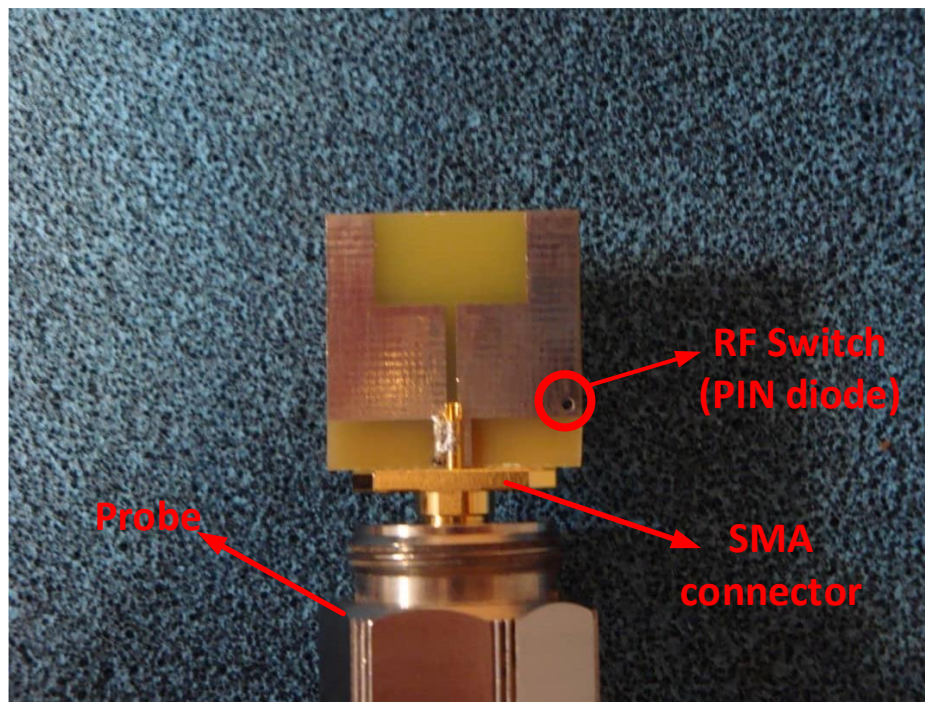


Fig.4.1 Fabricated prototype of the proposed pattern-reconfigurable antenna.

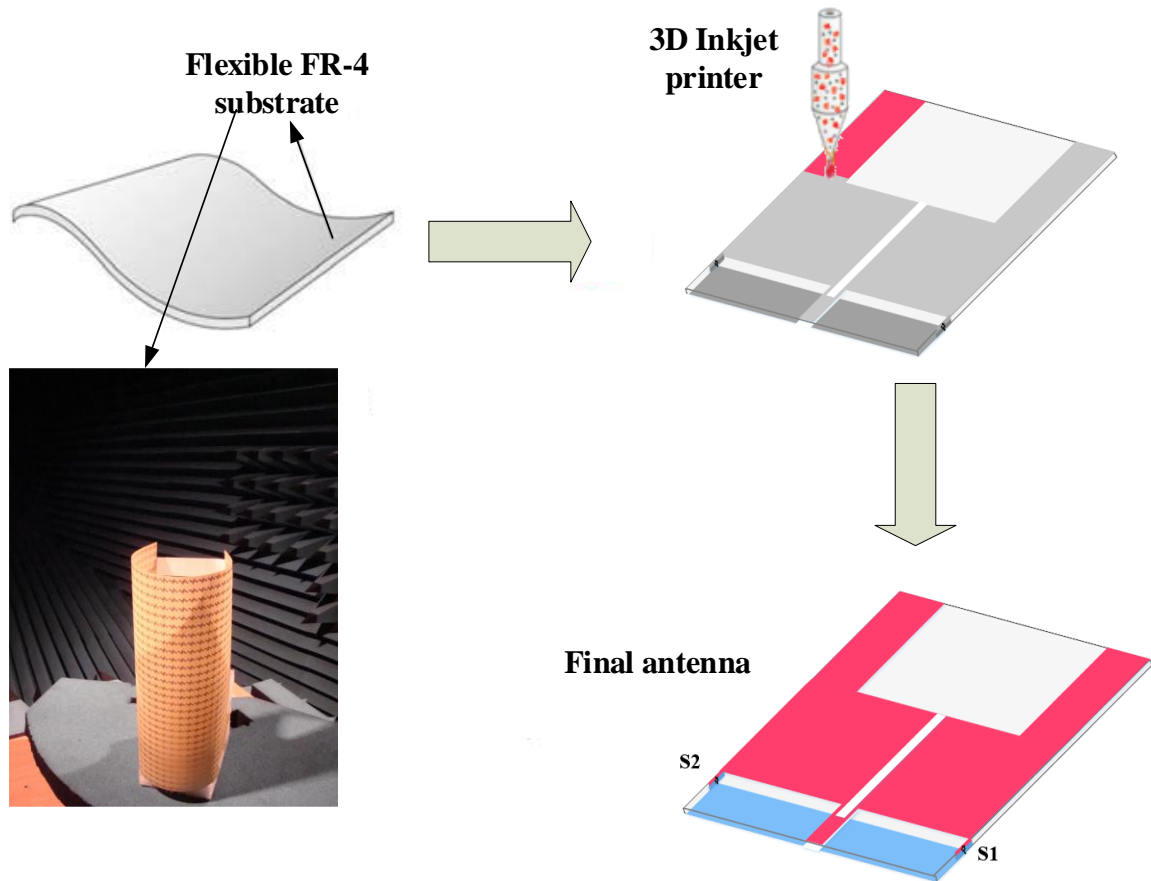


Fig.4.2 Fabrication process of the flexible radiation pattern-reconfigurable antenna.

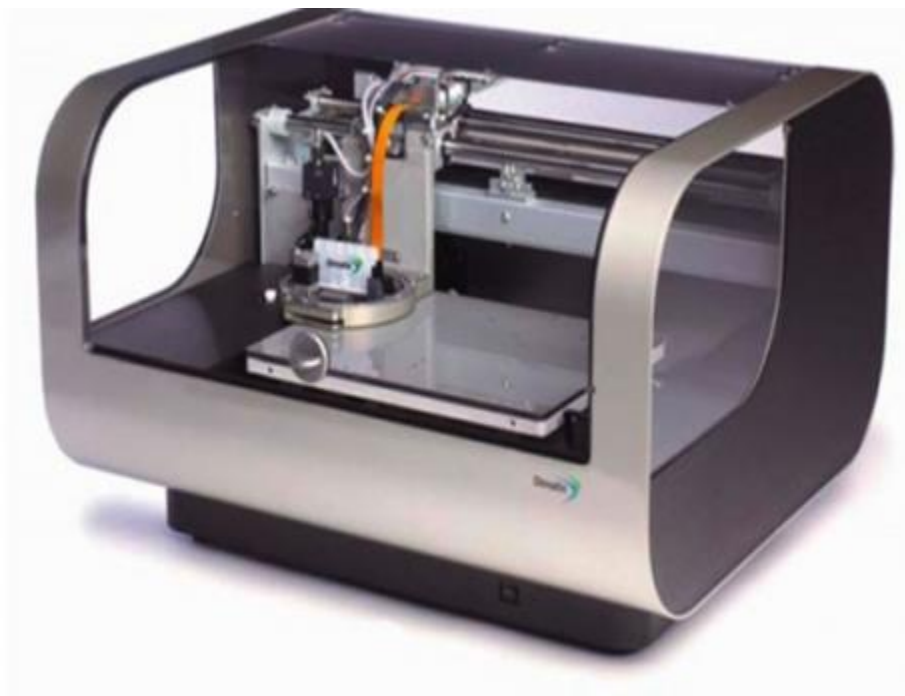


Fig.4.3 Fujifilm Dimatix 3D materials printer (DMP-2850)

Recently, the inkjet printing technique which employs accurate fused deposition modeling (FDM) to directly write highly conductive inks like silver nanoparticles on defined patterns to form an additive structure has been commercially introduced. This technique has been widely used to fabricate complex antenna structures on several of flexible materials such as the Kapton substrate and other textile materials. The fabrication process begins with the selection of the appropriate flexible substrate material and then the deposition of the conductive fluid material on a defined pattern on the substrate is performed by the micrometer nozzle of the inkjet printer as illustrated in Fig.4.2. A typical Fujifilm Dimatix materials printer (DMP-2850) is shown in Fig.4.3. The fabrication technique is known to provide high resolution, low cost, clean and fast manufacturing which enables rapid prototyping of printed devices.



Fig.4.4 Performance of the fabricated flexible pattern reconfigurable antenna on a stuffed animal body.

4.2 Far Field Measurements

4.2.1 On-Body Measurements

To practically characterize the conformable nature of the flexible reconfigurable antenna, it is mounted directly on a stuffed animal body, and the far-field properties are analyzed at different positions of the antenna in the anechoic chamber as shown in Fig.4.4. Further measurements of the antenna characteristics are verified by operating it directly on the hand of an average adult man as shown in Fig.4.5 to depict the wrist position operation. In Fig.4.6, the simulated 3D gain of the flexible pattern-reconfigurable antenna on the Hugo voxel model is shown. The two directional modes are realized by the appropriate switching of the incorporated PIN diodes. It is observed that the alternate switching of the PIN diodes achieves a directional pattern with a reasonable directivity of 2.11 dBi. It is stated for emphasis that, the proposed antenna ensures directional pattern even on the high-resolution Hugo phantom shown in Fig.4.6. The radiated energy is observed to be directed away from the body, hence, minimizing absorption and SAR. In all, the desired properties of an on-body antenna have been well achieved with the proposed flexible radiation pattern reconfigurable antenna. It is expedient to note that the measurement results are not compared with simulation due to its unavailability at the time of preparing this thesis. This is acknowledged as a limitation in this work, however, these results shall be presented in future publications.

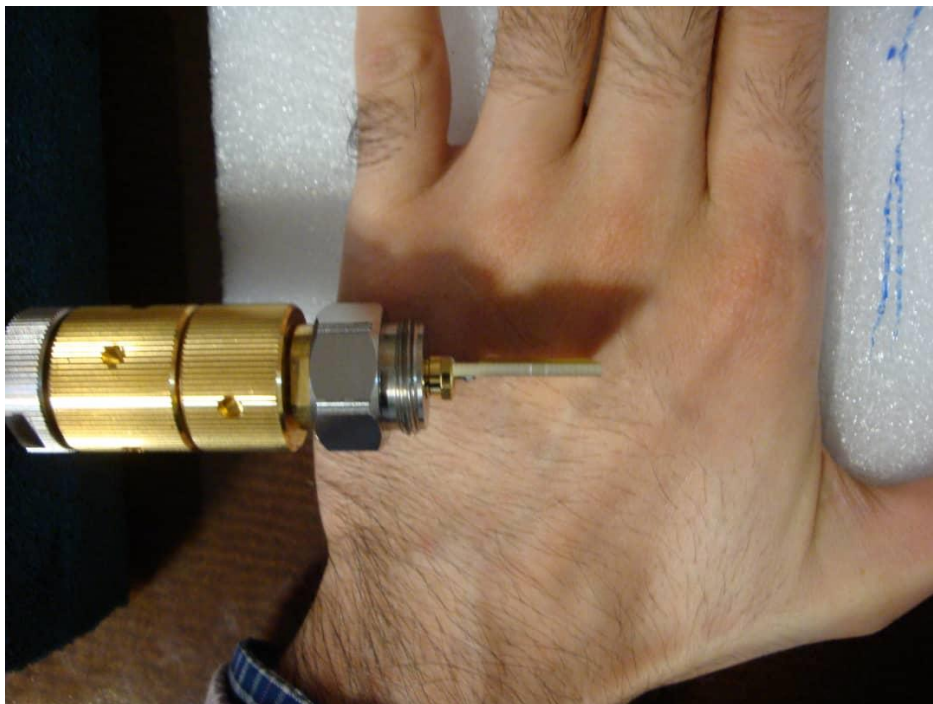


Fig 4.5 Performance of the fabricated flexible pattern reconfigurable antenna on an adult human hand.

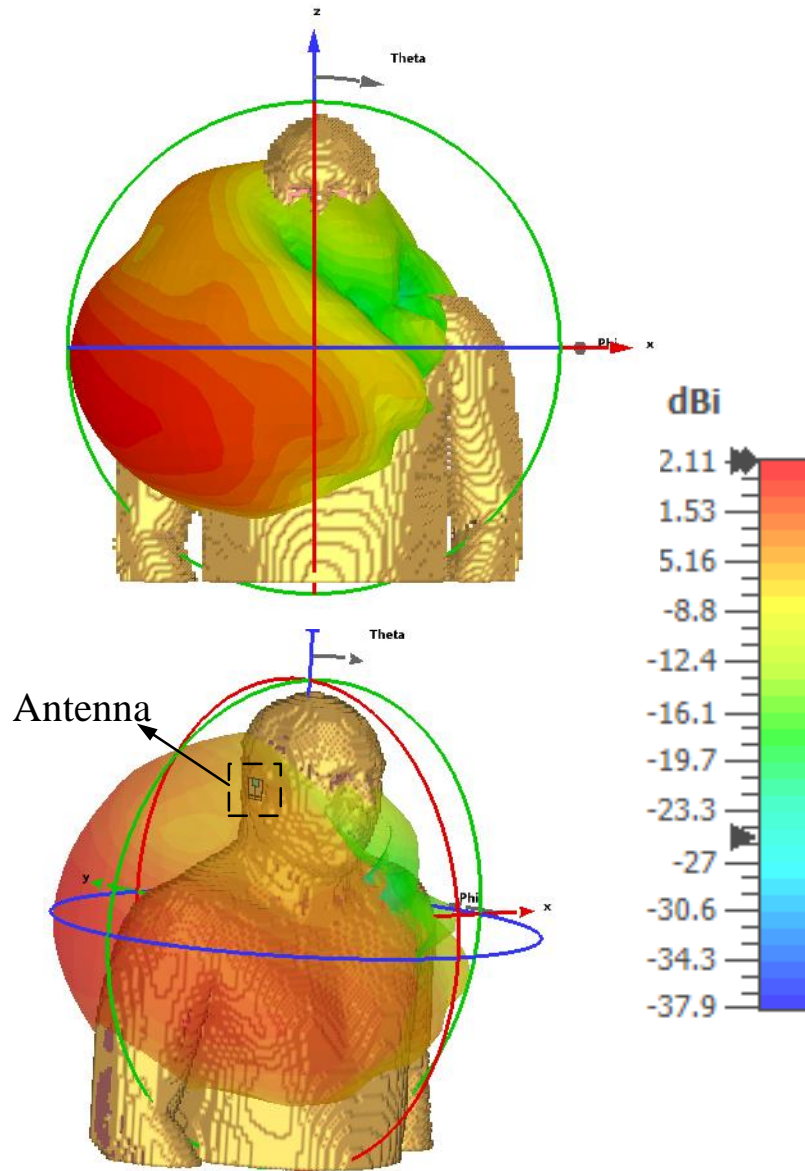


Fig.4.6 3D gain plot of the proposed antenna on human voxel model (front and side view)

4.2.2 Axial Ratio Bandwidth

Circular polarization (CP) of waves in space can generally be decomposed into the right-handed (RHCP) and left-handed (LHCP) rotational electric fields which are produced by two orthogonal waves that are 90° out of phase. The axial ratio (AR) specifies the purity of the CP waves and it is denoted by the ratio of the maximum to the minimum electric fields expressed in dB as:

$$AR = 20 \log \left(\frac{E_{max}}{E_{min}} \right) \quad (14)$$

As discussed in the earlier sections, the introduction of the side stub causes the necessary perturbation to detune the degenerate mode at the resonant frequency which satisfies the

required condition for CP radiation. Hence, the switching state of the RF PIN diodes effectively produces the clockwise and counter-clockwise RHCP and LHCP electric fields respectively. The simulated 3 dB AR bandwidth in the operational mode-1 and mode-2 of the reconfigurable antenna in the broadside direction was found to be 140 MHz (2.52 – 2.38 GHz) centered around the resonant frequency, 920 MHz (2.88 – 3.80 GHz) and 950 MHz (3.89 – 2.94 GHz) respectively as shown in Fig.4.7.

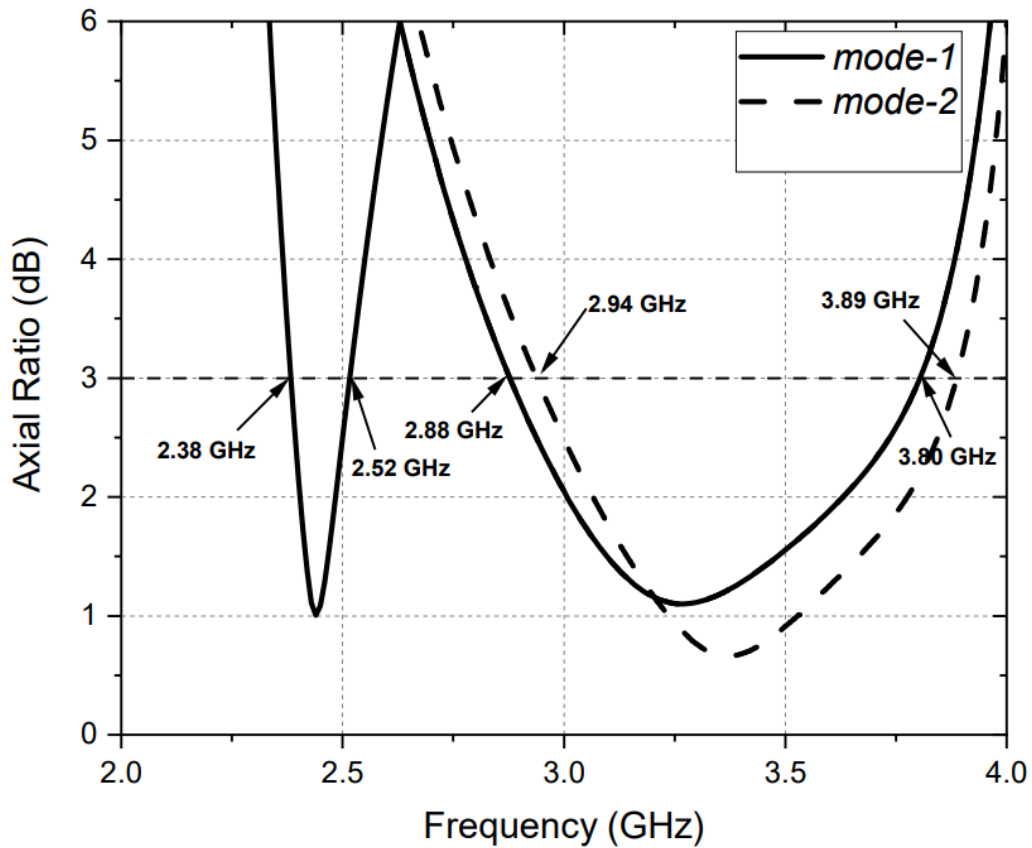


Fig.4.7 Simulated axial ratio of the proposed flexible reconfigurable antenna.

CHAPTER FIVE

CONCLUSION AND FUTURE WORKS

5.1 Conclusion

The radiation pattern reconfiguration of a compact, low-profile printed monopole antennas (PMAs) have been proposed in this current research for on-body communications. The design and operation of these antennas followed a comprehensive literature review of body-centric wireless communication (BWC) systems, planar monopole antennas, antenna reconfiguration mechanisms. Additional theory on flexible antenna and human body coupling effects on antennas were also explored. It has been established in the literature that strong body coupling effects lead to antenna mismatch that causes detuning and effectively renders an omnidirectional antenna unidirectional. This sets the first objective of this research to convert the conventional omnidirectional radiation of a PMA to unidirectional. To this end, the design and analysis of a directional printed monopole antenna using a simple metallic shorting side stub have been proposed for the 2.45 GHz ISM band. The reconfigurable extension of this antenna has also been realized via RF PIN diodes. Simulation results provided in chapter 3 verifies the operation of the reconfigurable antenna in generating three distinct radiation modes i.e. Mode-0, Mode-1 and Mode-2 based on the appropriate switching of the PIN diodes.

Moreover, the need to integrate conformable and wearable features into the reconfigurable antenna is essential in meeting the design requirements of an on-body antenna. The flexible configuration of the reconfigurable antenna was realized using flexible FR4 and Rogers RO4003 substrates. Flexibility and conformability tests in the form of antenna bending and subsequent placement on human phantoms were performed respectively. It is shown via simulation that body loading and various degrees of antenna curvature do not cause any severe detuning in the impedance bandwidth and radiation pattern of the antenna. Meanwhile, the characteristic linkage property that prevents the independent tuning of antenna properties is also shown in simulation to be successfully decoupled enabling the tuning of the radiation pattern without any effect on the resonant frequency. An $S_{11} < -20 \text{ dB}$ is achieved at 2.45 GHz.

Further analysis from the surface current distribution of the antenna reveals orthogonal electric fields that generate circular polarization with axial ratio ($A.R$) $< 3 \text{ dB}$ at the design frequency. This is a key feature particularly in on-body applications where random body postures lead to polarization mismatch. The circular polarization is immune to such body effects and maintains

the communication link. Table 5.1 compares this current work with some recently published BWC antennas in terms of compactness, the technique used, reconfigurability, flexibility, polarization, and SAR performance.

Experimental SAR measurements conducted on a real stuffed animal body and on an average adult human hand agree well with those performed in simulation. SAR levels of 0.46 W/kg and 0.28 W/kg averaged over 1g and 10g of tissue respectively were recorded on a Hugo voxel model. This is found to be well below the FCC limit. The overall size of the antenna measures a very compact square size of only $0.235\lambda_0$ and a low-profile of $0.002\lambda_0$. This suggests that the proposed flexible pattern-reconfigurable antenna is a strong candidate for flexible, wearable, and general body-centric wireless communication systems.

Table 5.1 Comparison of the Proposed Flexible Pattern-Reconfigurable Antenna with Previous Research Works

Reference work	Antenna Size (mm ³) (λ_0^3)	Technique used	Reconfigurable type	Substrate type	Polarization	SAR Performance (1 g / 10 g) W/kg
[68]	$13.4 \times 14 \times 13.77$ ($0.23\lambda \times 0.24\lambda \times 0.24\lambda$)	Microstrip -line monopole with a reflector.	N/A	Solid Rogers RO4003C and RO3010	Circular	0.182/0.106
[76]	$89 \times 83 \times 7.7$ ($0.727\lambda \times 0.678\lambda \times 0.063\lambda$)	Folded slot antenna with AMC backing	Frequency (2.45 GHz, 3.3 GHz) using PIN diodes	Flexible Rogers RO3003	Linear	0.29/–
[77]	$40 \times 50 \times 0.25$ ($0.22\lambda \times 0.27\lambda \times 0.001\lambda$)	Triangular monopole with semicircular stub	Frequency (1.8 GHz, 2.1 GHz) Radiation pattern (180°)	Flexible Rogers 5880LZ	Linear	N/A
[78]	$25 \times 25 \times 0.12$ ($0.20\lambda \times 0.20\lambda \times 0.00098\lambda$)	π – section CRLH antenna with AMC backing	N/A	Liquid Crystalline Polymer	Linear	0.22 / 0.105 at 100mW power with AMC
[79]	$170 \times 170 \times 17.5$ ($1.3\lambda \times 1.3\lambda \times 0.13\lambda$)	Dual feed stub-loaded circular patch antenna	Radiation Pattern (0°, 90°)	Solid metal-clad	Linear	N/A
[81]	$51.25 \times 51.25 \times 5.625$ ($0.41\lambda \times 0.41\lambda \times 0.045\lambda$)	Truncated loop ring resonator	N/A	Polydimethylsiloxane (PDMS)	Circular	0.18/–
This work	$28.8 \times 28.8 \times 0.25$ ($0.235\lambda \times 0.235\lambda \times 0.0020\lambda$)	Edge-stubbed slotted monopole antenna without reflector.	Radiation pattern (0°, ± 90°)	Flexible FR-4	Circular	0.46/0.28

5.2 Recommendation and Future Works

The recommendations derived from this research are geared towards future works and are discussed in the following;

- The design of the proposed radiation pattern reconfigurable printed monopole antenna with hard and flexible substrate materials using two RF PIN diodes has been examined. The performance characteristics have also been investigated for flat and curved configurations. However, the full radiation pattern scanning property of the antenna is limited by the solid-state switches implemented. This leads to discrete tuning that provides only three main degrees of freedom in the radiation pattern for this work. It is however desired to achieve active beam scanning that is particularly crucial in multipath scenarios. In this way, an active phased array mechanism can be implemented in replacement of the RF PIN diodes to achieve continuous beam steering and null effect to significantly improve coverage and capacity.
- Following the implementation of the phased array system, a dynamic and adaptive scanning extension of the antenna can be realized by introducing machine learning techniques that enables the antenna to switch features based on its environmental conditions rather than predefined logic states as in this current work. This conveniently makes the antenna intelligent for modern wearable applications. The next step is to redesign the antenna to include a full feature of smart properties.
- Further investigations performed on the antenna revealed both frequency and polarization reconfiguration capabilities. This can be extensively analyzed in simulation to achieve all reconfiguration types i.e. radiation pattern, frequency, and polarization on the same antenna. Additionally, it is recommended that the entire human body effects on the antenna be performed on higher resolution voxel models to ideally characterize the on-body antenna.

REFERENCES

- [1] J. Y. K. Mehmet R. Yuce, *Wireless Body Area Networks: Technology, Implementation, and Applications*, 1st Edition, Pan Stanford Publishing, 2012.
- [2] F. Farzami, S. Khaledian, B. Smida, and D. Erricolo, "Pattern-Reconfigurable Printed Dipole Antenna," *IEEE Antennas Wirel. Propag. Lett.*, vol. 16, pp. 1151–1154, 2017.
- [3] U. M. Antenna, T. Aboufoul, S. Member, C. Parini, X. Chen, and S. Member, "Pattern-Reconfigurable Planar Circular Ultra-Wideband Monopole Antenna," vol. 61, no. 10, pp. 4973–4980, 2013.
- [4] R. Li, H. Yang, B. Liu, Y. Qin, and Y. Cui, "Theory and Realization of a Pattern-Reconfigurable Antenna Based on Two Dipoles," *IEEE Antennas Wirel. Propag. Lett.*, vol. 17, no. 7, pp. 1291–1295, 2018.
- [5] S. Sam, H. Kang, and S. Lim, "Frequency reconfigurable and miniaturized substrate integrated waveguide interdigital capacitor (SIW-IDC) antenna," *IEEE Trans. Antennas Propag.*, vol. 62, no. 3, pp. 1039–1045, 2014.
- [6] N. Nguyen-Trong, A. Piotrowski, and C. Fumeaux, "A Frequency-Reconfigurable Dual-Band Low-Profile Monopolar Antenna," *IEEE Trans. Antennas Propag.*, vol. 65, no. 7, pp. 3336–3343, 2017.
- [7] M. Shirazi, J. Huang, T. Li, and X. Gong, "A Switchable-Frequency Slot-Ring Antenna Element for Designing a Reconfigurable Array," *IEEE Antennas Wirel. Propag. Lett.*, vol. 17, no. 2, pp. 229–233, 2018.
- [8] Y. J. Sung, T. U. Jang, and Y. S. Kim, "A reconfigurable microstrip antenna for switchable polarization," *IEEE Microw. Wirel. Components Lett.*, vol. 14, no. 11, pp. 534–536, 2004.
- [9] K. M. Mak, H. W. Lai, K. M. Luk, and K. L. Ho, "Polarization reconfigurable circular patch antenna with a C-Shaped," *IEEE Trans. Antennas Propag.*, vol. 65, no. 3, pp. 1388–1392, 2017.
- [10] P. S. Hall and Y. Hao, "Antennas and Propagation for Body-Centric Wireless Networks," *Artech House*, 2006.
- [11] P. S. Hall *et al.*, "Antennas and propagation for on-body communication systems," *ANTEM 2005 - 11th Int. Symp. Antenna Technol. Appl. Electromagn. Conf. Proc.*, 2005, doi: 10.1109/ANTEM.2005.7852088.
- [12] H. C. Mohanta, A. Z. Kouzani, and S. K. Mandal, "Reconfigurable antennas and their applications," *Univers. J. Electr. Electron. Eng.*, vol. 6, no. 4, pp. 239–258, 2019.
- [13] J. T. Bernhard, *Reconfigurable antennas*, vol. 4. 2007.
- [14] "IEEE Standard Definitions of Terms for Antennas.," vol. AP-31, no. 6. 2014.
- [15] E. Erdil, K. Topalli, M. Unlu, O. A. Civi, and T. Akin, "Frequency Tunable Microstrip Patch Antenna Using RF MEMS Technology," *IEEE Trans. Antennas Propag.*, vol. 55, no. 4, pp. 1193–1196, 2007.
- [16] M. Shrivastava, R. Agrawal, and P. Tapashetti, "Design and Development of Reconfigurable Antenna Using MEMS," *2018 Int. Conf. Adv. Comput. Telecommun. ICACAT 2018*, pp. 6–10, 2018.
- [17] S. Nikolaou *et al.*, "Pattern and frequency reconfigurable annular slot antenna using pin diodes," *IEEE Trans. Antennas Propag.*, vol. 54, no. 2, pp. 439–448, 2006.
- [18] A. Sonker, A. P. Deo, and R. Kumar, "Design of Reconfigurable Slot Antenna Using Varactor Diode," *Int. Conf. Comput. Commun. Electron.*, pp. 511–515, 2017.
- [19] C. Li, S. Xu, F. Yang, and M. Li, "Design and Optimization of a Mechanically Reconfigurable Reflectarray Antenna with Pixel Patch Elements Using Genetic Algorithm," *2019 IEEE MTT-S Int. Wirel. Symp. IWS 2019 - Proc.*, vol. 1, pp. 2019–2021, 2019.
- [20] Y. Tawk, "Physically Controlled CubeSat Antennas With an Adaptive Frequency

- Operation,” *IEEE Antennas Wirel. Propag. Lett.*, vol. 18, no. 9, pp. 1892–1896, 2020.
- [21] C. Wang, J. C. Yeo, H. Chu, C. T. Lim, and Y. X. Guo, “Design of a reconfigurable patch antenna using the movement of liquid metal,” *IEEE Antennas Wirel. Propag. Lett.*, vol. 17, no. 6, pp. 974–977, 2018.
- [22] A. Andy, P. Alizadeh, K. Z. Rajab, T. Kreouzis, and R. Donnan, “An optically-switched frequency reconfigurable antenna for cognitive radio applications,” *2016 10th Eur. Conf. Antennas Propagation, EuCAP 2016*, pp. 5–8, 2016.
- [23] C. J. Panagamuwa, A. Chauraya, and J. C. Vardaxoglou, “Frequency and beam reconfigurable antenna using photoconducting switches,” *IEEE Trans. Antennas Propag.*, vol. 54, no. 2, pp. 449–454, 2006.
- [24] C. G. Christodoulou, Y. Tawk, S. A. Lane, and S. R. Erwin, “Reconfigurable antennas for wireless and space applications,” *Proc. IEEE*, vol. 100, no. 7, pp. 2250–2261, 2012.
- [25] A. Ometov *et al.*, “A Survey on Wearable Technology: History, State-of-the-Art and Current Challenges,” *Comput. Networks*, vol. 193, no. December 2020, p. 108074, 2021.
- [26] D. Sim, J. H. Kwon, Y. J. Yoon, and S. il Kwak, “Design of PIFA With Metamaterials for Body-SAR Reduction in Wearable Applications,” vol. 59, no. 1, pp. 1–4, 2016.
- [27] A. H. Kusuma *et al.*, “A new low sar antenna structure for wireless handset applications,” *Prog. Electromagn. Res.*, vol. 112, no. May 2014, pp. 23–40, 2011.
- [28] K. Agarwal, Y. Guo, B. Salam, L. Chee, and W. Albert, “Latex based Near-Endfire Wearable Antenna backed by AMC Surface,” *IEEE MTT-S*, pp. 13–15, 2013.
- [29] R. L. Haupt and M. Lanagan, “Reconfigurable Antennas,” vol. 55, no. 1, pp. 49–61, 2013.
- [30] N. O. Parchin, H. J. Basherlou, Y. I. A. Al-Yasir, R. A. Abd-Alhameed, A. M. Abdulkhaleq, and J. M. Noras, “Recent developments of reconfigurable antennas for current and future wireless communication systems,” *Electron.*, vol. 8, no. 2, pp. 1–17, 2019.
- [31] N. O. Parchin, H. J. Basherlou, Y. I. A. Al-Yasir, A. M. Abdulkhaleq, and R. A. Abd-Alhameed, “Reconfigurable antennas: Switching techniques— a survey,” *Electron.*, vol. 9, no. 2, 2020.
- [32] L. A. N. Man, S. Committee, and I. Computer, *IEEE Standard for Local and metropolitan area networks - Wireless Body Area Networks*, no. February. 2012.
- [33] K. S. Sultan, H. H. Abdullah, E. A. Abdallah, and E. A. Hashish, “Low SAR, compact and multiband antenna for mobile and wireless communication,” *2nd Middle East Conf. Antennas Propagation, MECAP 2013*, vol. 2014, 2014.
- [34] G. A. Conway, W. G. Scanlon, and D. Linton, “Low-profile microstrip patch antenna for over-body surface communication at 2.45 GHz,” *IEEE Veh. Technol. Conf.*, pp. 392–396, 2007.
- [35] M. M. Khan, I. Mobin, G. Palikaras, and E. Kallos, “Study of a small printed quasi-self-complementary ultra wideband antenna for on-body applications,” *2012 4th Comput. Sci. Electron. Eng. Conf. CEEC 2012 - Conf. Proc.*, pp. 179–183, 2012.
- [36] K. R. Foster and H. P. Schwan, “Dielectric properties of tissues and biological materials: a critical review.,” *Crit. Rev. Biomed. Eng.*, vol. 17, no. 1, pp. 25–104, 1989.
- [37] F. A. Duck, *Physical Properties of Tissue. A Comprehensive Reference Book*, vol. 18, no. 4. 1990.
- [38] S. Gabriel, R. W. Lau, and C. Gabriel, “The dielectric properties of biological tissues: III. Parametric models for the dielectric spectrum of tissues,” *Phys. Med. Biol.*, vol. 41, no. 11, pp. 2271–2293, 1996.
- [39] B. Clarke, “Measurement of the dielectric properties of materials at RF and microwave frequencies,” *Microw. Meas. Third Ed.*, no. September 1993, pp. 409–458, 2007.
- [40] K. S. Cole and R. H. Cole, “Dispersion and absorption in dielectrics I. Alternating

- current characteristics,” *J. Chem. Phys.*, vol. 9, no. 4, pp. 341–351, 1941.
- [41] A. Mansoul, F. Ghanem, M. R. Hamid, and M. Trabelsi, “A selective frequency-reconfigurable antenna for cognitive radio applications,” *IEEE Antennas Wirel. Propag. Lett.*, vol. 13, pp. 515–518, 2014.
- [42] N. Nguyen-trong, L. Hall, and C. Fumeaux, “A Frequency- and Pattern-Reconfigurable Center-Shorted Microstrip Antenna,” *IEEE Antennas Wirel. Propag. Lett.*, vol. 15, pp. 1955–1958, 2016.
- [43] V. Sokol and M. Rütshlin, “Reconfigurable Antenna Simulation,” *IEEE Microw. Mag.*, no. November, p. 2014, 2014.
- [44] S. Bildik, S. Dieter, C. Fritsch, W. Menzel, and R. Jakoby, “Reconfigurable Folded Reflectarray Antenna Based Upon Liquid Crystal Technology,” *IEEE Trans. Antennas Propag.*, vol. 63, no. 1, pp. 122–132, 2015.
- [45] C. M. Lee and C. W. Jung, “Radiation-pattern-reconfigurable antenna using monopole-loop for fitbit flex wristband,” *IEEE Antennas Wirel. Propag. Lett.*, vol. 14, pp. 269–272, 2015.
- [46] Y. Y. Bai, S. Xiao, M. C. Tang, C. Liu, and B. Z. Wang, “Pattern reconfigurable antenna with wide angle coverage,” *Electron. Lett.*, vol. 47, no. 21, pp. 1163–1164, 2011.
- [47] S. P. Pinapati, S. J. Chen, D. Ranasinghe, and C. Fumeaux, “Detuning effects of wearable patch antennas,” *Asia-Pacific Microw. Conf. Proceedings, APMC*, pp. 162–165, 2017.
- [48] J. Buckley, K. G. McCarthy, B. O’Flynn, and C. O’Mathuna, “The detuning effects of a wrist-worn antenna and design of a custom antenna measurement system,” *Eur. Microw. Week 2010, EuMW2010 Connect. World, Conf. Proc. - Eur. Microw. Conf. EuMC 2010*, no. September, pp. 1738–1741, 2010.
- [49] W. Dorothy and R. Joos, “The Pin Diode Circuit Designers’ Handbook,” *Watertown*, no. 617, 1998, [Online]. Available: https://www.ieee.li/pdf/essay/pin_diode_handbook.pdf.
- [50] B. Doherty, “PIN diode Fundamentals, MicroNotes,” *MicroNote Ser. 701*, p. 2, 2017.
- [51] B. Mezghani, F. Tounsi, A. A. Rekik, F. Mailly, M. Masmoudi, and P. Nouet, *An Introduction to MEMS (Micro-electromechanical Systems) MEMS*, vol. 44, no. 12, 2013.
- [52] J.-M. Laheurte, *Compact Antennas for Wireless Communications and Terminals*, 1st Editio. John Wiley & Sons Inc., 2011.
- [53] S. M. Abbas, K. P. Esselle, L. Matekovits, M. Rizwan, and L. Ukkonen, “On-body antennas: Design considerations and challenges,” *2016 URSI Int. Symp. Electromagn. Theory, EMTS 2016*, pp. 109–110, 2016.
- [54] W. G. Scanlon, G. . Conway, and S. . Cotton, “Antennas and Propagation Considerations for robust wireless communications in medical body area networks,” vol. 1, 2007.
- [55] H. Kanaya, R. K. Pokharel, Y. Nakamura, and K. Yoshida, “Development of one-sided directional thin planar antenna for 5GHz wireless communication applications,” *IEEE Antennas Propag. Soc. AP-S Int. Symp.*, no. I, pp. 4–7, 2009.
- [56] R. A. Moody and S. K. Sharma, “Ultrawide bandwidth (UWB) planar monopole antenna backed by novel pyramidal-shaped cavity providing directional radiation patterns,” *IEEE Antennas Wirel. Propag. Lett.*, vol. 10, pp. 1469–1472, 2011.
- [57] V. Reghunath and S. K. Sukumaran, “Printed monopole UWB antenna with EBG structure for wireless body area network,” *Proc. 2014 Int. Conf. Contemp. Comput. Informatics, IC3I 2014*, pp. 1310–1314, 2014.
- [58] M. A. Antoniadis, M. A. B. Abbasi, M. Nikolic, P. Vryonides, and S. Nikolaou, “Conformal wearable monopole antenna backed by a compact EBG structure for body area networks,” *2017 11th Eur. Conf. Antennas Propagation, EUCAP 2017*, pp. 164–

- 166, 2017.
- [59] A. Arif, M. Zubair, M. Ali, M. U. Khan, and M. Q. Mehmood, "A Compact, Low-Profile Fractal Antenna for Wearable On-Body WBAN Applications," *IEEE Antennas Wirel. Propag. Lett.*, vol. 18, no. 5, pp. 981–985, 2019.
- [60] B. Yeboah-Akowuah, P. Kosmas, and Y. Chen, "A low profile microstrip patch antenna for body-centric communications at 2.45GHz band," *2015 9th Eur. Conf. Antennas Propagation, EuCAP 2015*, 2015.
- [61] B. S. Abirami and E. F. Sundarsingh, "EBG-Backed Flexible Printed Yagi-Uda Antenna for On-Body Communication," *IEEE Trans. Antennas Propag.*, vol. 65, no. 7, pp. 3762–3765, 2017.
- [62] M. Awais, M. Hamza, and W. T. Khan, "A Compact Ultra-wideband Single Element Planar Yagi Antenna," *2018 IEEE Antennas Propag. Soc. Int. Symp. Usn. Natl. Radio Sci. Meet. APSURSI 2018 - Proc.*, pp. 1939–1940, 2018.
- [63] M. Hamidkhani, "A Wideband Directional Microstrip Slot Antenna for On-Body Applications," *J. Electr. Electron. Eng.*, vol. 3, no. 3, p. 48, 2015.
- [64] S. A. Rezaeieh and A. Abbosh, "Broadband CPW-fed slot antenna with circular polarization for on-body applications at ISM band," *Asia-Pacific Microw. Conf. Proceedings, APMC*, pp. 1184–1186, 2012.
- [65] T. Alves, B. Poussot, and J. M. Laheurte, "PIFA-top-loaded-monopole antenna with diversity features for WBAN applications," *IEEE Antennas Wirel. Propag. Lett.*, vol. 10, pp. 693–696, 2011.
- [66] H. I. Hraga, C. H. See, R. A. Abd-Alhameed, and N. J. McEwan, "Miniaturised UWB antenna for a Wireless Body Area Network," *LAPC 2012 - 2012 Loughbrgh. Antennas Propag. Conf.*, no. November, pp. 3–6, 2012.
- [67] S. Chaimool, C. Rakluea, and P. Akkaraekthalin, "Mu-near-zero metasurface for microstrip-fed slot antennas," *Appl. Phys. A 2013 1123*, vol. 112, no. 3, pp. 669–675, Apr. 2013.
- [68] U. Ullah, I. Ben Mabrouk, and S. Koziel, "A Compact Circularly Polarized Antenna with Directional Pattern for Wearable Off-Body Communications," *IEEE Antennas Wirel. Propag. Lett.*, vol. 18, no. 12, pp. 2523–2527, 2019.
- [69] A. Hirata, T. Adachi, and T. Shiozawa, "Folded-loop Antenna with A Reflector for Mobile Handsets," *Wiley Period. Inc.*, vol. 40, no. 4, pp. 272–275, 2004.
- [70] K. Kwon, J. Ha, S. Lee, and J. Choi, "Design of a dual-band on-body antenna for a wireless body area network repeater system," *Int. J. Antennas Propag.*, vol. 2012, 2012.
- [71] G. Zhang, J. Hong, B. Wang, G. Song, and P. Zhang, "Compact Wideband Unidirectional Antenna With a Reflector Connected to the Ground Using a Stub," *IEEE Antennas Wirel. Propag. Lett.*, vol. 10, pp. 1186–1189, 2011.
- [72] M. S. Ellis, A. Ahmed, J. J. Kponyo, J. Nourinia, C. Ghobadi, and B. Mohammadi, "Unidirectional Planar Monopole Antenna Using a Quasi-Radiator," *IEEE Antennas Wirel. Propag. Lett.*, vol. 18, no. 1, pp. 157–161, 2019.
- [73] A. Fhager, T. McKelvey, and M. Persson, "Stroke detection using a broadband microwave antenna system," *EuCAP 2010 - 4th Eur. Conf. Antennas Propag.*, pp. 1–3, 2010.
- [74] K. N. Paracha, A. D. Butt, A. S. Alghamdi, S. A. Babale, and P. J. Soh, "Liquid metal antennas: Materials, fabrication and applications," *Sensors (Switzerland)*, vol. 20, no. 1, Jan. 2020.
- [75] S. Zhang *et al.*, "Highly conductive, flexible and stretchable conductors based on fractal silver nanostructures," *J. Mater. Chem. C*, vol. 6, no. 15, pp. 3999–4006, 2018.
- [76] S. M. Saeed, C. A. Balanis, C. R. Birtcher, A. C. Durgun, and H. N. Shaman, "Wearable Flexible Reconfigurable Antenna Integrated with Artificial Magnetic Conductor," *IEEE*

- Antennas Wirel. Propag. Lett.*, vol. 16, no. c, pp. 2396–2399, 2017.
- [77] A. Ghaffar *et al.*, “A flexible and pattern reconfigurable antenna with small dimensions and simple layout for wireless communication systems operating over 1.65–2.51 ghz,” *Electron.*, vol. 10, no. 5, pp. 1–13, 2021.
- [78] M. El Atrash, M. A. Abdalla, and H. M. Elhennawy, “A Compact Highly Efficient Π -Section CRLH Antenna Loaded with Textile AMC for Wireless Body Area Network Applications,” *IEEE Trans. Antennas Propag.*, vol. 69, no. 2, pp. 648–657, 2021.
- [79] W. Lin, H. Wong, and R. W. Ziolkowski, “Wideband Pattern-Reconfigurable Antenna with Switchable Broadside and Conical Beams,” *IEEE Antennas Wirel. Propag. Lett.*, vol. 16, pp. 2638–2641, 2017.
- [80] and C. L. Xiaohui Guo, Ying Hang, Zhicheng Xie, Can Wu, Le Gao, “Flexible and Wearable 2.45 GHz CPW-Fed Antenna Using Inkjet Printing of Silver Nano Particles on PET Substrate,” *Microw. Opt. Technol. Lett.*, vol. 55, no. 11, pp. 2562–2568, 2017.
- [81] Z. H. Jiang, Z. Cui, T. Yue, Y. Zhu, and D. H. Werner, “Compact, Highly Efficient, and Fully Flexible Circularly Polarized Antenna Enabled by Silver Nanowires for Wireless Body-Area Networks,” *IEEE Trans. Biomed. Circuits Syst.*, vol. 11, no. 4, pp. 920–932, 2017.
- [82] G. Li and M. Li, *Broadband Microstrip Antennas*, vol. 26, no. 6. 1998.
- [83] D. Sheet, “DSM8100-000 : Mesa Beam-Lead PIN Diode Applications :,” pp. 1–5, 2008.
- [84] M. S. Khan, A. D. Capobianco, S. M. Asif, A. Iftikhar, B. D. Braaten, and R. M. Shubair, “A pattern reconfigurable printed patch antenna,” *2016 IEEE Antennas Propag. Soc. Int. Symp. APSURSI 2016 - Proc.*, vol. 1, no. Patch 2, pp. 2149–2150, 2016.
- [85] K. C. Gupta, R. Garg, I. Bahl, and P. Bhartia, *Microstrip Lines and Slotlines*, Second Edi. Artech House, 2013.
- [86] E. S. Ahmed, “Wearable conformal antennas for 2.4 GHz wireless body area networks,” *Telkomnika*, vol. 11, no. 1, pp. 175–180, 2013.
- [87] J. C. Wang, E. G. Lim, M. Leach, Z. Wang, and K. L. Man, “Conformal Wearable Antennas for WBAN Applications,” *IAENG Int. J. Comput. Sci.*, vol. 43, no. 4, pp. 474–480, 2016.

APPENDIX A

Table 5.2 Parameters Needed to Find Body Tissue Dielectric Constant and Conductivity at Any Frequency [10].

	ϵ_∞	$\Delta\epsilon_1$	τ_1 (ps)	α_1	$\Delta\epsilon_2$	τ_2 (ns)	α_2	σ	$\Delta\epsilon_3$	τ_3 (ms)	α_3	$\Delta\epsilon_4$	τ_4 (ms)	α_4
Aorta	4.000	40.00	8.842	0.100	50	3.183	0.100	0.250	1.00E+5	159.155	0.200	1.00E+7	1.592	0.000
Bladder	2.500	16.00	8.842	0.100	400	159.155	0.100	0.200	1.00E+5	159.155	0.200	1.00E+7	15.915	0.000
Blood	4.000	56.00	8.377	0.100	5200	132.629	0.100	0.700	0.00E+0	159.155	0.200	0.00E+0	15.915	0.000
Bone (cancellous)	2.500	18.00	13.263	0.220	300	79.577	0.250	0.070	2.00E+4	159.155	0.200	2.00E+7	15.915	0.000
Bone (cortical)	2.500	10.00	13.263	0.200	180	79.577	0.200	0.020	5.00E+3	159.155	0.200	1.00E+5	15.915	0.000
Brain (gray matter)	4.000	45.00	7.958	0.100	400	15.915	0.150	0.020	2.00E+5	106.103	0.220	4.50E+7	5.305	0.000
Breast fat	2.500	3.00	17.680	0.100	15	63.660	0.100	0.010	5.00E+4	454.700	0.100	2.00E+7	13.260	0.000
Cartilage	4.000	38.00	13.263	0.150	2500	144.686	0.150	0.150	1.00E+5	318.310	0.100	4.00E+7	15.915	0.000
Cerebro spinal fluid	4.000	65.00	7.958	0.100	40	1.592	0.000	2.000	0.00E+0	159.155	0.000	0.00E+0	15.915	0.000
Cornea	4.000	48.00	7.958	0.100	4000	159.155	0.050	0.400	1.00E+5	15.915	0.200	4.00E+7	15.915	0.000
Eye tissues (sclera)	4.000	50.00	7.958	0.100	4000	159.155	0.100	0.500	1.00E+5	159.155	0.200	5.00E+6	15.915	0.000
Fat (average infiltrated)	2.500	9.00	7.958	0.200	35	15.915	0.100	0.035	3.30E+4	159.155	0.050	1.00E+7	15.915	0.010
Gall bladder bile	4.000	66.00	7.579	0.050	50	1.592	0.000	1.400	0.00E+0	159.155	0.200	0.00E+0	15.915	0.200
Heart	4.000	50.00	7.958	0.100	1200	159.155	0.050	0.050	4.50E+5	72.343	0.220	2.50E+7	4.547	0.000
Kidney	4.000	47.00	7.958	0.100	3500	198.944	0.220	0.050	2.50E+5	79.577	0.220	3.00E+7	4.547	0.000
Liver	4.000	39.00	8.842	0.100	6000	530.516	0.200	0.020	5.00E+4	22.736	0.200	3.00E+7	15.915	0.050
Lung (inflated)	2.500	18.00	7.958	0.100	500	63.662	0.100	0.030	2.50E+5	159.155	0.200	4.00E+7	7.958	0.000
Muscle	4.000	50.00	7.234	0.100	7000	353.678	0.100	0.200	1.20E+6	318.310	0.100	2.50E+7	2.274	0.000
Skin (dry)	4.000	32.00	7.234	0.000	1100	32.481	0.200	0.000	0.00E+0	159.155	0.200	0.00E+0	15.915	0.200
Skin (wet)	4.000	39.00	7.958	0.100	280	79.577	0.000	0.000	3.00E+4	1.592	0.160	3.00E+4	1.592	0.200
Small intestine	4.000	50.00	7.958	0.100	10000	159.155	0.100	0.500	5.00E+5	159.155	0.200	4.00E+7	15.915	0.000
Stomach	4.000	60.00	7.958	0.100	2000	79.577	0.100	0.500	1.00E+5	159.155	0.200	4.00E+7	15.915	0.000
Testis	4.000	55.00	7.958	0.100	5000	159.155	0.100	0.400	1.00E+5	159.155	0.200	4.00E+7	15.915	0.000
Tongue	4.000	50.00	7.958	0.100	4000	159.155	0.100	0.250	1.00E+5	159.155	0.200	4.00E+7	15.915	0.000

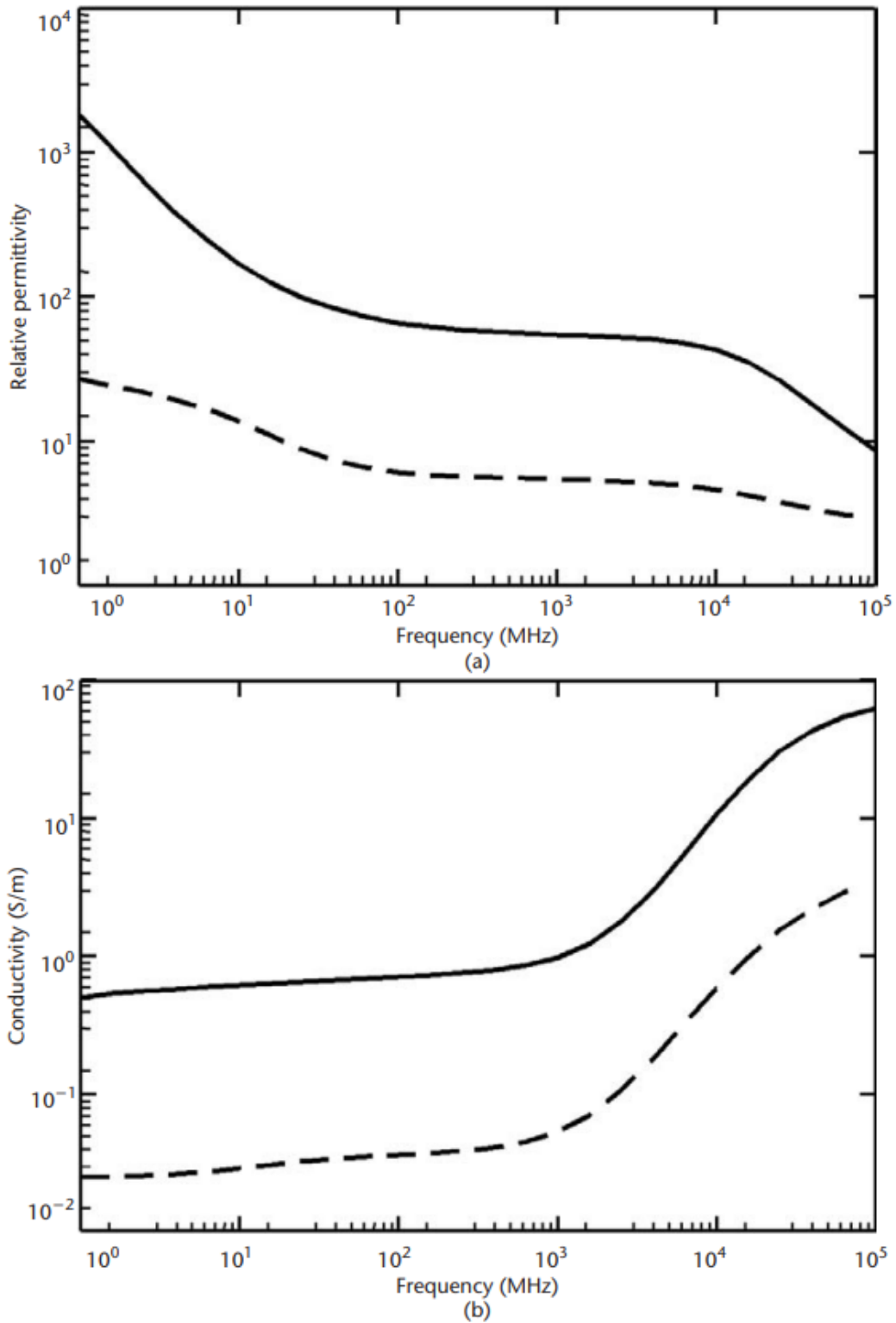


Fig.5.1 Electrical characteristics of tissues [8]: (a) relative permittivity; and (b) conductivity. Solid: muscle; dotted: fat.

APPENDIX B

Design and Simulation of the Flexible Pattern-Reconfigurable Antenna Based on 0.2 mm Rogers RO4003 Substrate.

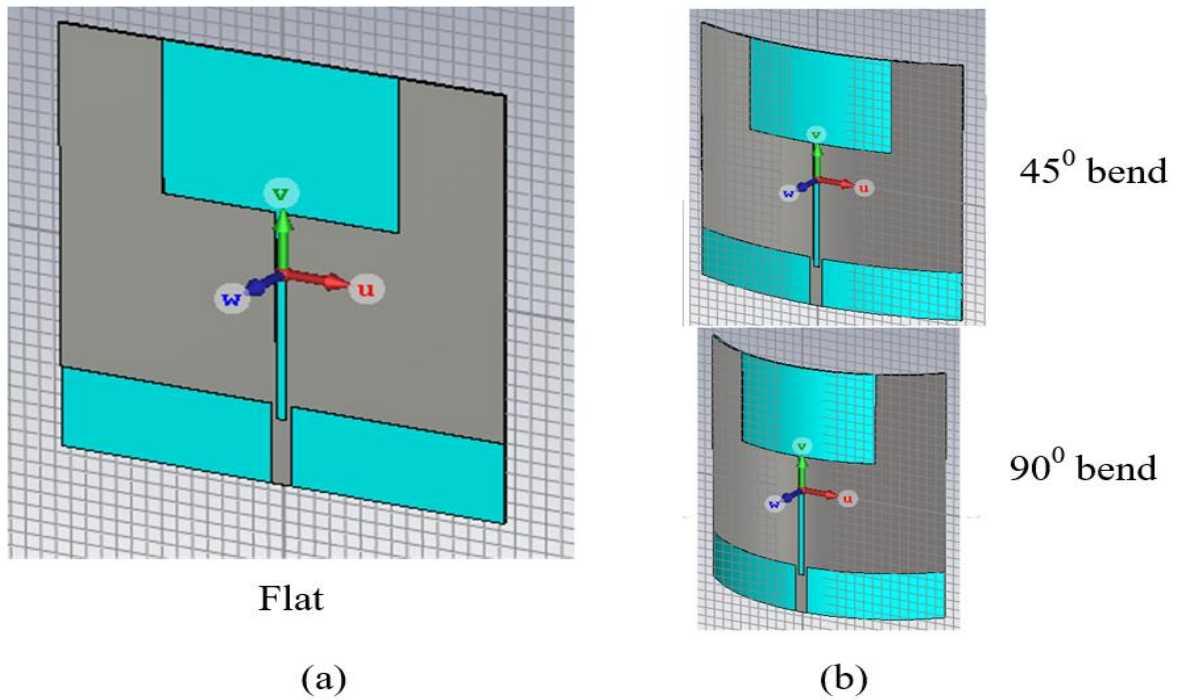


Fig.5.2 Design layout of the flexible reconfigurable antenna based on Rogers substrate (a) Flat (unbend, 0°) antenna (b) 45° and 90° bending.

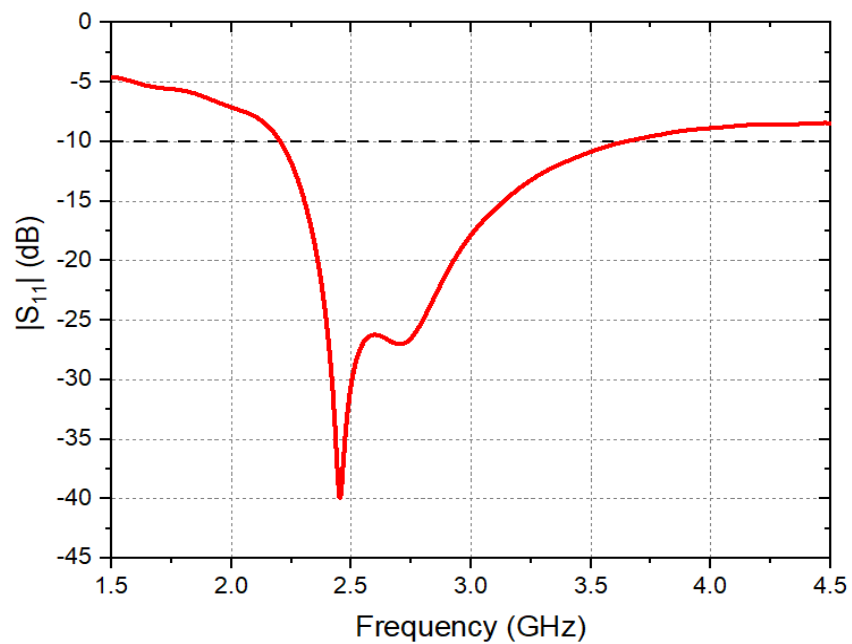


Fig.5.3 Simulated reflection coefficient (S_{11}) of the proposed flexible reconfigurable antenna without bending (flat, 0°).

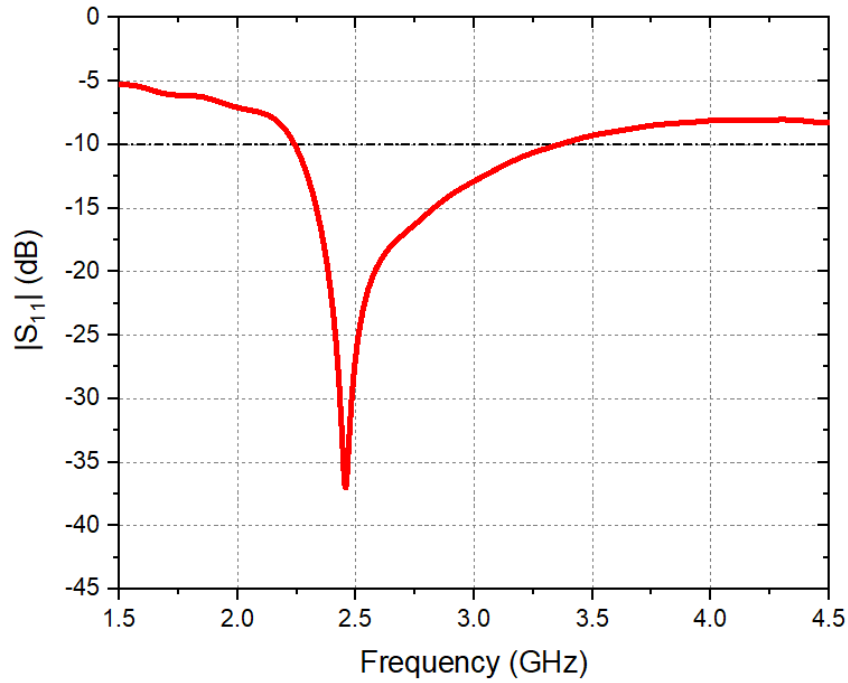


Fig.5.4 Simulated reflection coefficient (S_{11}) of the proposed flexible reconfigurable antenna at 90° based on Rogers substrate.

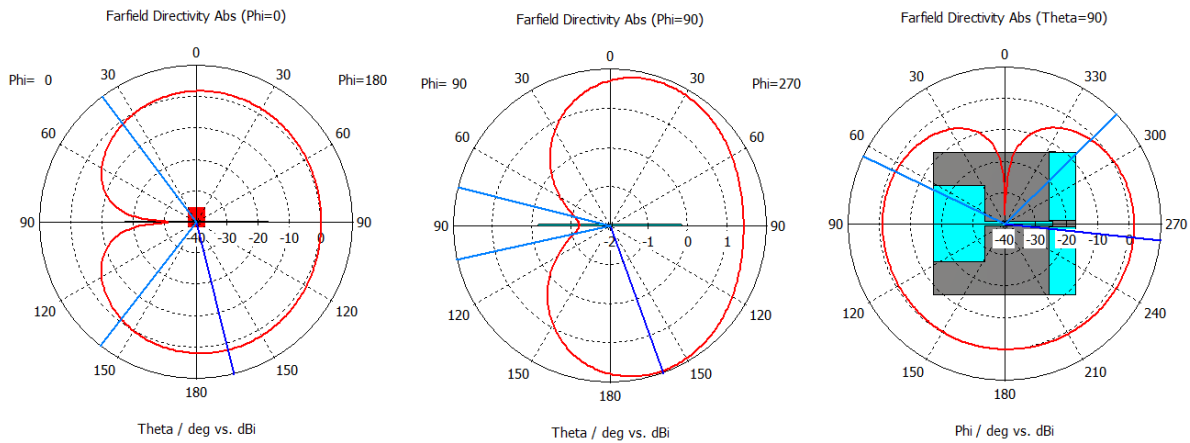


Fig.5.5 Normalized radiation pattern of the proposed antenna without bending (flat, 0°).

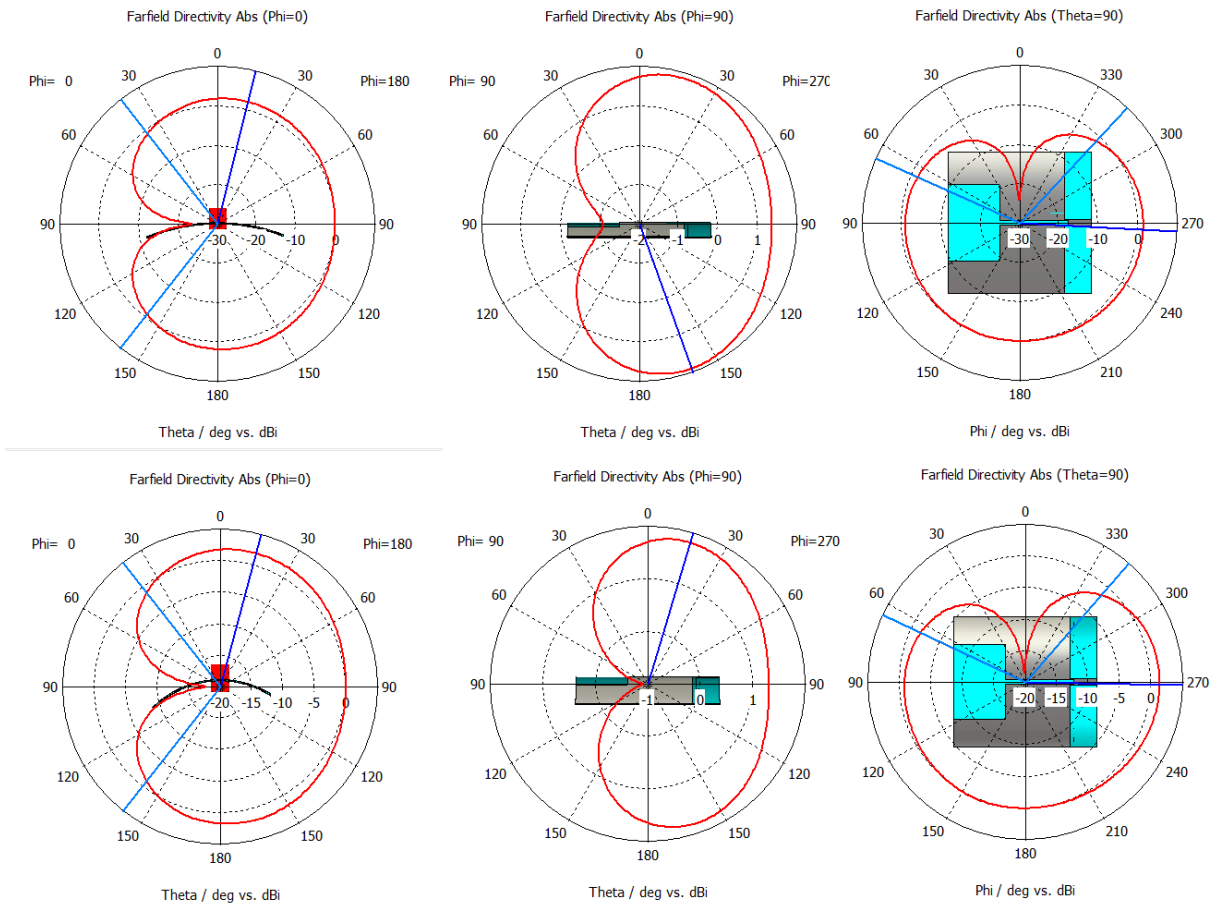


Fig.5.6 Normalized radiation pattern of the proposed antenna with bending at 45° (top) and 90° (down).